Propulsion System Analysis for Conceptual Design:
Drag and Losses of Nozzles and Mixed Compression Inlets

by

Arthur H. Warren

Thesis submitted to the Faculty of the
Virginia Polytechnic Institute and State University
in partial fulfillment of the requirements for the degree of

Master of Science

in

Mechanical Engineering

APPROVED:

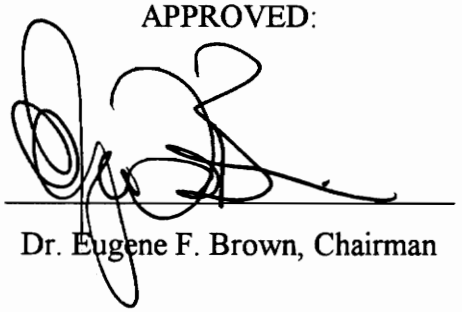

Dr. Eugene F. Brown, Chairman

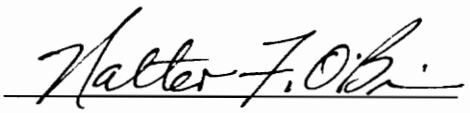

Dr. Walter F. O'Brien

Dr. Arvid Myklebust

July, 1993

Blacksburg, Virginia

Propulsion System Analysis for Conceptual Design:
Drag and Losses of Nozzles and Mixed Compression Inlets

Arthur H. Warren
Committee chairman: Dr. E. F. Brown
Department of Mechanical Engineering

(ABSTRACT)

This thesis describes the development and implementation of new computational techniques to predict installation losses for mixed compression inlets and a study of advanced technology nozzles.

The new computational techniques have been created to predict drag and total pressure recovery for both axisymmetric and 2-D mixed compression inlet configurations. These inlets are designed for use in aircraft with sustained supersonic cruise capabilities such as the HSCT. The drag and pressure recovery prediction methods have been added to ACSYNT, an aircraft conceptual design program.

Also included in this thesis is a survey of the performance of advanced technology nozzles. Axisymmetric and nonaxisymmetric geometries are considered, as are non thrust-vectoring nozzles. Only the internal losses of these nozzles are considered, and these losses are characterized by the thrust coefficient. The results of this survey have also been added to ACSYNT to extend the thrust prediction capabilities of the code.

Acknowledgements

I would like to thank the following people:

Professor E. F. Brown, for his involving me in the project, willingness to help, overall understanding and for not beating me over the head with large blunt objects, even when I deserved it.

Professors Joseph Schetz and Walter O'Brien, for agreeing to serve on my graduate committee.

I am particularly indebted to the ACSYNT institute for supporting this project financially, and Anthony Midea of the Sverdrup Corporation (in association with NASA-Lewis) for providing many mixed compression inlet design suggestions.

Finally, thanks to the rest of the ACSYNT team for their help, and to my parents, whose moral support has really helped me more than they, or anyone else, can possibly imagine.

Table of Contents

List of Figures

List of Tables

Inlet Nomenclature

A ..... Area

A_c ..... Area of capture face

A_i ..... Area of streamtube exit

A_m ..... Maximum projected cowl area

A_s ..... Projected cone area upstream of bow shock

A_t ..... Area at throat

A_∞ ..... Streamtube area at upstream (undisturbed) station

$C_{D_{inlet}}$ ..... Inlet drag coefficient (referenced to A_c)

$C_{D_{prof}}$ ..... Profile drag coefficient (referenced to A_c)

$C_{D_{spill}}$ ..... Spillage drag coefficient (referenced to A_c)

$C_{D_{wave}}$ ..... Wave drag coefficient (referenced to A_c)

$\tilde{C}_D$ ..... Transonic wave drag function for a wedge

$C_{D_{wedge}}$ ..... Wedge wave drag coefficient (referenced to A_c)

$\bar{C}_{D_{wedge}}$ ..... Wedge wave drag coefficient (referenced to cowl frontal area)

C_f ..... Skin friction coefficient

D_{add} ..... Additive drag force

D_b ..... Bleed and bypass drag force

D_{inlet} ..... Inlet drag force

D_f ..... Nacelle viscous drag force

D_p ..... Nacelle form drag force

D_{prof} ..... Profile drag force

D_{spill} ..... Spillage drag force

D_{wave} ..... Wave drag force

D_x ..... Auxiliary air systems drag force

F_{ramp} ..... Total force on forebody ramps

F_{cone} ..... Force on centerbody cone

f ..... Additive drag calculation factor

f_f ..... Friction factor

g_c ..... Gravitational constant

L_1 ..... Length of first forebody ramp

L_2 ..... Length of second forebody ramp

L_c ..... Length of cowl

M ..... Mach number

MFR ..... Mass flow ratio

MFR_{ref} ..... Reference mass flow ratio

$\dot{m}$ ..... Mass flow rate

$\dot{m}_{max}$ ..... Maximum mass flow rate

P ..... Static pressure

P_{c_1} ..... Cone pressure downstream of conical shock

P_{c_2} ..... Cone pressure downstream of bow shock

P_i ..... Pressure at streamtube exit

P_o ..... Total pressure

P_{R1} ..... Pressure on the first forebody ramp

P_{R2} ..... Pressure on the second forebody ramp

P_{R3} ..... Pressure after the bow shock (unstarted only)

q_∞ ..... Freestream dynamic head

R ..... Ideal gas constant

R_c ..... Cowl radius at capture face

R_{cone} ..... Cone radius at streamtube exit station

R_i ..... Cone radius at capture face

R_m ..... Maximum cowl radius

T ..... Static temperature

T_o ..... Total temperature

V ..... Velocity

$W\&R$ ..... Willis and Randall

w ..... Inlet width

wv ..... Control volume dimension

X_c ..... Length of centerbody cone

X_{ramp_1} ..... Length of first forebody ramp

X_{ramp_2} ..... Length of second forebody ramp

Y_c ..... Cowl height at capture face

Y_i ..... Height of inlet capture streamtube

Y_m ..... Maximum cowl height

ΔX ..... Distance from cowl lip to inlet throat

α ..... Internal cowl angle for axisymmetric inlet

β ..... $\sqrt{M_\infty^2 - 1}$

γ ..... Specific heat ratio

η ..... Cowl slope

θ ..... Ramp angles, cone half angle

ρ ..... Density of air

τ_w ..... Viscous shear stress

χ ..... Wedge wave drag function

Subscripts

b ..... Bleed, bypass

c ..... Capture plane

des ..... Value at design conditions

s ..... Over a surface

t ..... At the throat station

x ..... In the streamwise direction

∞ ..... Upstream (undisturbed) flow station

min ..... Minimum

shk ..... Station immediately downstream of normal shock

Nozzle Nomenclature

A_e ..... Exit area

A_t ..... Throat area

AR ..... Area ratio $\equiv \frac{A_e}{A_t}$

NPR ..... Nozzle pressure ratio

T ..... Actual thrust

T_i ..... Ideal thrust, given by: $\gamma\sqrt{\frac{2}{\gamma-1}\left(\frac{2}{\gamma+1}\right)\left[1-\left(\frac{P_\infty}{P_o}\right)^{\frac{\gamma-1}{\gamma}}\right]}$

T_r ..... Resultant thrust

$\delta_{v,p}$ ..... Pitch thrust vectoring angle, degrees

$\delta_{v,y}$ ..... Yaw thrust vectoring angle, degrees

1.0 Introduction

The process of designing an aircraft is a laborious task, especially considering the complexity of current aircraft. Conceptual design, that part of the design process which determines project feasibility, has become increasingly important for supersonic aircraft, as small geometrical changes can result in large changes in performance, particularly in the transonic regime. The conceptual design process is complex and well suited to computer analysis due to the iterative nature of the calculations performed.

In the mid 70's a computer program called ACSYNT (AirCraft SYNThesis) was developed to assist in the conceptual design process. In its original form, it was non-interactive; it determined drag, thrust, fuel requirements, and other conceptual design considerations from a user-created input file. The current version of ACSYNT bears little resemblance to its ancestor, employing an interface that shows the final design to users in graphical form. Along the way, the analysis portion of the program has been significantly updated, by incorporating state of the art computational techniques wherever possible, and by adding new capabilities. Recent examples are the addition of new inlet geometries (Malan, 1989), and improved afterbody drag prediction (Squire, 1992). The currently targeted deficiencies are the lack of a high speed inlet calculation, and the lack of thrust prediction capabilities to support recent revisions made in the afterbody drag prediction calculation.

Inlets decelerate the freestream air to a velocity that the compressor can efficiently process. Ideally, the deceleration process would be accomplished without reducing the total pressure of the freestream air using an isentropic compression inlet. Isentropic compression inlets provide perfect total pressure recovery at the design Mach number, but have serious performance degradation at flight speeds below this design Mach number. The

design of aircraft such as the high speed civil transport, or HSCT, demands an inlet that is capable of processing Mach two to Mach three air efficiently, but without these severe off-design penalties. The external compression inlets of Malan (1989), which substitute a single compression surface for the isentropic ramp, do not exhibit such a serious off-design performance problem. These inlets do, however, have large total pressure losses at higher Mach numbers and should not be used for continuous high Mach number operation. Supersonic cruise aircraft require an inlet that offers on-design performance similar to an isentropic compression inlet and off-design performance comparable to an external compression supersonic inlet. One solution is what is termed "mixed compression" inlets.

Mixed compression inlets are so named because the compression process, consisting in part of a series of shocks, is performed both externally and internally. These inlet types offer a number of design advantages over external compression inlets, such as increased total pressure recovery and reduced drag at higher Mach numbers. Analysis of the flow through mixed compression inlets is complicated by the additional shock structure and the need to avoid unstarting. In its simplest terms, starting refers to the inlet operating in true mixed-compression mode, with the terminal normal shock occurring downstream of the inlet throat. When the inlet is unstarted, it behaves similarly to an external compression inlet, with an external bow shock. Thus, analysis of these inlet types can be seen as a straightforward extension of external compression inlet analysis, and many of the same techniques can be used for both external and mixed compression inlets. The focus of the research for this thesis has been to develop mixed compression inlet analysis methods. Implementation of these methods is fully described in Appendix B.

1.1 Research Objectives

The objectives of the research conducted for this thesis were as follows:

- Select representative axisymmetric and 2D mixed compression inlet geometries
- Determine geometric parameters describing these inlets
- Develop solution algorithms to solve for drag and internal performance
- Create FORTRAN subroutines using these methods
- Verify the results obtained from the FORTRAN routines by comparing against experimental results
- Conduct a literature search for nozzle installation data (internal losses)
- Develop a FORTRAN subroutine to predict thrust using a variety of nozzles, using this installation data

2.0 Background Theory

2.1 Thrust & Drag Accounting

In November of 1991 it was brought to the author's attention by Tony Midea that a thrust and drag accounting standard was developed by NASA-LeRC, NASA-Ames, and Virginia Polytechnic Institute and State University. This standard is based on current industry methodology as seen in Crosthwait et al (1967), Tinney et al (1983) and an SAE Committee (1985). The work presented in this report follows this procedure. A detailed explanation of this accounting method follows, beginning with a standard definition of installed thrust:

$$T_{inst} = \left(F_g C_v - D_{ram}\right) - D_{prop}$$

where T_{inst} is the installed thrust, $\left(F_g C_v - D_{ram}\right)$ is the uninstalled thrust, and D_{prop} is the propulsion system drag. F_g and C_v are the engine gross thrust and engine gross thrust coefficient, respectively. The engine gross thrust and engine ram drag, D_{ram} can be calculated using cycle analysis routines; the gross thrust coefficient is determined from table lookup routines. D_{prop} is defined as the sum of the throttle dependent drags.

$$D_{prop} = D_{nozzle} + D_{inlet} + D_{nacelle}$$

These terms are defined in more detail; the terms of interest are inlet and nacelle drag, defined as:

$$D_{inlet} = D_{spillage} + D_{bld} + D_{byp} + D_{ecs}$$

$$D_{nacelle} = D_{wave} + D_{friction}$$

The nacelle drag is composed of wave and friction drag over the entire nacelle. Nacelle drag at the reference setting is assigned to vehicle drag. Drag at the reference throttle setting subtracted from the throttle dependant nacelle drag. For further information on choice of reference throttle setting, consult Squire (1992).

Inlet drag is the sum of spillage, bleed, bypass, and environmental control system (or auxiliary) drags. Spillage drag is defined to be the difference between additive drag and cowl suction. Bleed, bypass, and auxiliary drags are determined from momentum losses. These drag terms are explained in further detail in the following section.

2.2 Inlet Drag

Inlet drag, for the purposes of ACSYNT, includes not only inlet drag terms as defined above, but also the nacelle drag terms. This is done primarily for the sake of convenience, since all the information needed to calculate throttle dependant nacelle drag is available to the routines that determine inlet drag. This section explains the origin of these drag terms; later sections will focus on applying these formulae to specific geometries.

Additive drag is the pressure integral along the capture streamline in the streamwise direction. While this is not a drag force in the conventional sense, the concept of additive drag is used as a correction to account for viscous and non-one-dimensional flow effects ignored in the calculation of installed thrust. For a complete explanation additive drag and the cancellation of additive drag under ideal conditions, consult Appendix A of Malan (1988). Additive drag is given by the expression $D_{add} = \int_{c}^{\infty} \left(P - P_{\infty}\right) dA_x$, where dA_x is the projected area of the streamtube in the streamwise direction.

Form drag:

$D_p = \int_c^e \left(P - P_\infty\right) dA_x$, where dA_x is the projected area of the nacelle in the streamwise direction.

Viscous drag:

$D_f = \int_c^e \tau_w dA_x$, where dA_x is the projected area of the nacelle in the streamwise direction.

Bleed and bypass drag:

$D_b = \left[\dot{m}_b\left(V_\infty - V_b\right) + A_b\left(P_b - P_\infty\right)\right]\cos\theta_b$, where θ_b is the exit angle for bleed and bypass air.

Auxiliary or ECS drag:

$\dot{m}_x V_\infty$ where $\dot{m}_x$ is the ECS mass flow rate in the streamwise direction and V_∞ is the freestream velocity.

In conformity with the standards set for ACSYNT, form drag and viscous drag, defined for the entire nacelle, are calculated only for that part of the nacelle that is upstream of the maximum diameter, and are called cowl drags. The drag over the remainder of the nacelle is computed as afterbody drag.

During subsonic operation, the form drag and viscous drag are combined and called profile drag. Typically, as Mach numbers near unity, the flow will become locally supersonic, which causes a high form drag. The Mach number at which drag rises significantly is called the drag-rise Mach number. The high form drag is due to the appearance of locally supersonic flow on the nacelle.

2.3 Inlet Performance

Inlet performance is measured by total pressure losses. These losses are computed by determining the pressure losses through the shock system plus the losses in the subsonic portion of the inlet. The subsonic loss calculation depends only on the throat Mach number, and is based on the experimental correlations of Ball (1972). This correlation is intended to determine subsonic diffuser losses due to frictional effects and separation. It is important to note that this correlation assumes no knowledge of diffuser geometry, as none is available within ACSYNT.

2.4 Nozzle Performance

Adjustments to idealized nozzle performance are required because of frictional effects, flow nonuniformities, and non-axially directed flow. These losses are typically split into two components: discharge and thrust coefficients. For the purposes of the ACSYNT standard, only the thrust coefficient is explicitly considered.

2.4.1 Thrust Coefficient

The definition of the thrust coefficient is $\frac{T_a}{\dot{m}_a V_{ideal}}$ where T_a is the actual thrust, $\dot{m}_a$ is the actual mass flow rate through the nozzle and V_{ideal} is the ideal nozzle exit velocity.

Alternatively, the thrust coefficient can be defined as $\frac{T_a}{C_d \dot{m}_{ideal} V_{ideal}}$ where C_d is the discharge coefficient, and $\dot{m}_{ideal}$ is the ideal mass flow rate through the nozzle.

2.4.2 Ideal Thrust Ratio

The ideal thrust ratio is not a coefficient that accounts for non-ideal effects, it is used to relate the thrust of a perfectly expanded convergent-divergent nozzle to that of a choked convergent nozzle with the same upstream flow characteristics. This ratio is conveniently defined only in terms of the nozzle pressure ratio. One method of computing the thrust of a convergent nozzle is to multiply the thrust of an equivalent convergent-divergent nozzle by the ideal thrust ratio. The original convergent nozzle correlations in ACSYNT use a similar method. A complete derivation of the ideal thrust ratio is given in Appendix A.

3.0 Inlets

3.1 Literature Survey

This section is a review of literature containing enhanced methods for the prediction of inlet drag and internal performance. Specific references will be cited in later sections as the details of drag and performance are discussed.

Shock standoff distance is critical to accurately predict additive drag; as will be shown, the force on the ramp after the normal shock depends on the area and average pressure downstream of the shock. Kapoor et al. (1992) have developed a different method for predicting this shock standoff distance, which yields similar results to that used in the current ACSYNT code (Osmon, 1967).

As flight Mach numbers increase, so does the importance of bleed and bypass systems, especially with mixed compression inlets. Bleed air flow is used to reduce or eliminate the shock/boundary layer interactions and bypass air flow is used to control the inlet unstart problem. Inlet unstart can occur during slight fluctuations of the mass flow rate, such as throttle reduction, but a bypass system can provide a margin of tolerance to the intake system (Fujimoto et al., 1992).

Additional work has been done to review the analytical methods in use; Malan (1989) has been the most helpful single source for an explanation of inlet system operation in general, and of the methods used in ACSYNT in particular. Although originally intended for external compression inlets, the procedures used by Malan to predict spillage drag, wave

drag, and profile drag are still in use with specific changes to account for alternative geometries and higher Mach numbers present in mixed compression inlets. These changes are detailed in later sections.

The literature used to test the results from these methods are Anderson and Wong (1973) for the 2D inlet, and Smeltzer and Sorensen (1973) for the axisymmetric inlet.

3.2 Overview of the Prediction Methods

3.2.1 Sizing Methodology

Inlets are sized according to design mass flow conditions. This condition is determined by the user-specified geometry (ramp angles, engine face area and Mach number), design Mach number and design total pressure recovery. The sizing of the inlet determines the required capture face area, the required bleed and bypass mass flow, auxiliary mass flow, and the actual mass flow processed by the inlet. The process of determining bleed and bypass requirements is virtually identical to that used in the original version of ACSYNT, with the exception that, for off-design calculations, the amount of bypass air required is determined according to that which will provide a started flow condition. See the flowcharts on the following pages (figures 1 and 2) for an overview of the inlet calculation.

Any reduction in total mass flow through the inlet from the maximum amount of total mass flow the inlet can process at a given flight condition will cause immediate unstart of the inlet. Bypass air is used to keep the total mass flow processed by the inlet independent of engine mass requirements. This approach to determining the bypass and total mass

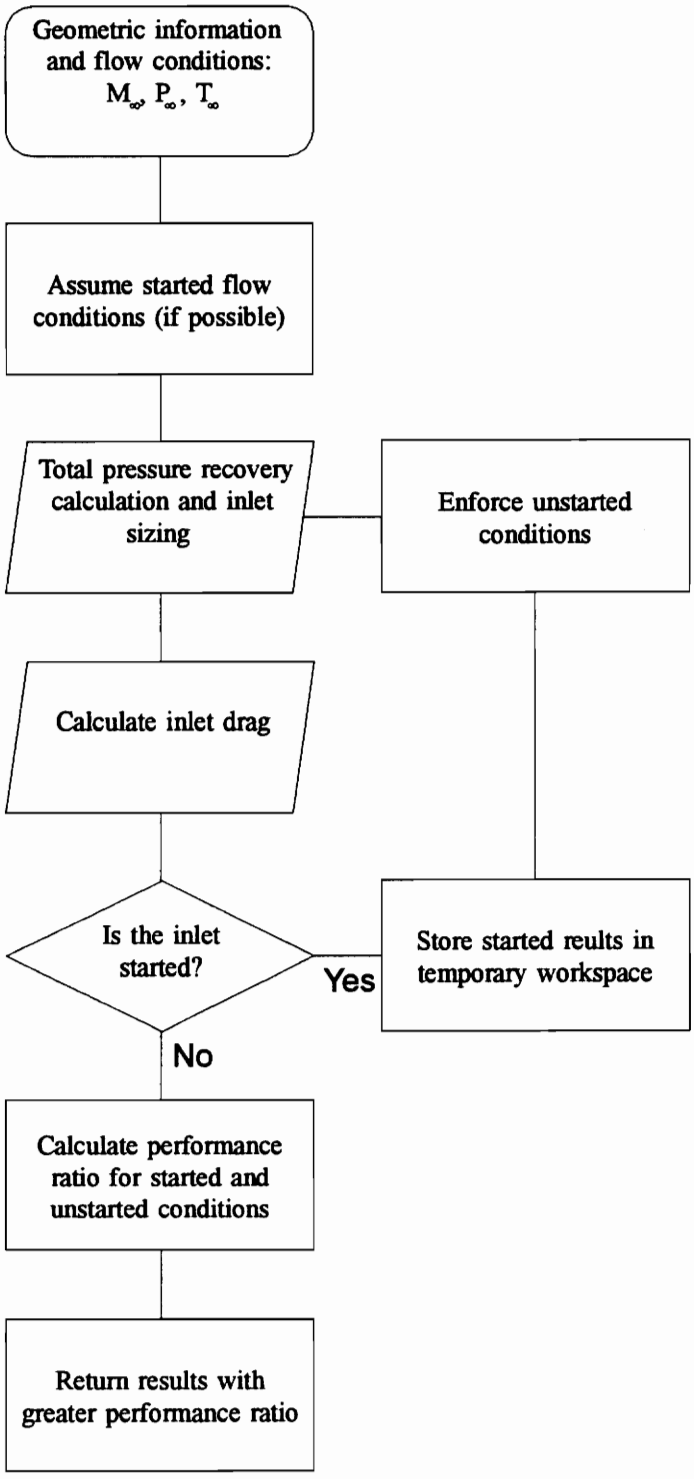

Figure 1 Overview of inlet calculation.

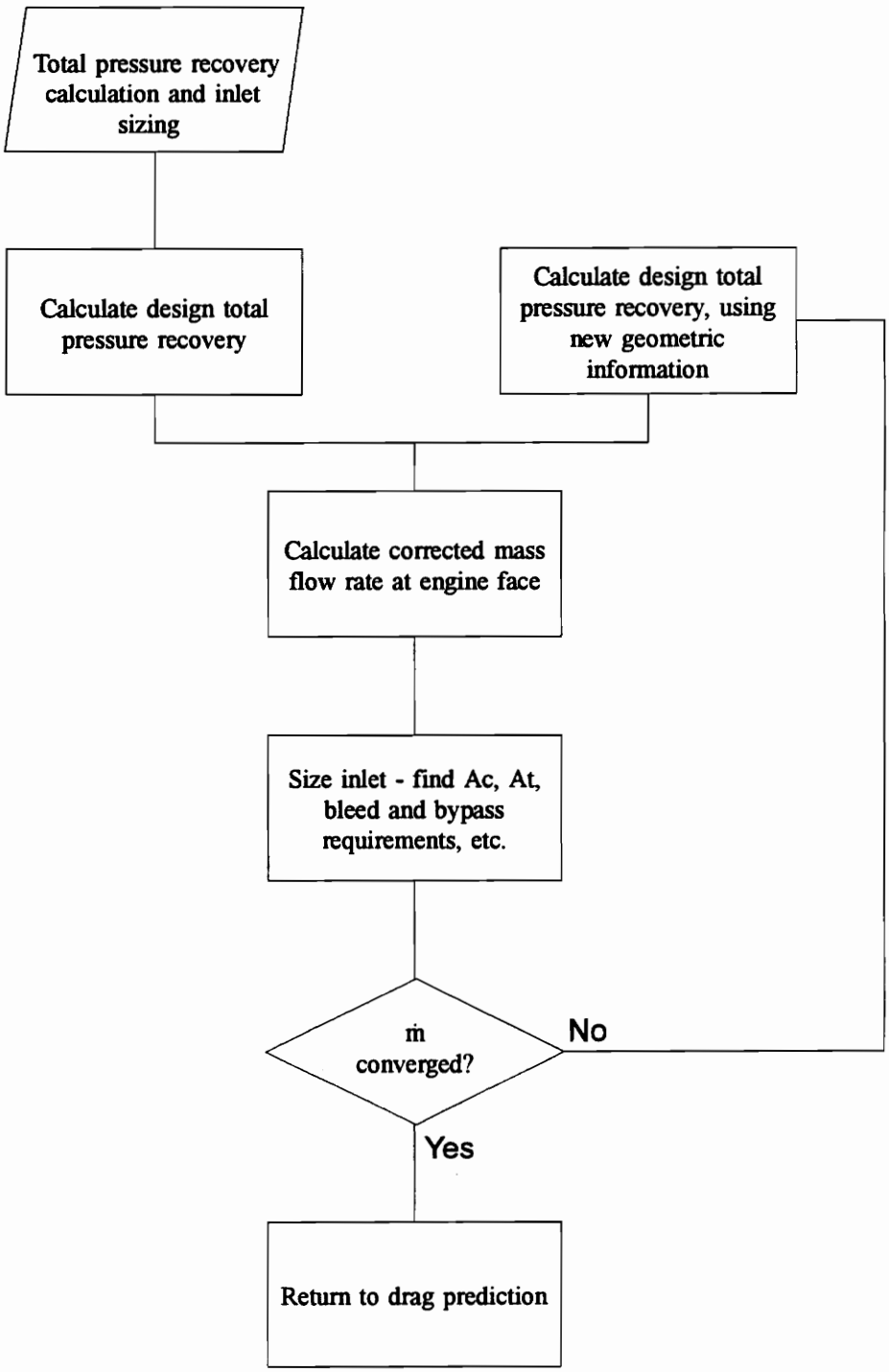

Figure 2 Overview of pressure recovery and sizing calculation.

flow rate requires an iterative scheme, since inlet sizing is a function of design total pressure recovery, which is dependant on total mass flow processed by the inlet. The standard ACSYNT correlations for bypass are used when the iterated results are less than those from the correlations.

The bleed mass flow is determined in the following manner; for design Mach numbers between 1.0 and 2.8:

$$\frac{A_{bl}}{A_c} = 0.1\left(\frac{M_{des}}{3.0}\right)^3\left(\frac{M_\infty - 1}{M_{des} - 1}\right) \qquad [3.2.1]$$

For design Mach numbers greater than 2.8:

$$\frac{A_{bl}}{A_c} = 0.10\left(.344M_{des} - 0.0113\right) \qquad [3.2.2]$$

Equation [3.2.1] comes from a curve-fit to data from Ball (1972); the origin of [3.2.2] is unknown.

3.2.3 Pressure Recovery

Total pressure recovery is a measure of the efficiency of the inlet, expressed as a ratio of total pressure at the compressor face to total ambient pressure. If one considers a Brayton cycle, the higher this ratio, the less work the compressor needs to perform for the engine to achieve the thrust. Ideally, the pressure recovery for an inlet would be unity; this can be (theoretically) achieved using an isentropic compression inlet. Unfortunately, this type of inlet yields perfect recovery only at the design Mach number. Off this design point, the total pressure recovery drops off dramatically. Furthermore, the cowl drag for an isentropic

inlet will be large due to the amount of flow turning required. A properly designed inlet system, utilizing a series of shock waves, can provide good on and off-design performance.

The total pressure recovery calculation consists of separate total pressure recovery calculations for the supersonic and subsonic portions of the inlet. Subsonic pressure recovery is determined as for the external compression inlets, with the exception of determining the throat Mach number. For the mixed compression inlet, the Mach number used in the calculation of subsonic pressure recovery is the actual throat Mach number when the inlet is unstarted, or the Mach number directly behind the normal shock if the inlet is started. The correlations used to determine subsonic pressure recovery come from Ball (1972), and a curve fit by Morris et al. (1977).

The supersonic pressure recovery is determined using shock calculations; no provisions exist to use either Military Specification 5008B or AIA standard ram recovery (two standard ACSYNT correlations), as these underpredict the total pressure recovery at higher Mach numbers.

3.2.2 Drag Prediction

Drag prediction is based on the summation of spillage drag, wave drag, nacelle viscous drag, and bleed and bypass drag — these are the terms described in Chapter two. A flowchart on the following page illustrates the general prediction methodology; the techniques used to evaluate each of the drag terms will depend on inlet type and operating conditions. These drag prediction methods all assume zero angle of attack and undisturbed freestream conditions.

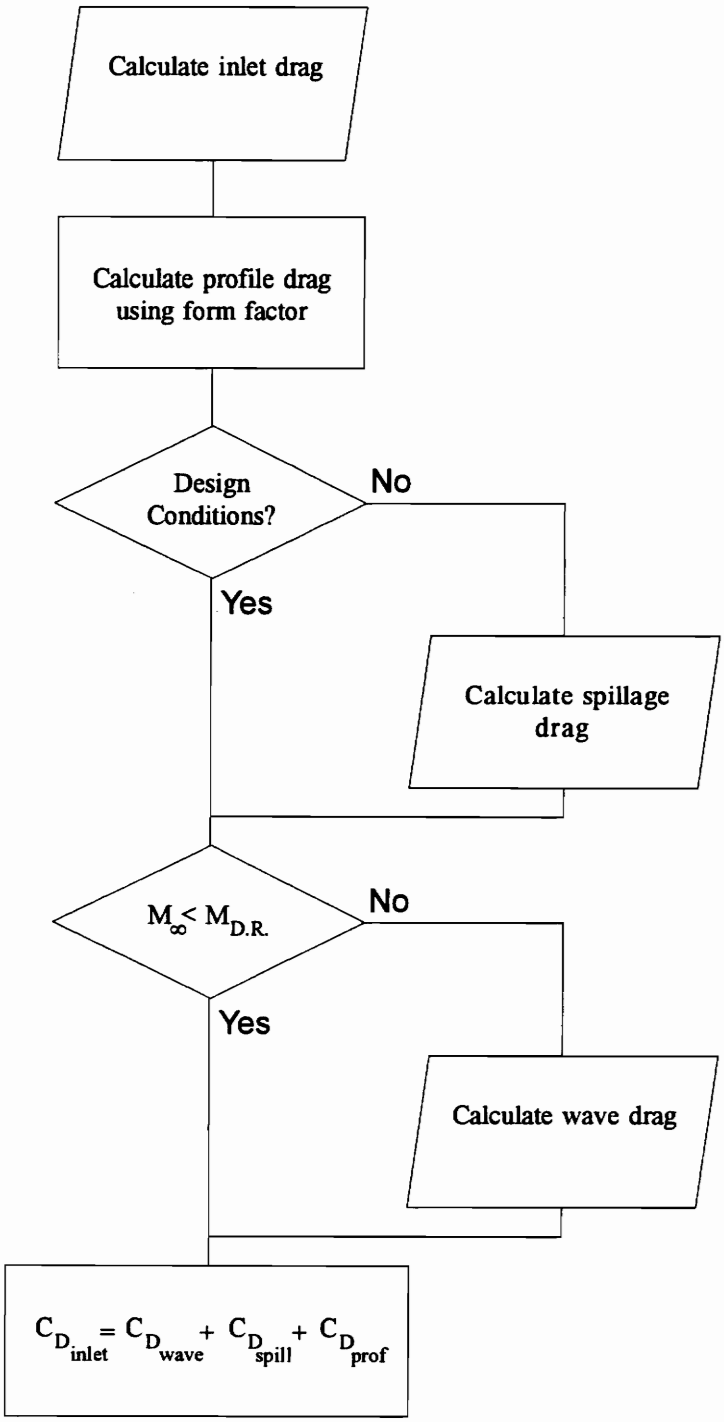

Figure 3 Overview of drag prediction calculation.

Spillage drag is typically composed of two separate drag calculations, additive drag and cowl suction. For the purposes of this calculation, the cowl lip is assumed to be sharp, and the cowl profile to be wedge shaped. Because of this, the cowl suction term is zero (or near zero), and spillage drag is equal to additive drag. Additive drag is calculated using a control volume approach identical to that used in the external compression inlet calculation. Viscous nacelle drag is determined using a turbulent mean skin friction coefficient, corrected for surface roughness and localized heating that may occur at high Mach numbers. This method is virtually identical to that used in the aerodynamics portion of the ACSYNT code, and is carried over from the external compression inlets of Malan (1989).

The procedure used to calculate wave drag is independent of the freestream Mach number, since linear theory is used to extend transonic wave drag over a wedge to any Mach number. Note that wave drag is calculated assuming that the Mach number immediately upstream of the cowl is the freestream Mach number. This assumption is less restrictive for mixed compression inlets, which operate started in the higher Mach number ranges, than for external compression inlets, which have a bow shock in front of the cowl for much of their operating range.

3.3 Planar Inlet

3.3.1 Overview

For the purposes of the calculation the planar mixed compression inlet is a two ramp, four shock inlet. The two ramp angles are assumed to be the same, and the final oblique shock

turns the flow through an angle of 2θ back to horizontal (Figure 4 on following page). The upper and lower cowls are assumed to be sharp lipped and wedge shaped. This sharp lip assumption was used because the actual cowl lip radius is very small compared to that used on external compression inlets. This small radius, in conjunction with the linear cowl profile, makes calculation of cowl suction unnecessary.

Prediction of maximum mass flow for a given freestream Mach number is critical for several reasons. The first is to limit the engine mass flow requirements. Since the calculated drag is also based partially on the engine mass flow rate, this prevents overprediction of drag for the inlet. Also, the maximum mass flow is used to calculate the amount of bypass needed to control starting of the inlet.

Figures 5 and 6 on the following pages are flow charts showing the solution procedure for the planar mixed compression inlet. Details of this procedure follow throughout the remainder of this chapter. Prediction of bow shock location is detailed in Malan (1989) and comes from the correlations of Moeckel (1955) and Osmon (1967).

3.3.2 Total Pressure Recovery

Determination of total pressure recovery, consisting of supersonic and subsonic procedures, is part of the iterative process used to calculate the total inlet mass flow rate. Supersonic pressure recovery is calculated using the same technique throughout the iterative process, whereas the subsonic pressure recovery calculation method depends on the start/unstart state of the inlet.

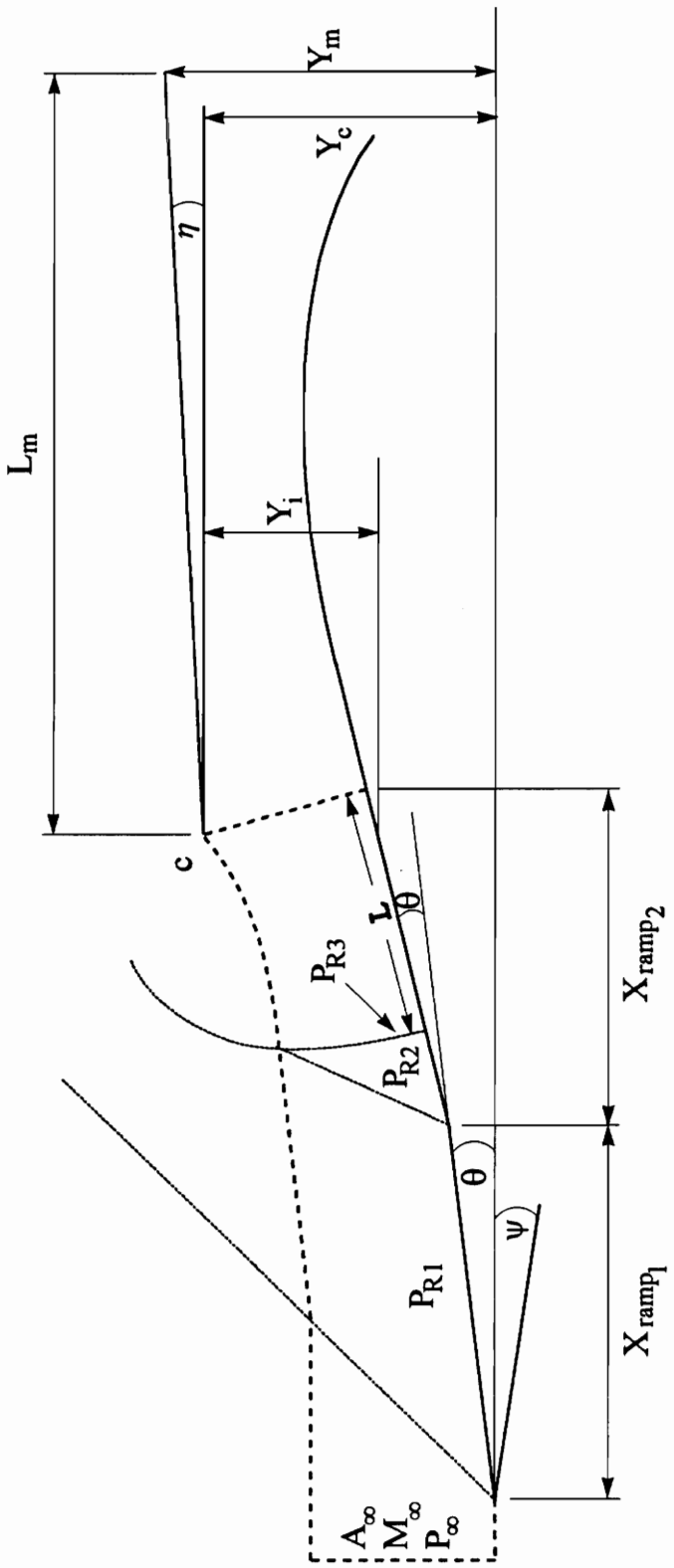

Figure 4 2D Mixed Compression Inlet and Control Volume.

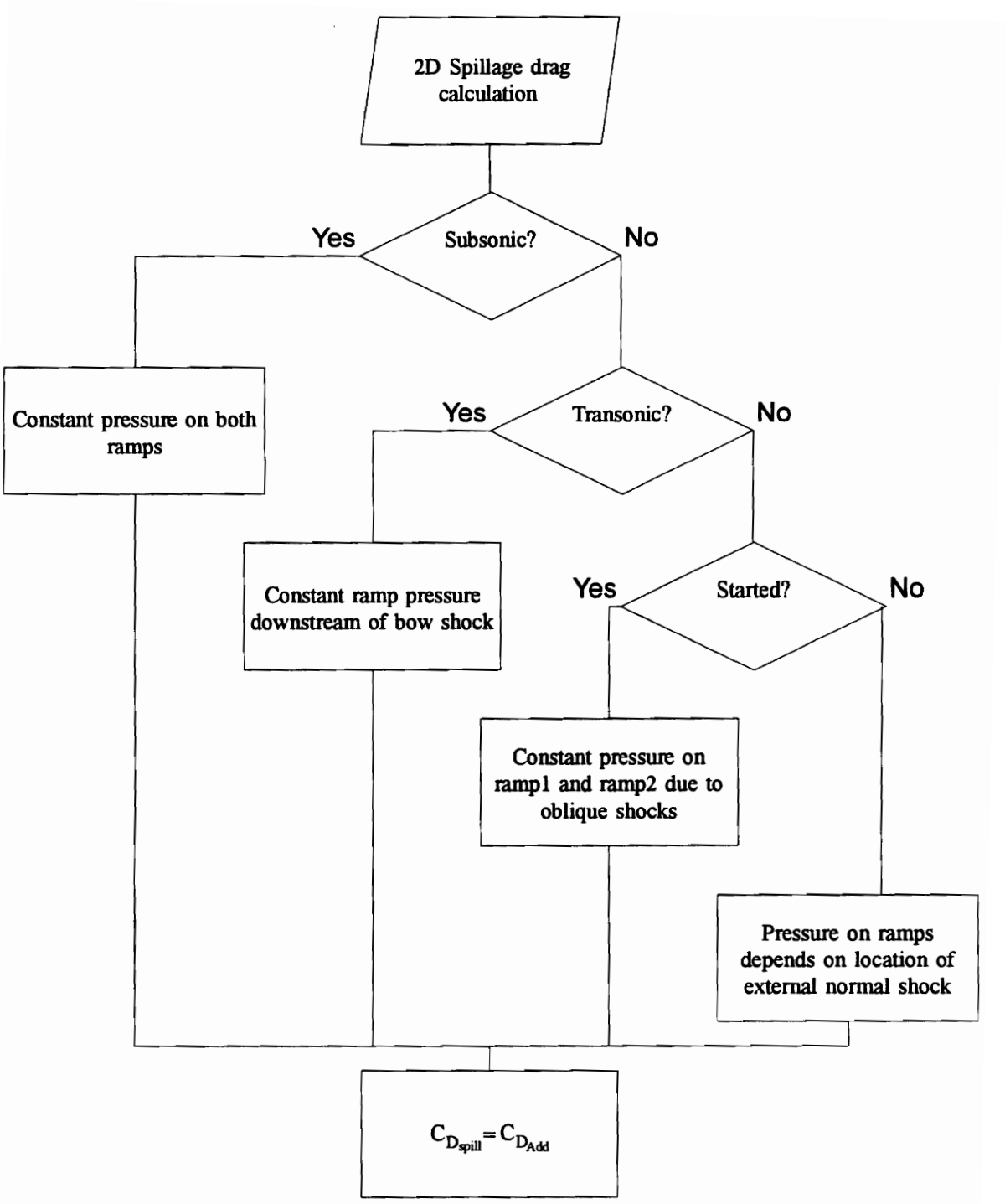

Figure 5 Spillage drag prediction for the 2D inlet.

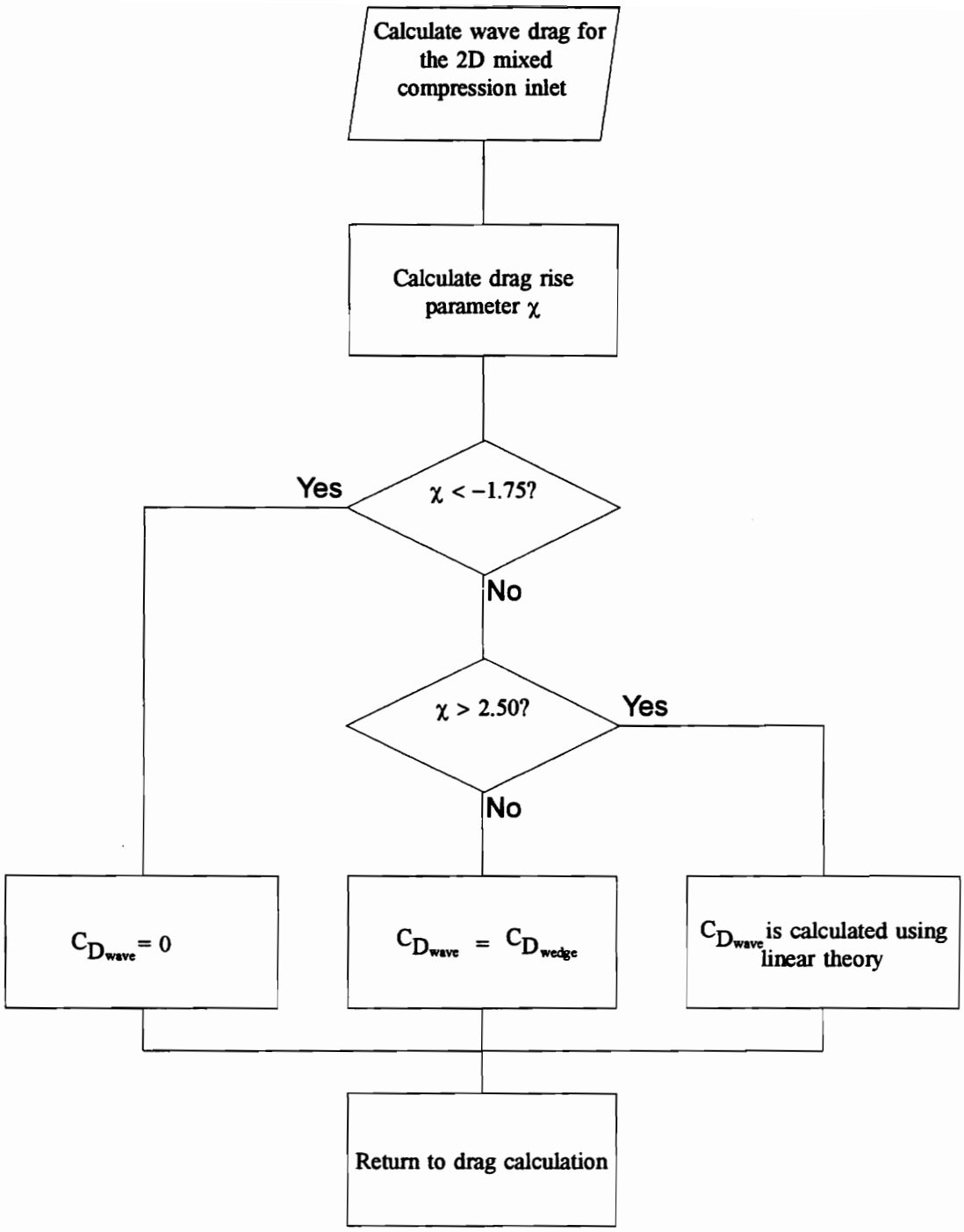

Figure 6 Wave drag prediction for the 2D inlet.

The procedure used to calculate supersonic pressure recovery is identical during each iteration. The pressure loss across each shock is calculated, and the product of these terms is the supersonic pressure recovery. It is important to note that, for unstarted conditions, it is assumed that the air flow passes entirely through the oblique shocks and then through the bow shock. This is not necessarily true; in that case the supersonic total pressure recovery would be reduced slightly. Prediction of this shock interaction phenomena is complex, and the effect is small enough that for the purposes of conceptual design, this is ignored.

Subsonic pressure recovery is calculated from an experimental correlation relating total pressure recovery to the throat Mach number by the empirical method of Ball (1972). This method was used by Malan (1989) and in the original version of ACSYNT. The formula given below is for γ=1.4.

$$PR_{sub} = 1.0 - \varepsilon\left[1 - \frac{1}{\left(1 + .2M_t^2\right)^{3.5}}\right] \qquad [3.3.1]$$

where PR_{sub} is the ratio of the total pressure at the throat (as defined above) to the total pressure at the compressor face. The parameter ε is a function of the throat Mach number, M_t. This parameter, ε, is determined by the subsonic diffuser geometry, and is a measure of losses due to viscous effects and flow separation. Morris et al. (1977) fit the following curve to data presented by Ball:

$$\varepsilon = 0.37148M_t^2 - 0.231428M_t^2 + 0.0 \qquad [3.3.2]$$

From equations 3.3.1 and 3.3.2 it can be seen that the subsonic total pressure recovery is solely a function of the throat Mach number.

3.3.3 Determination of the Throat Mach Number

When the inlet is started, the value of M_t used to determine subsonic recovery is the Mach number directly behind the normal shock. When the inlet is unstarted, the actual throat Mach number is calculated and used to determine the subsonic pressure recovery. The method used to calculate the throat Mach number for the latter case changes after the first iteration, since additional information about the inlet geometry is available at that time.

To provide a first guess for the iterative procedure, the reference mass flow ratio is calculated and from this, the ratio of throat area to upstream flow tube area is calculated using the following equation:

$$\frac{A_t}{A_\infty} = \left(\frac{1}{MFR_{ref}} - \frac{\tan(\theta)}{\tan(\sigma_{des})} \right) \cos(\theta) \qquad [3.3.3]$$

This ratio is calculated for supersonic freestream Mach numbers and is combined with mass continuity to determine the throat Mach number. The shock losses upstream of the throat will have been determined by the supersonic pressure recovery calculation.

For subsonic freestream Mach numbers, the above ratio is assumed to be unity. Because there is no supersonic pressure loss in this case, the throat Mach number will be identically equal to the freestream Mach number.

In the transonic flight regime, A_t/A_∞ is again assumed to be one, but the pressure loss due to the bow shock prevents simply setting the throat Mach number to the freestream Mach number. Mass continuity can then be applied to solve for the Mach number at this point. Unfortunately this solution is completely independent of the actual mass flow. Intuitively, we suspect that this must be ignoring some of the physics of the problem; however, it does produce a good first estimate in most cases.

For the second iteration, the solution is broken up into pieces depending on the number of oblique shocks that precede the normal shock. In all cases, the computed mass flow rate and throat area from the previous iteration is used for the current iteration. With these values known, the area ratio used in the continuity equation is:

$$\frac{A_t}{A_{sub}} = \frac{\dot{m}A_t}{M_{sub}P_{sub}\sqrt{\frac{\rho g_c T_{sub}}{\gamma}}} \qquad [3.3.4]$$

Where M_{sub}, P_{sub} and T_{sub} are the Mach number, pressure and temperature behind the last oblique shock, or are the freestream values if the inlet is operating subsonically.

3.3.4 Additive Drag

Additive drag is calculated by balancing forces and momentum flux using a control volume formulation to solve for the pressure integral along the streamline that intersects the cowl lip. Additive drag prediction requires that both the force on the compression ramp and the pressure at the inlet capture face must be accurately predicted. When the inlet is started, both of those quantities, and thus the additive drag, can be easily determined. When the inlet is not started, predicting the force on the ramp becomes more difficult. The pressure integral to be evaluated is:

$$D_{add} = \int_{\infty}^{c} \left(P - P_{\infty}\right) dA_x$$

$$= F_{ramp} + \left(P - P_{\infty} + \gamma M_c^2 P_c\right) w Y_i \cos^2 2\theta - \gamma M_{\infty}^2 A_{\infty} P_{\infty} \qquad [4.3.5]$$

where the flow enters the inlet at an angle of 2θ, w is the width of the inlet, and F_{ramp} is the force on the ramp. There are five cases that must be separately considered to evaluate

F_{ramp} and P_c: subsonic, three transonic flight cases, and full supersonic, all detailed below. These five cases, plus design conditions, are depicted in Figure 7 on the following page.

For the subsonic case, the air is assumed to be isentropically expanded from $M_\infty, P_\infty, A_\infty$ to M_c, P_c, A_c and the pressure on the ramp is assumed to be the average of P_∞ and P_c. Thus:

$$F_{ramp} = w\left(Y_{ramp1} + Y_{ramp2}\right)\frac{P_c - P_\infty}{2} \qquad [3.3.6]$$

There are three locally transonic cases; the first is a "true" transonic case; $M_\infty \geq 1$, but is too low for the first shock to attach to the ramp. This case is very similar to the subsonic case, except for the bow shock in front of the inlet system. The air isentropically expands from the shock to the capture face. Again, the pressure is constant over the length of the ramp and so:

$$F_{ramp} = w\left(Y_{ramp1} + Y_{ramp2}\right)\left(\frac{P_n + P_c}{2} - P_\infty\right) \qquad [3.3.7]$$

where P_n is the pressure directly behind the bow shock.

The following two cases are locally transonic cases; the inlet is not started, and a bow shock exists somewhere along the forebody ramp.

In the first locally transonic case, one oblique shock exists and the bow shock is located on the first ramp. Between the oblique shock and the normal shock, the pressure is constant; after the bow shock the air expands isentropically to the capture face. The bow shock is assumed to occur at the vertex of the second ramp due to the nature of the experimental correlation used to predict bow shock standoff distance. The force on the ramp is thus:

$$F_{ramp} = w\left(Y_{ramp1}\left(P_1 - P_\infty\right) + Y_{ramp2}\left(\frac{P_n + P_c}{2} - P_\infty\right)\right) \qquad [3.3.8]$$

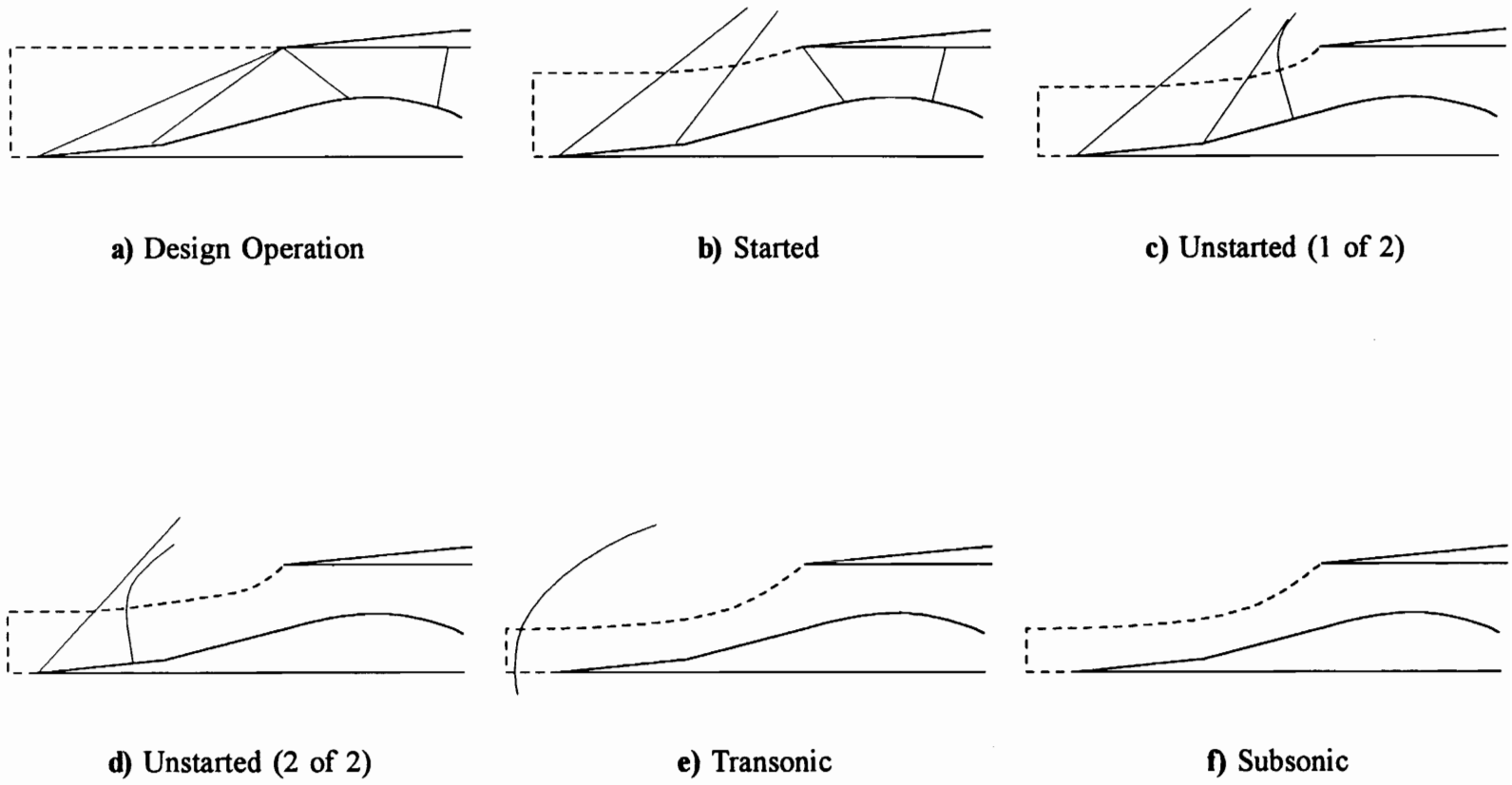

Figure 7 The six idealized operating modes for the 2D inlet.

where P_n is the pressure behind the bow shock, and P_1 is the pressure behind the first oblique shock.

In the second case there are two oblique shocks that can exist. A check must be made to ensure that the location of the normal shock is not upstream of the vertex of the second ramp. If this occurs, this case collapses into the previously described transonic case, and is evaluated according to equation [3.3.8]. If the normal shock is downstream of the second oblique shock, then the pressure on the first ramp is constant, and is constant again on the second ramp until the normal shock, and then expands isentropically to the capture face. The force on the ramp is given by:

$$F_{ramp} = w\left[Y_{ramp1}\left(P_1 - P_\infty\right) + \left(Y_{ramp2} - L\sin 2\theta\right)\left(P_2 - P_\infty\right) + L\sin 2\theta\left(\frac{P_n + P_c}{2} - P_\infty\right) \right]$$

[3.3.9]

where P_n is the pressure behind the normal shock, P_1 is the pressure behind the first oblique shock, and P_2 is the pressure behind the second oblique shock.

If the inlet is started, then all three oblique shocks are present, pressure is constant between the shocks, and the force on the ramp is simply given by:

$$F_{ramp} = w\left[Y_{ramp1}\left(P_1 - P_\infty\right) + Y_{ramp2}\left(P_2 - P_\infty\right) \right] \qquad [3.3.10]$$

where P_1 is the pressure behind the first oblique shock and P_2 is the pressure behind the second oblique shock.

3.3.5 Cowl Drag

Cowl drag is split into wave drag, and profile drag for both the upper and lower cowls. Both cowls are wedge shaped, and so the same procedures are used to determine drag on the upper and lower cowls.

3.3.5.1 Cowl Profile Drag

The method of computing profile drag is a form factor method similar to that used to calculate drag on wings,

$$f_f = 1 + \frac{t}{c} + 100\left(\frac{t}{c}\right)^4 \qquad [3.3.11]$$

where the ratio $\frac{t}{c}$ is the thickness to cord ratio for the cowl. This ratio is defined to be:

$$\frac{t}{c} = \frac{Y_m - Y_c}{L_c} = \tan\eta \qquad [3.3.12]$$

where η is the angle of the cowl (see Figure 4).

The cowl profile drag coefficient is determined using:

$$C_{d_{profile}} = C_f \frac{A_s}{A_c} f_f \qquad [3.3.13]$$

where A_s is the cowl wetted area, given by $A_s = wL_c/\cos\eta$, and C_f is the skin friction coefficient.

3.3.5.2 Cowl Wave Drag

Calculation of wedge wave drag is based on methods of Liepmann and Roshko (1965). Data used in this approach was manually digitized by Malan (1989) to calculated transonic wave drag, and linear theory (Liepmann and Roshko, 1965) is used to extend these results to supersonic solutions.

Cowl wave drag is strongly dependant on the drag-rise Mach number, M_d. Instead of calculating M_d directly, a parameter χ is calculated according to:

$$\chi = \frac{M_\infty^2 - 1}{\left[(\gamma+1)M_\infty^2 \tan\eta\right]^{\frac{2}{3}}} \qquad [3.3.14]$$

where η is the wedge angle. If this value is less than the smallest value in table 1, then $M_\infty < M_d$, and therefore the cowl wave drag is zero. Otherwise the cowl wave drag is computed according to the equation:

$$C_{d_{cowl}} = \bar{C}_d \frac{Y_m - Y_c}{Y_c} \qquad [3.3.15]$$

where, for values of χ included in table 1, $\bar{C}_d$ is defined by:

$$\bar{C}_d = \frac{\tilde{C}_d\left(\tan\eta\right)^{\frac{2}{3}}}{\left[(\gamma+1)M_\infty^2\right]^{\frac{1}{3}}} \qquad [3.3.16]$$

where η is the wedge angle.

If the computed value of χ is greater than the largest tabulated value, then the value of $\bar{C}_d$ is computed according to:

Table 1. Data for wave drag of a wedge in supersonic flow

χ	$\tilde{C}_d$
-1.75	0.00
-1.00	0.17
-0.75	0.37
-0.50	0.78
0.00	1.78
0.25	2.25
0.50	2.73
0.75	3.10
1.00	3.20
1.25	2.56
1.50	2.00
2.00	1.57
2.50	1.27

Digitized by Malan (1989) from Liepmann and Roshko (1963), figure 10.2b

$$\bar{C}_d = \frac{2\tan\eta}{\sqrt{M_\infty^2 - 1}} \qquad [3.3.17]$$

The table shown below is from data manually digitized by Malan (1989) for use in transonic wave drag calculations. These values are valid, using linear theory detailed above, for wedge flows at any Mach number and wedge angle.

3.3.6 Results

The following section details selected results demonstrating the capability of the methods presented above. Included are plots showing total pressure recovery as a function of free-stream Mach number, and additive drag as a function of Mach number. Additive drag is shown since it tends to be the largest drag term. Together, additive drag and total pressure recovery characterize the overall performance of the inlet.

In Figure 8, the calculated total pressure recovery is compared against data from Anderson and Wong (1973). Overall, the trend seems to be overprediction of pressure recovery, possibly due to neglecting the boundary layer and viscous effects in the supersonic portion of the inlet. Pressure recovery has been enforced to agree with experimental results at the design Mach number of 3.0 by adjusting the location at which the normal shock occurs.

Transonic additive drag results are shown in Figure 9. Again, computational results tend to be overpredicted. The trends, however, tend to follow experimental data closely. This is believed to be partially due to ignoring cowl suction. Experimental data is again from Anderson and Wong (1973).

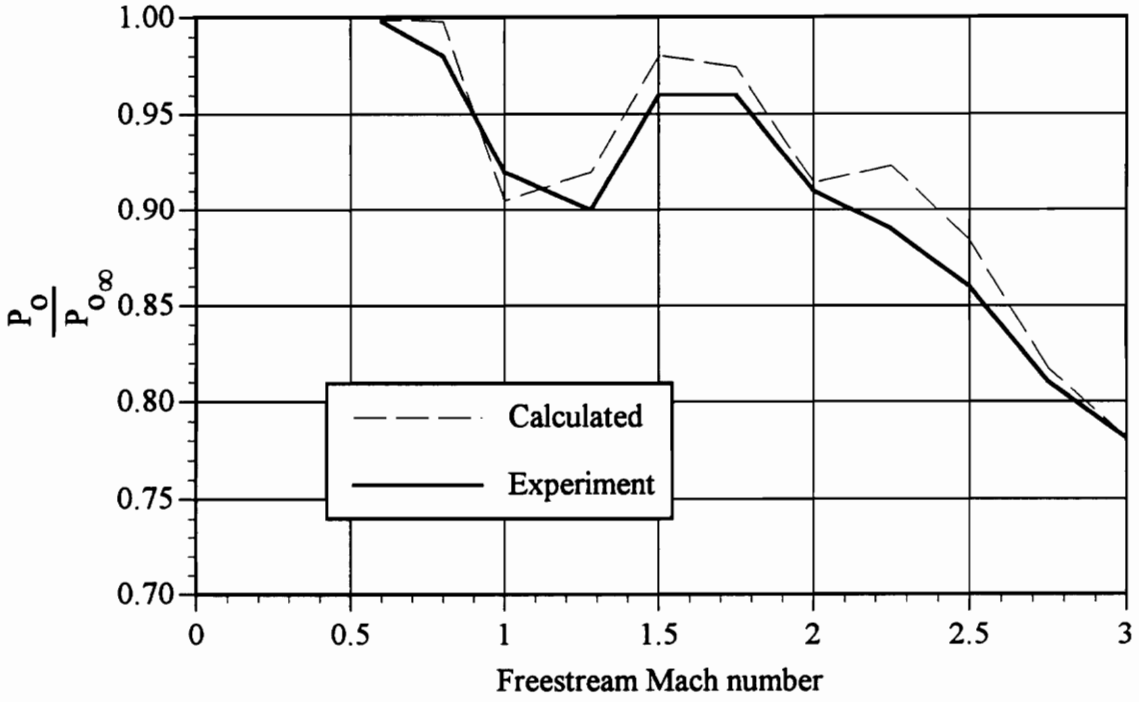

Figure 8 2D Total pressure recovery.

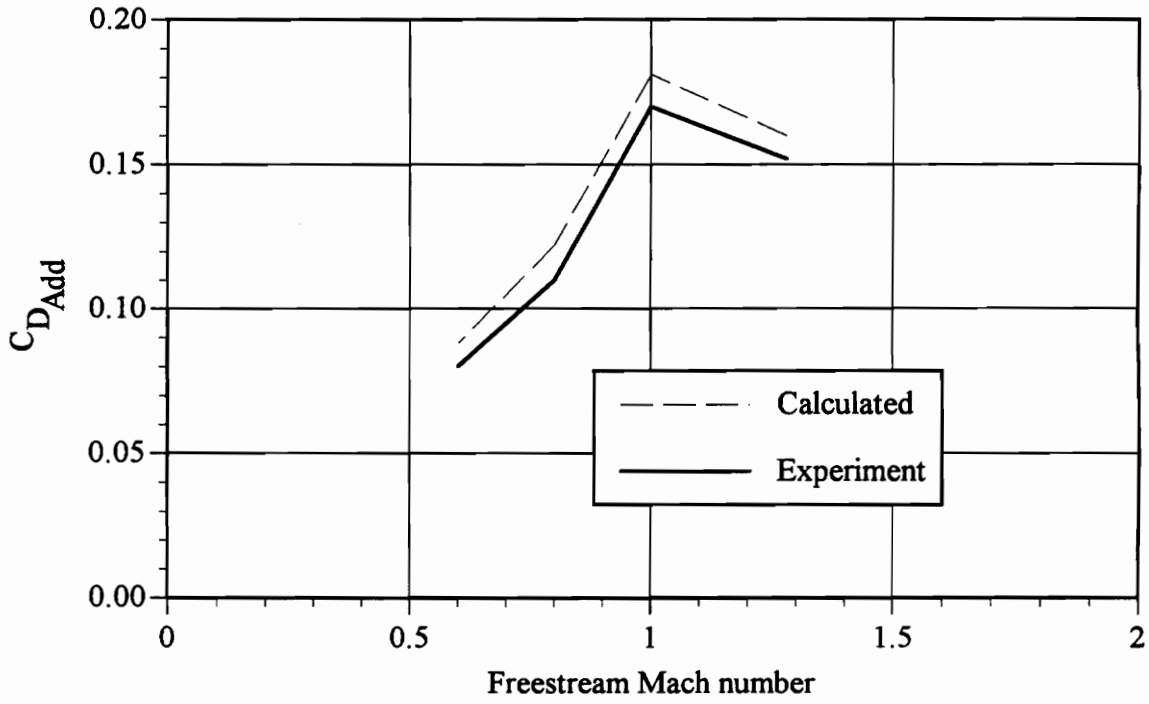

Figure 9 Additive drag prediction for 2D inlet

3.4 Axisymmetric Inlet

3.4.1 Overview

The axisymmetric inlet modelled is a three shock, single compression surface inlet similar to the P-inlet developed by NASA. A sketch of the inlet modelled, along with pertinent dimensions is shown in Figure 10. Again, the cowl profile is linear with a sharp cowl lip, and cowl suction is not computed for this inlet design.

Flow downstream of the conical shock is assumed to be at a constant Mach number equal to the average of the Mach number immediately behind the shock then Mach number on the cone surface. This assumption allows for simple methods to be used downstream of the conical shock, instead of using discretized methods to account for Mach number as a function of the cone radius.

As is the case with the planar inlet, determination of maximum mass flow is critical. In order to keep started flow conditions over as much of the operating range as possible, a translating centerbody is employed. Unlike the external compression inlet with translating centerbody, which used translation to minimize additive drag, the mixed compression inlet uses translation to keep a constant throat Mach number. This, combined with bypass air flow, as determined by the maximum mass flow, helps to ensure started flow conditions over much of the operating range of the inlet.

The flow chart of the solution procedure and the diagram of the inlet on the following pages (figures 11 and 12) provide a summary of the solution methodology. Detailed explanations of each of the flowchart steps will follow in subsequent sections.

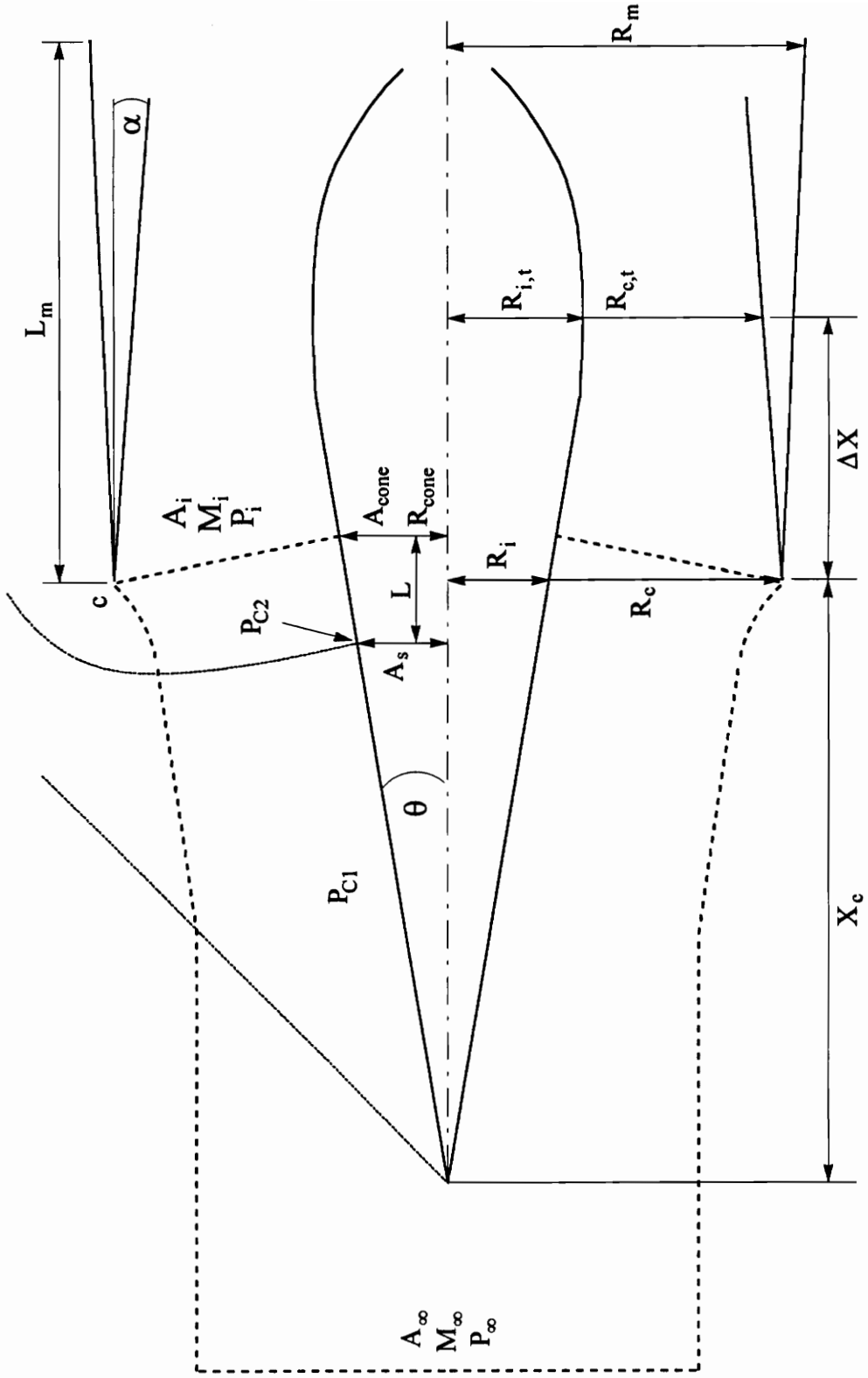

Figure 10 Axisymmetric Mixed Compression Inlet and Control Volume.

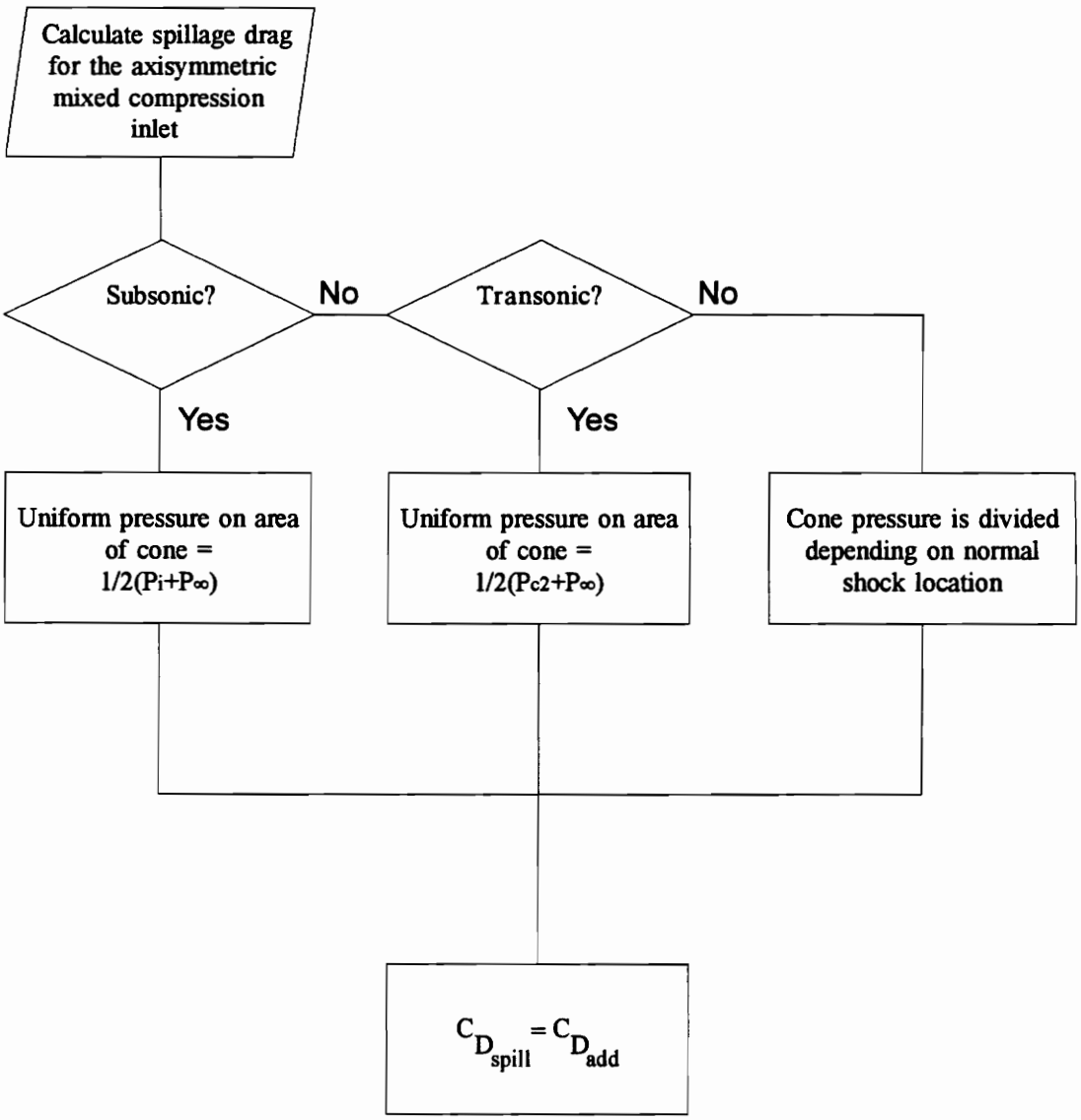

Figure 11 Spillage drag prediction for the axisymmetric inlet.

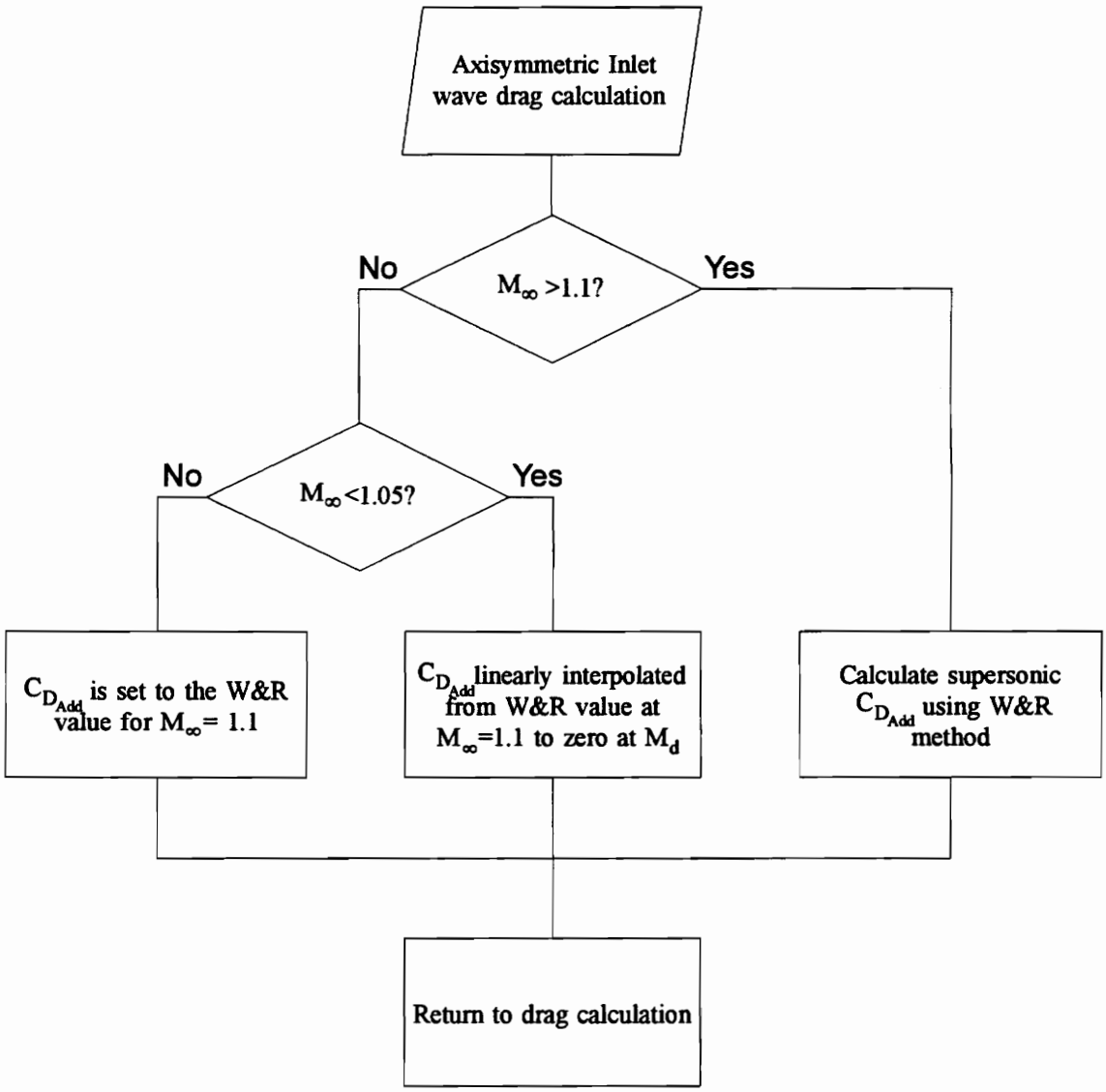

Figure 12 Wave drag prediction for the axisymmetric inlet.

3.4.2 Pressure Recovery

Pressure recovery is calculated using an iterative scheme that involves the maximum mass flow of the inlet, bleed and bypass air flow requirements, and the position of the translating centerbody. The solution for pressure recovery is split into supersonic and subsonic components; the dividing line between these two is dependant upon the start/unstart state.

When the inlet is started, the subsonic pressure recovery calculation begins directly behind the normal shock, which is located downstream of the throat. If the inlet is not started, then the calculation begins at the throat. In both cases, the calculation of subsonic pressure recovery extends to the compressor face, and the extent of the supersonic pressure recovery calculation is from the freestream conditions up to and including the normal shock. The correlation used to determine the subsonic total pressure loss is identical to that used for the planar mixed compression inlet.

Supersonic pressure recovery is calculated directly by computing pressure losses across the shocks. Conical shock relationships are used to determine the pressure loss across the first shock. Losses across the second shock, assumed to be attached to the cowl lip, are computed using oblique shock relationships. The Mach number used for the oblique shock calculation is the average of the cone Mach number and the Mach number immediately downstream of the cone shock. The data required for the conical flow solutions were incorporated into ACSYNT by Malan (1989)

3.4.3 Additive Drag

Additive drag is calculated using a control volume method similar to that used for the planar inlet. One important feature of the axisymmetric inlet is the translating centerbody. Unlike the axisymmetric external compression inlet of Malan, the centerbody does not translate to minimize additive drag. The centerbody instead is positioned to help prevent inlet unstart.

The equation used to compute additive drag is as follows:

$$D_{add} = F_{cone} + \left(P_i - P_\infty + \gamma M_i^2 P_i\right) A_c f - \gamma M_\infty^2 A_\infty P_\infty \qquad [3.4.1]$$

Note the presence of the factor f, introduced by Malan (1989) that is used to ensure that on design additive drag will be zero. Zero additive drag on design is not guaranteed the factor f is simply equal to $\cos\theta$, as it would be from purely geometrical considerations. This is primarily due to the assumptions made for the cone pressure. The calculation to determine this factor is as follows.

Solve for f in equation [3.4.1] by setting D_{add} to zero, and substituting $M_{des} = M_\infty$ and $A_c = A_\infty$ to get:

$$f = \frac{\gamma M_{des}^2 A_c P_\infty - F_{cone_{des}}}{\left(P_{i_{des}} - P_\infty + \gamma M_{i_{des}}^2 P_{i_{des}}\right) A_i} \qquad [3.4.2]$$

Where $F_{cone_{des}}$ is calculated assuming that the inlet is started at design conditions. One simplifying assumption was made; the area A_i is calculated assuming that the flow angle at the inlet capture face is equal to the cone half angle. This was done to prevent an unnecessarily complicated iterative solution.

The resulting expressions for inlet area, and cone projected area are as follows:

$$A_i = \left(A_c - \pi R_i^2\right)\cos\theta \qquad [3.4.3]$$

$$A_{cone_x} = A_c - A_t \cos\theta \qquad [3.4.4]$$

Once again, the difficulty in calculating additive drag is in the calculation for the force on the cone. As with the planar inlet, there are several cases, as determined by the freestream Mach number and starting conditions, that must be individually considered. These are: subsonic, transonic, supersonic unstarted, and supersonic started, and are represented, with the design conditions, in Figure 13.

3.4.3.1 Subsonic Additive Drag

For subsonic freestream conditions, the pressure on the cone is determined by the average of the freestream pressure and the pressure at the inlet capture face. The pressure at the capture face is determined by continuity, assuming zero total pressure losses. Therefore, the force on the cone is expressed as:

$$F_{cone} = \tfrac{1}{2}\left(P_i - P_\infty\right)A_{cone_x} \qquad [3.4.5]$$

3.4.3.2 Transonic Additive Drag

The transonic calculation for additive drag is performed when the freestream Mach number is greater than one, but is insufficient to permit a conical shock to be attached to the centerbody. In this case, the calculation proceeds as though a normal shock exists ahead

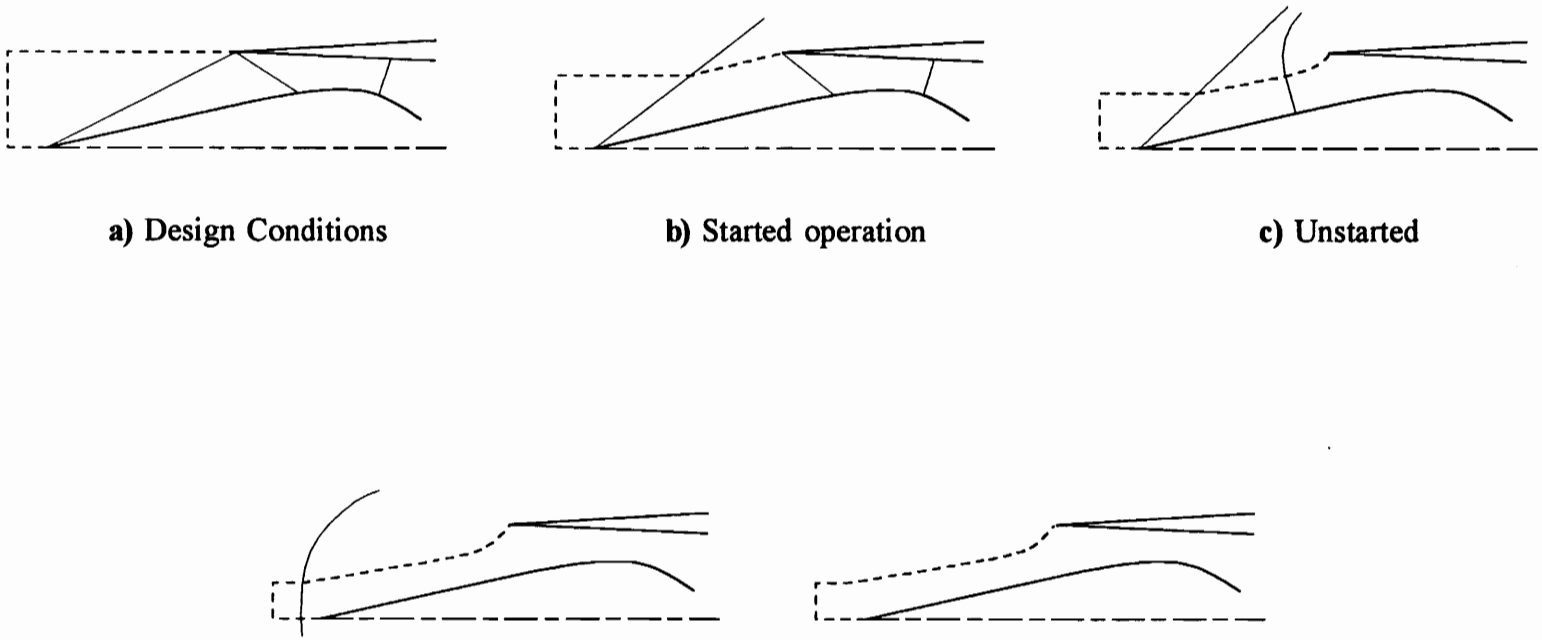

Figure 13 The idealized operating modes for the axisymmetric inlet.

of the inlet. The cone pressure in this case is the average of the pressure behind the normal shock, P_{c_2}, and the pressure at the inlet capture face. Accordingly, the force on the cone is:

$$F_{cone} = \left[\tfrac{1}{2}\left(P_{c_2} + P_i\right) - P_\infty\right] A_{cone_x} \qquad [3.4.6]$$

The expression to determine the minimum Mach number for conical shocks comes from a curve fit by Malan to the data of Sims (1964), and is as follows:

$$M_{\min} = 1.0 + .35955\theta + 1.89161\theta^2 - .24535\theta^3 \qquad [3.4.7]$$

where θ is the cone half angle in radians

3.4.3.3 Unstarted Supersonic Additive Drag

For supersonic unstarted conditions, a conical shock is attached to the centerbody, and a bow shock exists somewhere along the centerbody. The pressure along the cone from the vertex to the bow shock is constant. The pressure on the cone from the bow shock to the capture face is assumed constant as the average of the pressure behind the shock and the pressure at the capture face. The force on the cone is thus:

$$F_{cone} = \tfrac{1}{2}\left[\left(P_{c_2} + P_i\right) - P_\infty\right]\left(A_{cone_x} - A_s\right) + \left(P_{c_1} - P_\infty\right)A_s \qquad [3.4.8]$$

where A_s is the projected area of the cone ahead of the bow shock:

$$A_s = \pi\left(R_{cone} - L\tan\theta\right)^2 \qquad [3.4.9]$$

where R_{cone} is the cone radius at the capture face, and L is the bow shock position.

The method used to calculated bow shock position is identical to that used for the external compression inlets of Malan (1989). It is important to note here that an assumption is made that **all** the mass flow passes through both the conical shock and bow shock.

3.4.3.4 Started Supersonic Additive Drag

The supersonic started inlet has only the attached conical shock to influence additive drag. The pressure on the cone is constant, and thus the force on the cone is given by:

$$F_{cone} = \left(P_{c_1} - P_\infty\right) A_{cone_x} \qquad [3.4.10]$$

3.4.3.5 Determination of Centerbody Location

The centerbody is positioned to maintain a throat Mach number that is slightly supersonic, typically between 1.2 and 1.4. This will tend to minimize the amount of bypass air required to maintain started conditions. When the freestream Mach number is too low for the inlet to be started, it is assumed that the centerbody remains fixed in the design position.

The dimension $X_{\max}$ is used as a reference dimension and an explicit expression can be written for it that depends only on values determined from design conditions.

$$X_{\max} = X_{cone_{des}} + \Delta X_{des} \qquad [3.4.11]$$

where ΔX_{des} is determined from the following equations:

$$R_{ct} = R_c - \Delta X_{des} \tan\alpha \qquad [3.4.12]$$

$$R_{it_{des}} = R_{i_{des}} + \Delta X_{des} \tan\theta \qquad [3.4.13]$$

$$A_{t_{des}} = \pi\left(R_{ct}^2 - R_{it_{des}}^2\right) \qquad [3.4.14]$$

where $A_{t_{des}}$ is the design throat area and $R_{i_{des}}$ is given by:

$$R_{i_{des}} = X_{cone_{des}} \tan\theta \qquad [3.4.15]$$

To determine the centerbody location for a given operating condition, the following expression is employed:

$$X_{cone} = X_{cone_{des}} - \Delta X \qquad [3.4.16]$$

In this case, the term ΔX is a function of X_{cone}, and so equation [3.4.15] must be solved iteratively.

3.4.4 Cowl drag

Cowl profile drag is calculated using a form factor approach similar to that used for the planar mixed compression inlet. The computation of the form factor is the same as for the axisymmetric external compression inlet:

fineness ratio: $f_r = \frac{5}{3}\frac{L}{D_m} + 1$

form factor: $f_f = 1 + 3f_r^{-\frac{3}{2}} + 7f_r^{-3}$

As noted by Malan (1989) this form factor comes from the original version of ACSYNT, and is for a podded nacelle. The source of the expression is unknown.

The profile drag is thus:

$$C_{d_{prof}} = C_f \frac{A_s}{A_c} f_f \qquad [3.4.17]$$

where A_s is the cowl wetted area, and C_f is the skin friction coefficient. The skin friction coefficient calculation is identical to that used for the external compression inlet.

Wave drag is also computed in a manner similar to the axisymmetric external compression inlets, with the exception that the cowl profile is assumed to be linear. Transonic wave drag is calculated assuming a drag rise Mach number of about 0.9, where the wave drag is zero, and peaks at Mach 1.05, and is given by the expression:

$$C_{d_{wave}} = \left[\frac{M_\infty - M_d}{1.05 - M_d}\right]^{\frac{5}{3}} C_{d_{WR}} \qquad [3.4.18]$$

where $C_{d_{WR}}$ is the wave drag given by the Willis and Randall method for $M_\infty = 1.1$.

Wave drag calculated using the Willis and Randall method is (Seddon and Goldsmith, 1985):

$$C_{D_{wave}} = \frac{1}{2}\left(\frac{d_m}{L}\right)^2 \left(1 - \frac{d_c}{d_m}\right)^2 \frac{A_m}{A_c}$$

$$\times \left\{\frac{d_c}{d_m} - \left(1 + \frac{A_c}{A_m}\right)\left[\frac{1}{2} - \log\left(\frac{4L}{\beta d_m}\right)\right] - \frac{A_c}{A_m}\log\left(\frac{d_c}{d_m}\right)\right\}\frac{A_m}{A_c} \qquad [3.4.19]$$

where $\beta = \sqrt{M_\infty^2 - 1}$.

3.4.5 Results

Figure 14 shows a comparison of computed total pressure recovery to experimental results from Smeltzer and Sorensen (1973). The trends exhibited are arguably better than that seen for the 2D inlet, although these results also tend to overpredict the pressure recovery. The starting Mach number (characterized by the increase in pressure recovery) is well predicted; design total pressure recovery is forced to agree with experimental results by proper positioning of the normal shock downstream of the throat.

Additive drag predictions also follow the trends shown by experiment, as seen in Figure 15, but tends to overpredict the amount of additive drag. This overprediction is possibly due to the method of determining the Mach number downstream of the conical shock, and can be also seen in the results of Malan (1989). Data is again from Smeltzer and Sorensen (1973).

3.5 Summary

Methods for computing internal performance and drag of mixed compression inlets have been presented and documented to be sufficiently accurate for use in preliminary design work. The 2D inlet modelled is a four-shock, two-ramp inlet. Both ramps turn the flow through the same angle. The axisymmetric inlet modelled is a three-shock single-cone design, similar to the NASA P-Inlet. In both cases the cowl lips are assumed to be sharp, and the cowl profiles are linear. Cowl suction is not computed for either of the inlet types. Results for both types of inlets follow the trends of the comparison data well, tending towards overprediction of both drag and total pressure recovery.

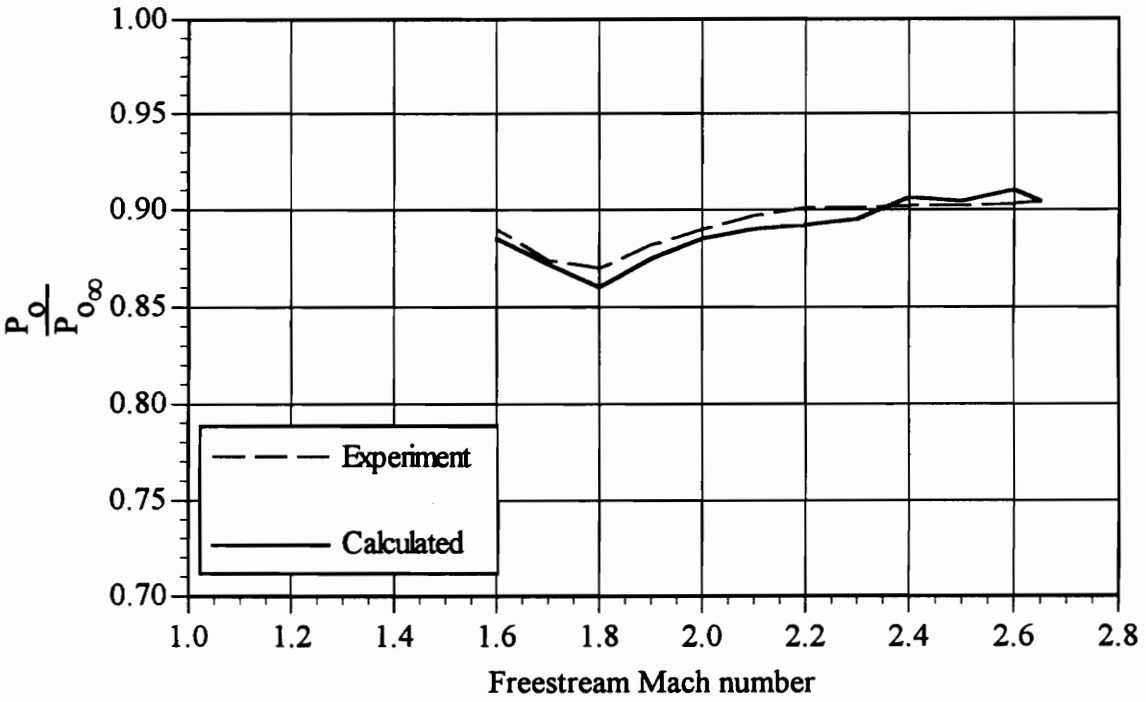

Figure 14. Axisymmetric inlet total pressure recovery.

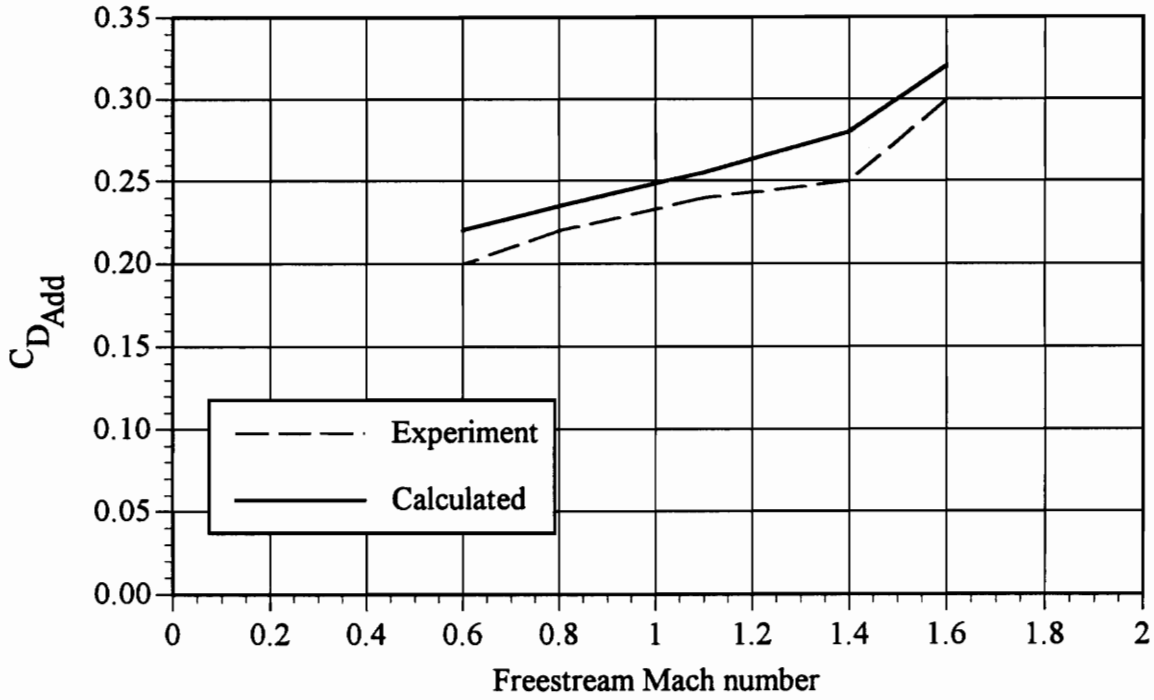

Figure 15. Axisymmetric inlet additive drag.

4.0 Nozzles

4.1 Literature Survey

The focal point of this chapter is advanced nozzle technology. Advanced nozzles are characterized as having any or all of the following: non-axisymmetric geometry, thrust vectoring capability, and variable ratio convergent-divergent design. As will be graphically shown, thrust vectoring can be performed with only small reductions in resultant thrust if the flow is turned subsonically. These nozzles are typically intended for military use where nozzle/airframe integration, ability to use short airfields, or a high degree of maneuverability is important.

There are several ways to conceptualize "short" (typically considered to be under 1000 feet in length) airfield capabilities: Short Take-Off and Landing (STOL), Short Take-Off and Vertical Landing (STOVL), and Vertical Take-Off and Landing (VTOL). Both STOVL and VTOL designs require special controls systems for low speed flight that add to aircraft complexity and required maintenance, and may reduce payload and range. STOL aircraft designs are typically less complex and thus less expensive (Curry, et al, 1983).

Thrust vectoring, critical to STOL designs, can be produced using several methods, using both axisymmetric and 2-Dimensional (2-D) nozzle configurations. Research has been focused on 2-D designs as they are mechanically simpler. Unfortunately, nonaxisymmetric nozzles tend to suffer from poorer internal performance than their axisymmetric counter-

parts. Much of the research conducted thus far has concentrated on decreasing weight, reducing the internal losses, and increasing nozzle cooling.

Wolfe and Fanning (1977) discuss the benefits of three different nonaxisymmetric nozzles, considering internal performance, cooling effectiveness, and structural integrity at minimum weight. All of these nozzles have transition ducting upstream and a rectangular cross section throat, although these conditions are not required for nonaxisymmetric nozzles.

The first is a simple 2-D Convergent-Divergent (C-D) nozzle with thrust vectoring and reversing capabilities. This nozzle has two planar internal and external flaps to control the exhaust flow. The internal flaps control the throat area, and the external flaps provide the thrust vectoring (pitch only) and reversing capabilities. Also considered is a Single Exhaust Ramp Nozzle (SERN), and a 2-D plug nozzle. The main advantage of the plug nozzle for thrust vectoring is that it turns the flow subsonically, reducing the losses due to vectoring. The simple nozzle turns the flow supersonically, using shocks, and is accordingly penalized.

4.2 Motivation for work

There were three reasons for enhancing the thrust prediction coding within ACSYNT: coordination with improved afterbody drag calculations; updating the nozzle database and developing a library of nozzle types, similar in scope to the inlet library; ensuring self-consistency and state of the art methodology is used.

Recently, Squire (1992) has developed an improved afterbody drag prediction scheme, allowing drag prediction over a variety of afterbody geometries. It was desired that the cal-

culation of geometry used to calculate thrust be consistent with this new method. The nozzle library has therefore been expanded to include a variety of nonaxisymmetric nozzles. In addition to 2-D nozzle performance data, other nozzle types have been incorporated, and will be explained in detail later. Overall, the size of the nozzle library has been expanded by a factor of 14. This allows the user additional flexibility in the specification of the propulsion system. The thrust routine has been written such that new nozzle types can easily be added as new nozzle information becomes available.

The thrust calculation has been made more self-consistent. The original routine calculated thrust as though all nozzles, convergent and convergent-divergent were perfectly expanded, then applied a nozzle dependent gross thrust coefficient to determine actual thrust. While this thrust calculation procedure is consistent with industry standard, and has been retained, the routine then returned values for nozzle exit conditions that were not consistent with the actual nozzle geometry. These inconsistent values were then used in other routines, such as afterbody drag prediction. The new routine assumes choked flow at the throat for C-D nozzles, and returns the exit area as determined by A_e/A_t for that nozzle type. Given this exit area, the proper values of pressure, temperature, and Mach number at the exit plane can be determined.

4.3 Enhanced Nozzle Library

A total of six new axisymmetric convergent-divergent nozzles and eleven 2D nozzles have been added to the nozzle library. Refer to Tables 2 and 3 for a summary of the nozzles added. The following section contains a geometrical description of each nozzle type and graph of the gross thrust coefficient. All of the nozzle graphs are accompanied by the equation that was fit to the data using a least squares method, and the data is from static testing. While the thrust coefficient will be different at various freestream Mach numbers

Table 2. Summary of new axisymmetric nozzle types

Figure	A_e/A_t	Dry	Afterburning	$\delta_{v,p}$
16a	1.35	•		0
16b	1.35		•	0
17a	1.35	•		20
17b	1.35		•	20
18a	1.10	•		0
18b	1.34		•	0
19a	1.10	•		0
19b	1.34		•	0
20a	1.10	•		35
20b	1.10	•		70

Table 3. Summary of new nonaxisymmetric nozzle types

Figure	A_e/A_t	AR	Dry	Afterburning	$\delta_{v,p}$	$\delta_{v,y}$
21a	1.35	2.33	•		0	0
21b	2.20	2.33	•		0	0
21c	1.20	1.33		•	0	0
22a	1.35	2.12	•		0	0
22b	1.10	2.59	•		0	0
23a	1.80	1.14		•	0	0
23b	1.35	1.18		•	0	0
24a	N/A	N/A	•		60	0
24b	N/A	N/A	•		70	0
25a	1.00	1.50	•		0	0
25b	1.00	1.50	•		0	20
26a	1.00	4.00	•		0	0
26b	1.00	4.00	•		0	20
27a	1.09	1.50	•		0	0
27b	1.09	1.50	•		0	20
28a	1.08	4.00	•		0	0
28b	1.08	4.00	•		0	20

N/A -- Not available; authors were unable to accurately determine exit area

due to afterbody interference, it is believed that the correlations presented herein are suitably accurate for conceptual design.

4.3.1 Axisymmetric Nozzles

All of the axisymmetric nozzles presented here use a convergent-divergent geometry, and most are suitable for thrust vectoring applications. These nozzles were chosen to represent advanced nozzle technology suitable for next generation military aircraft.

The first series of graphs come from Carson and Capone (1991), and show the thrust coefficient for multiaxis thrust vectoring nozzles. Thrust vectoring has been achieved by deflection of the divergent portion of the nozzle only. The first graph, Figure 16, shows results for the case of pure axial thrust for both dry and afterburning conditions. It is interesting to compare these to the results for the same nozzles at $\delta_{v,p}$=20°, as seen in Figure 17. The peaks on both graphs, particularly for the dry configurations, indicate that the losses due to turning the flow are very small. This result is due to the position of the actual throat, which has moved downstream from the geometric throat; thus most of the turning of the flow occurs subsonically. Similar results occur for yaw vectoring (not shown).

The next three figures come from the data of Mason and Burley (1986). Figure 18 shows thrust coefficient results for a conventional axisymmetric C-D nozzle in both dry and afterburning states. These results were included for comparison to the next two figures; Figure 19 shows the results of unvectored thrust and Figure 20 shows results for thrust vectoring nozzles at $\delta_{v,p}$=35° and 70°. These vectoring nozzles have special counter rotating ducting that allow the flow to be turned at nearly any angle. This, like the nozzles of Carson and Capone, allow the flow to be turned subsonically, minimizing the losses due to turn-

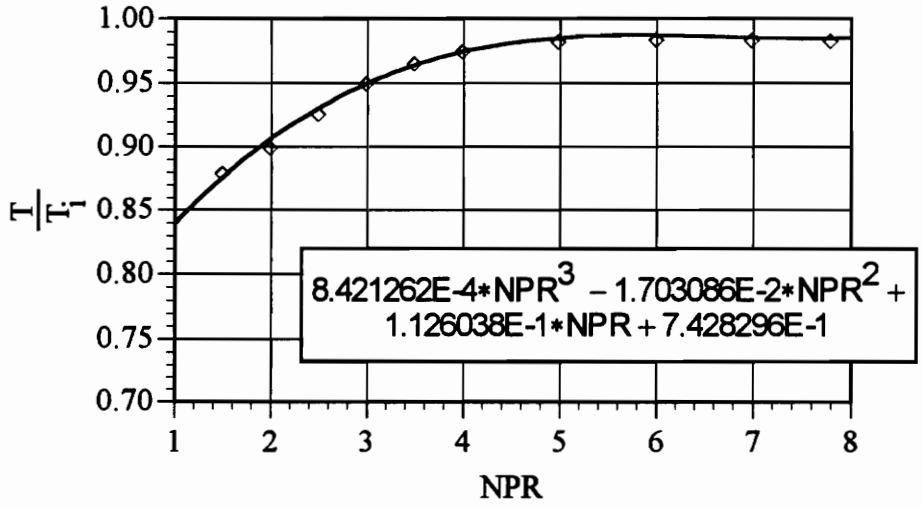

a) Dry configuration

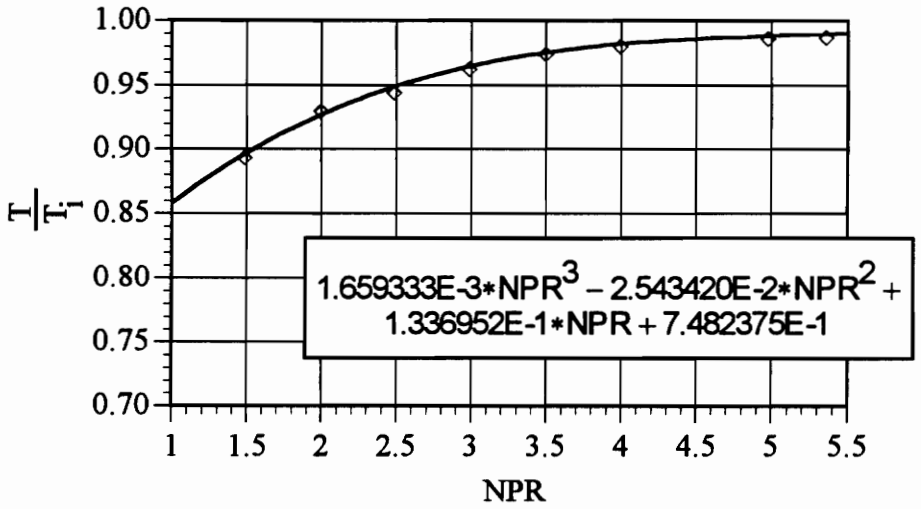

b) Afterburning configuration

Figure 16 Thrust Coefficient for axisymmetric nozzles with multiaxis thrust vectoring capacity.

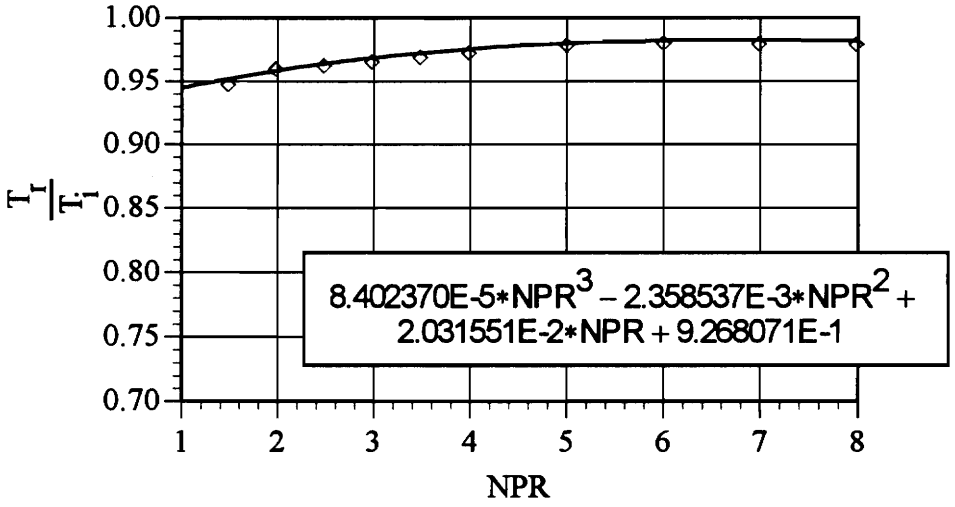

a) Dry Configuration

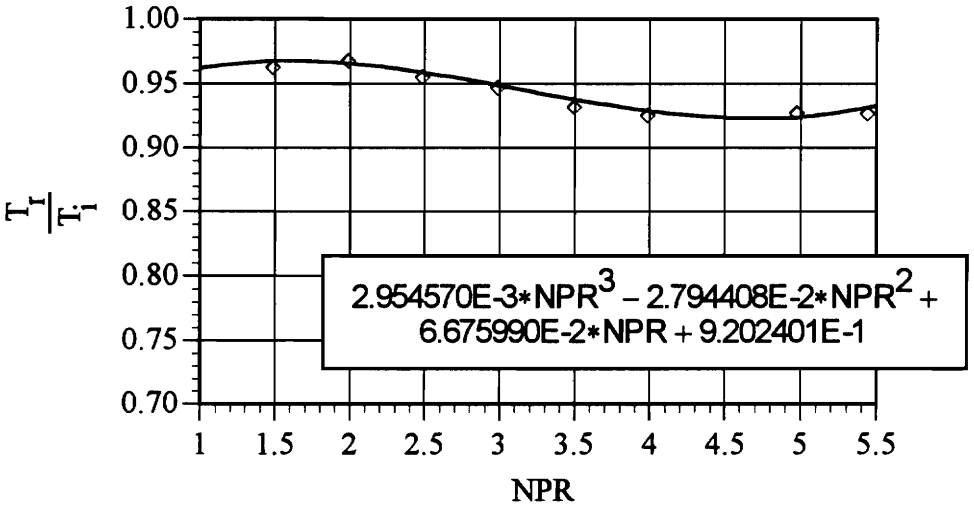

b) Afterburning Configuration

Figure 17. Thrust coefficient for axisymmetric thrust vectoring nozzles at 20° pitch.

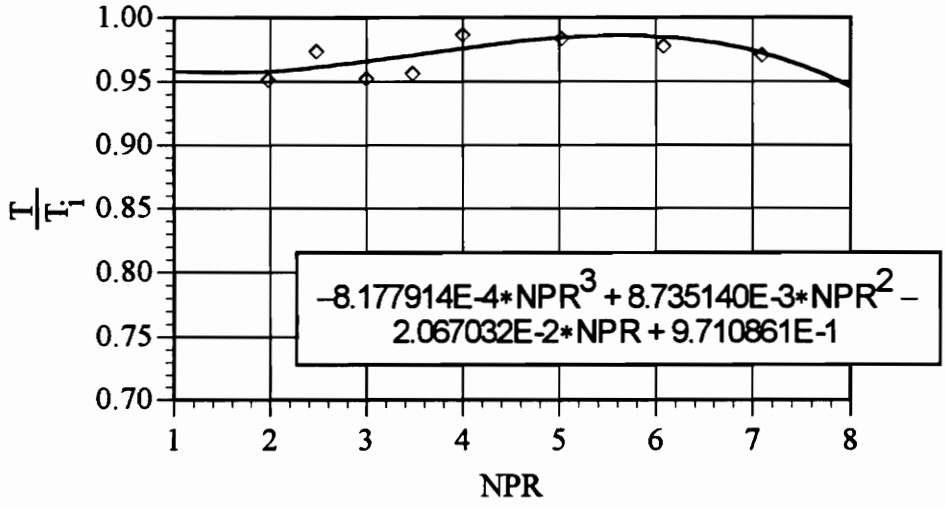

a) Dry

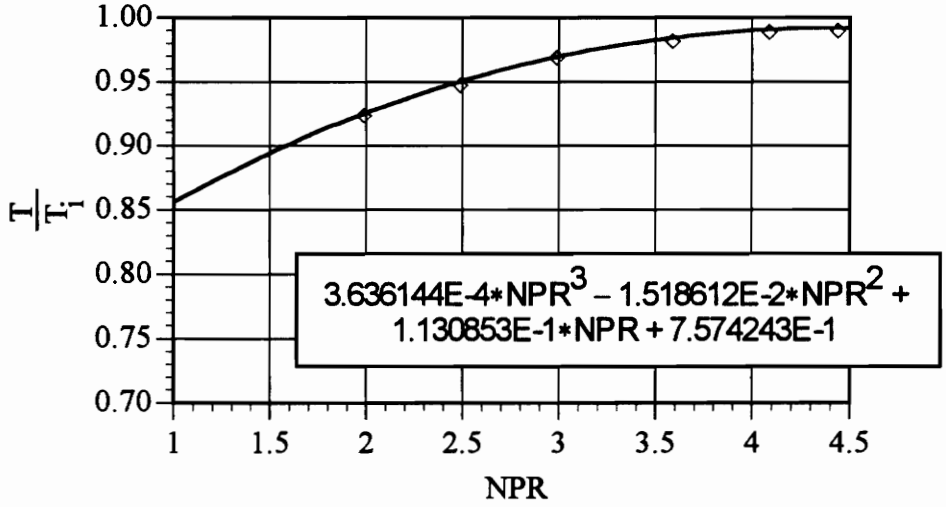

b) Afterburning

Figure 18 Thrust coefficient for axisymmetric C-D nozzles.

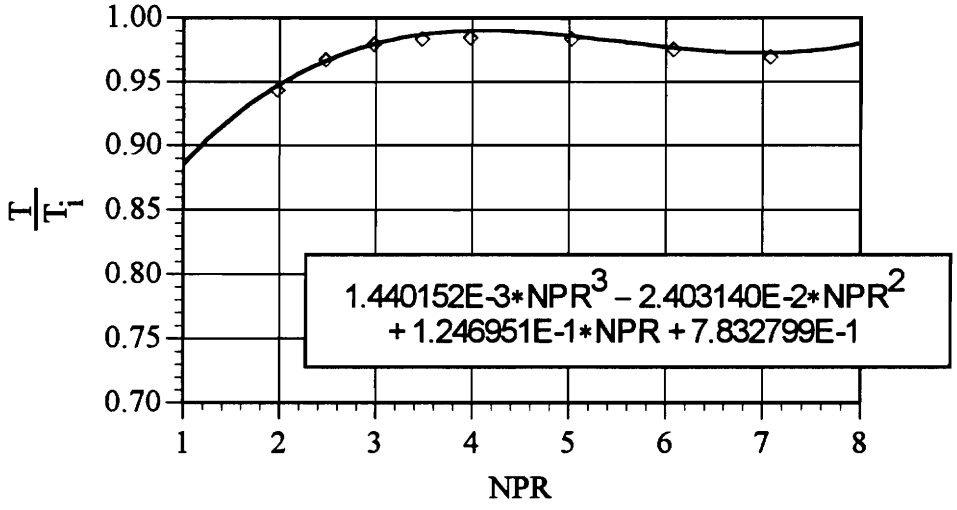

a) Dry

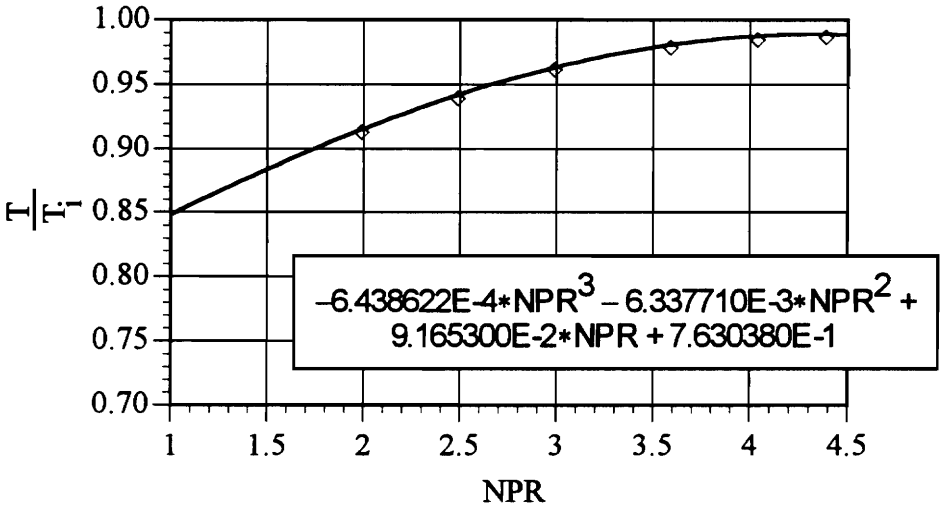

b) Afterburning

Figure 19 Thrust Coefficients for axisymmetric CD thrust vectoring nozzles; $\delta_{v,p} = 0$.

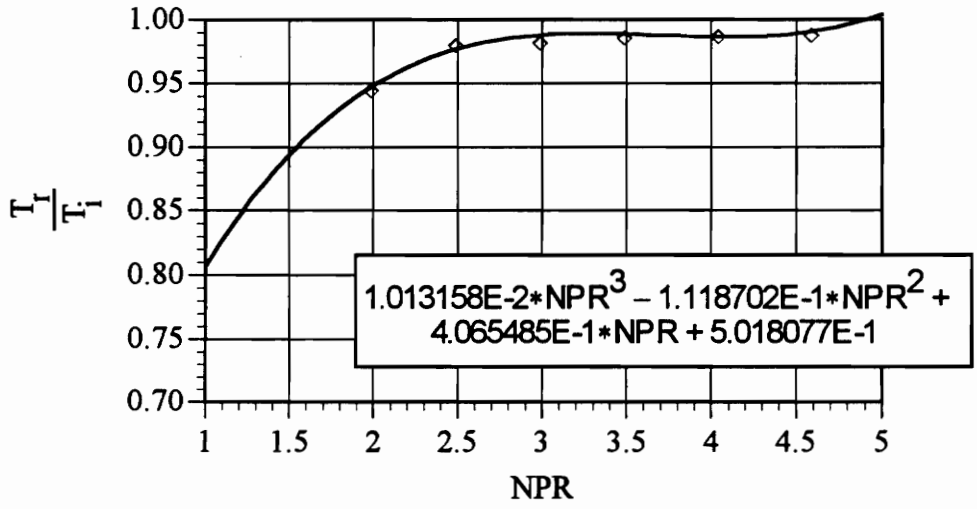

a) $\delta_{v,p} = 35°$

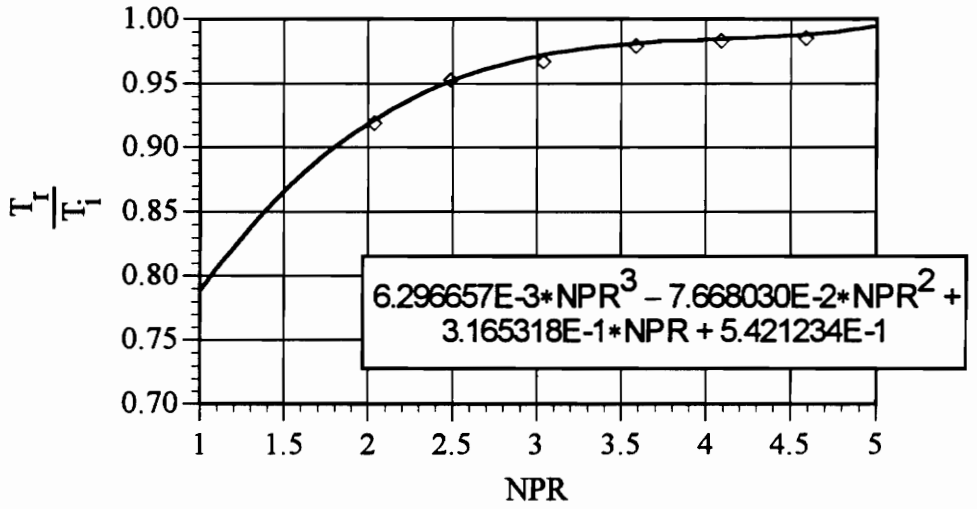

b) $\delta_{v,p} = 70°$

Figure 20 Thrust Coefficients for axisymmetric CD thrust vectoring nozzles.

ing. Some of the reduction in performance can be attributed to the additional complexity of the counter rotating duct, but losses for 70° vectoring are substantial. Even so, the overall performance of these vectoring nozzles remains good, particularly at and above nozzle pressure ratios above 2.5, where the thrust coefficient never falls below 0.94.

4.3.2 Nonaxisymmetric Nozzles

The first nonaxisymmetric nozzle results, shown in Figure 21, are for a hybrid nozzle. This nozzle has an axisymmetric geometry in the convergent segment, and nonaxisymmetric through the divergent section. This nozzle geometry was developed by Taylor (1991) and is designed to gain the advantages of the nonaxisymmetric nozzle without the necessary transition ducting. The results shown are for three power level settings, subsonic cruise, supersonic cruise, and full afterburner. All of the nozzles suffer from poor performance until the nozzle pressure ratio nears the design point.

Nonaxisymmetric convergent-divergent pitch vectoring nozzle results from Mason and Burley (1986) are shown in figures 22 through 24. Figure 22 shows the thrust coefficients for two thrust vectoring nozzles with different design nozzle pressure ratios, and Figure 23 shows the results for similar nozzles configured for afterburning. Figure 24 demonstrates the one possible result of pitch vectoring. In this case, vectoring was achieved by blocking the nozzle exit and opening a passage in the lower flap. Mason and Burley acknowledge that this is an inefficient method of turning the flow. An alternative is to use the flaps to turn the flow in the divergent section, but this will incur shock losses, as the flow will be supersonic in this region.

The final set of nozzles come from a report by Mason and Berrier (1988). These are yaw vectoring nozzles, both convergent, and convergent-divergent. Results are shown for

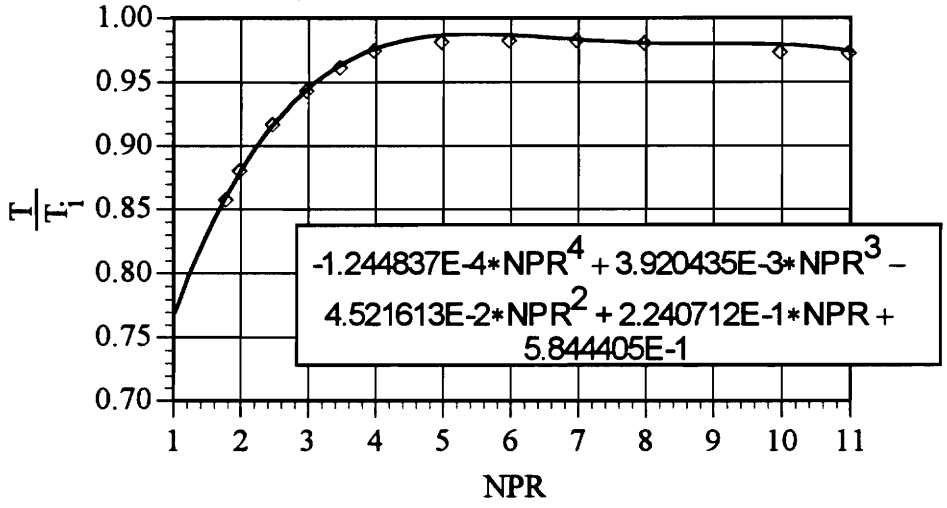

a) Subsonic cruise

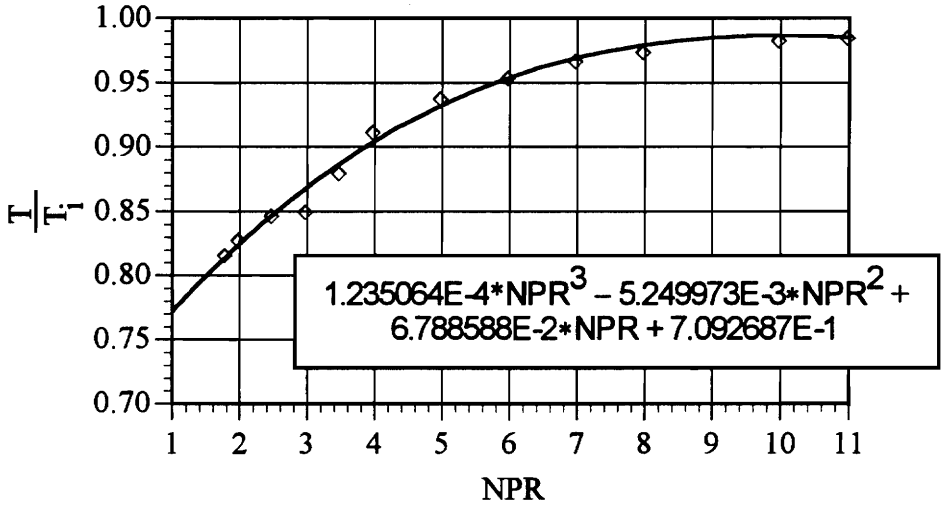

b) Supersonic Cruise

Figure 21 Thrust coefficients of hybrid Convergent-Divergent nozzles.

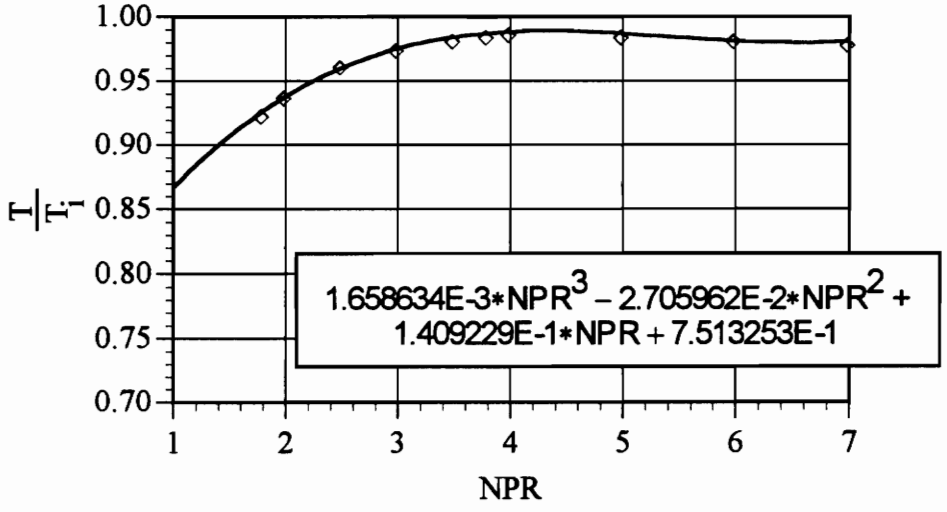

c) Maximum thrust -- Full Afterburners

Figure 21 concluded

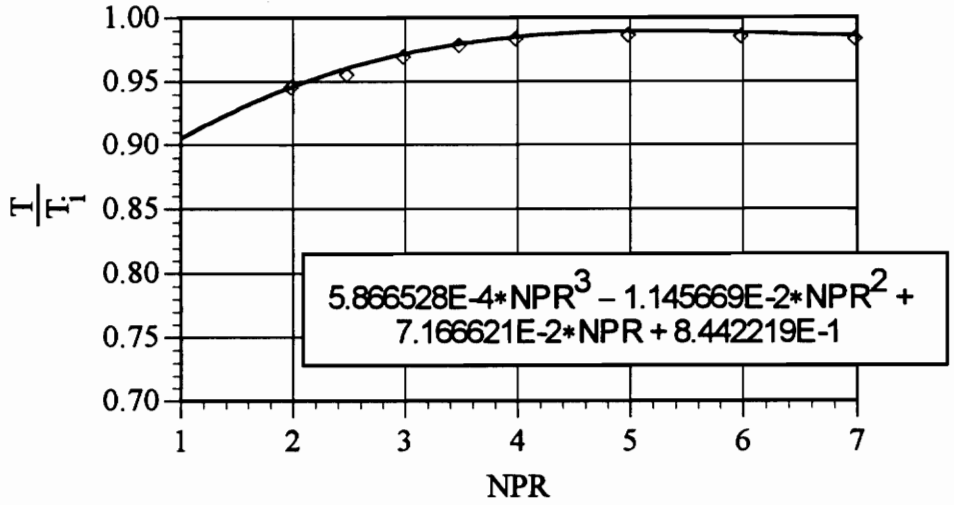

a) $\frac{A_e}{A_t} = 1.35$

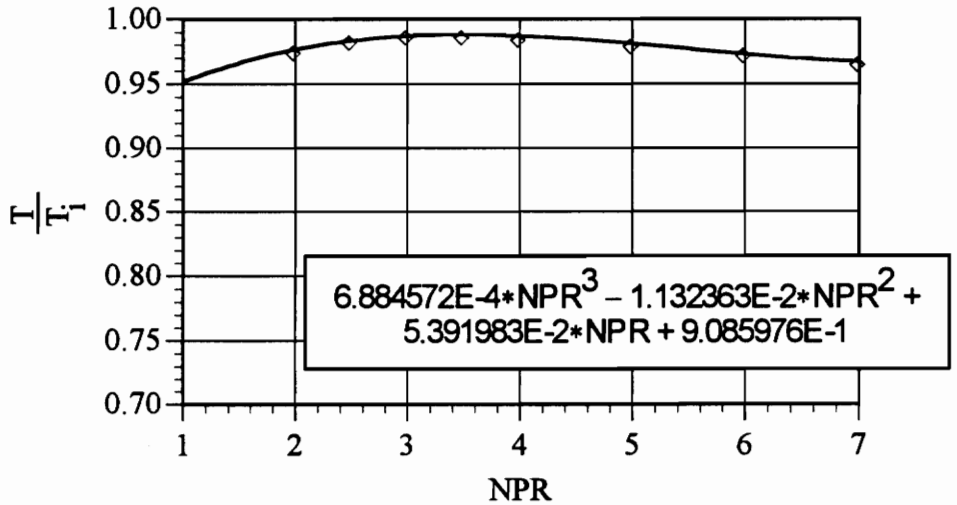

b) $\frac{A_e}{A_t} = 1.1$

Figure 22 Thrust coefficients for 2D, C-D thrust vectoring nozzles.

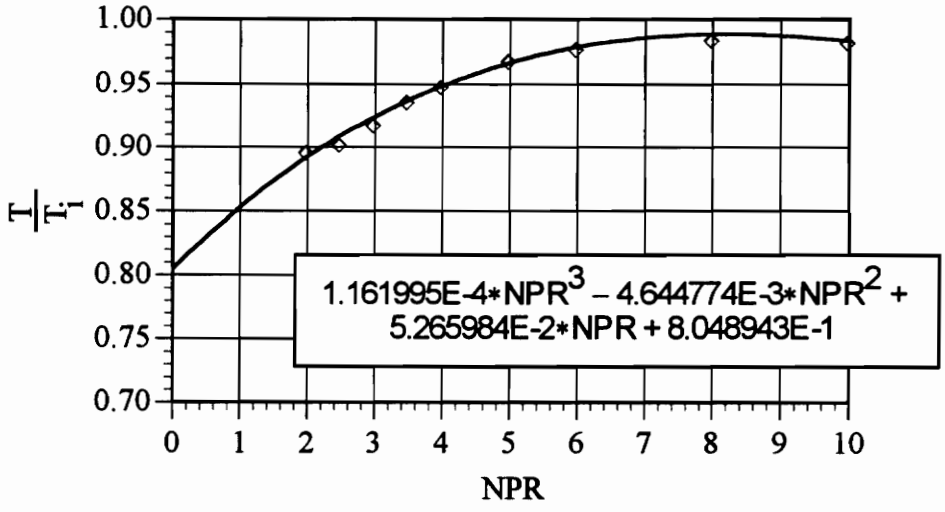

a) $\frac{A_e}{A_t} = 1.8$

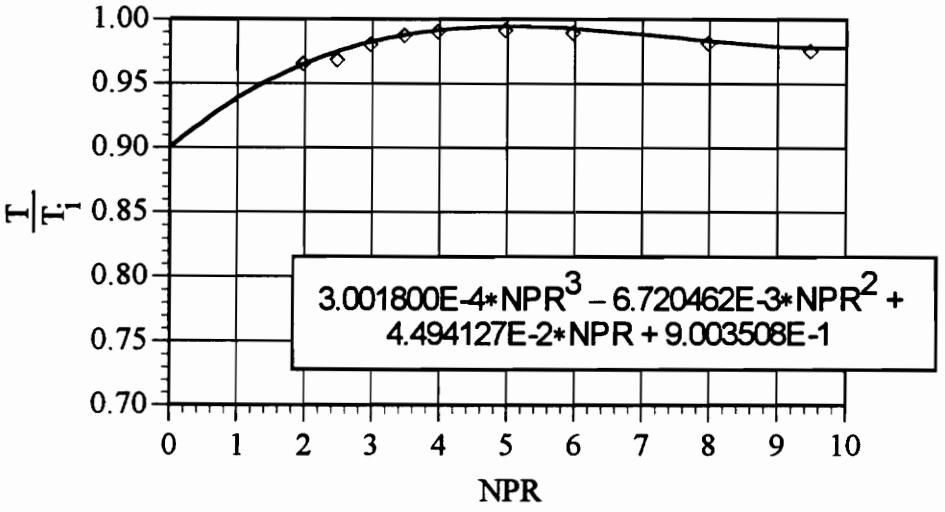

b) $\frac{A_e}{A_t} = 1.35$

Figure 23. Thrust coefficient for 2D, C-D thrust vectoring nozzles, afterburning configuration, $\delta_{v,p}$=0.

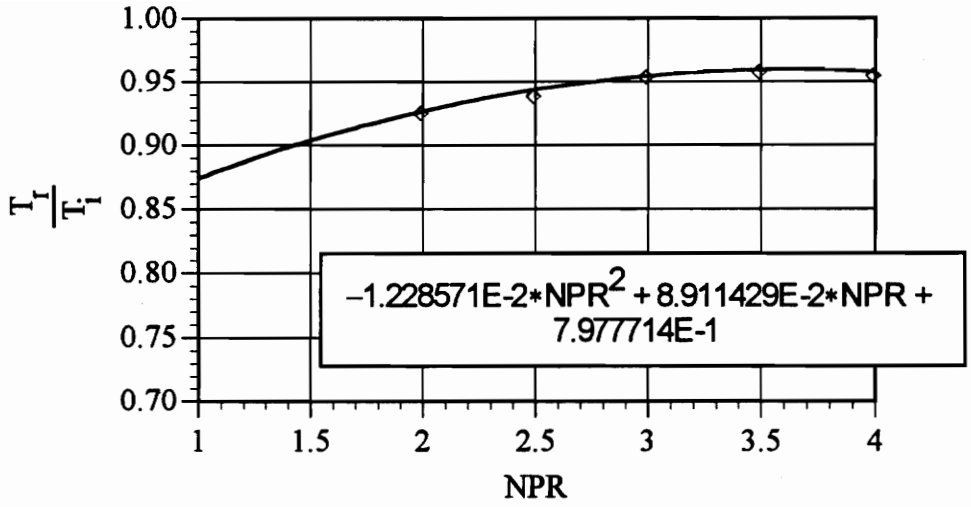

a) $\delta_{v,p}=60°$

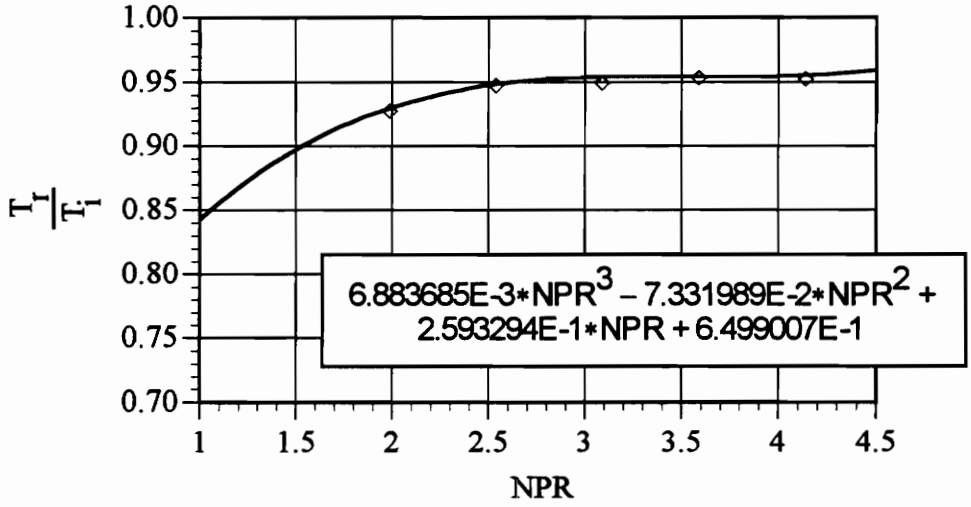

b) $\delta_{v,p}=70°$

Figure 24. Thrust coefficient for 2D, C-D thrust vectoring nozzles

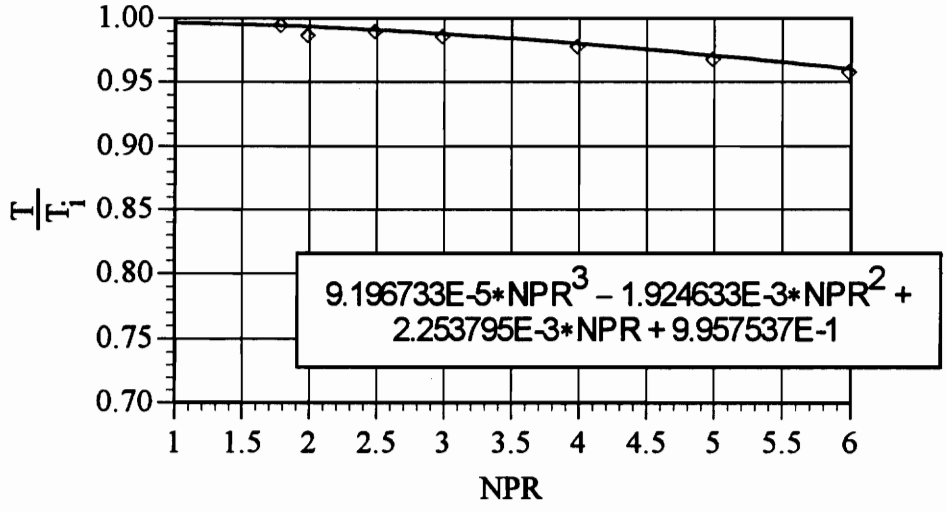

a) $\delta_{v,y}=0°$

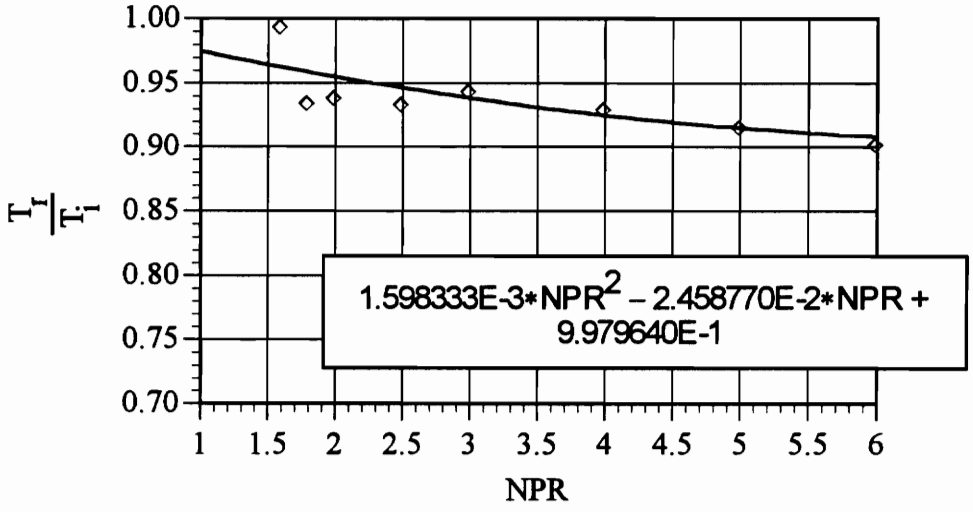

b) $\delta_{v,y}=20°$

Figure 25. Thrust coefficient for 2D, convergent thrust vectoring nozzles, AR=1.5.

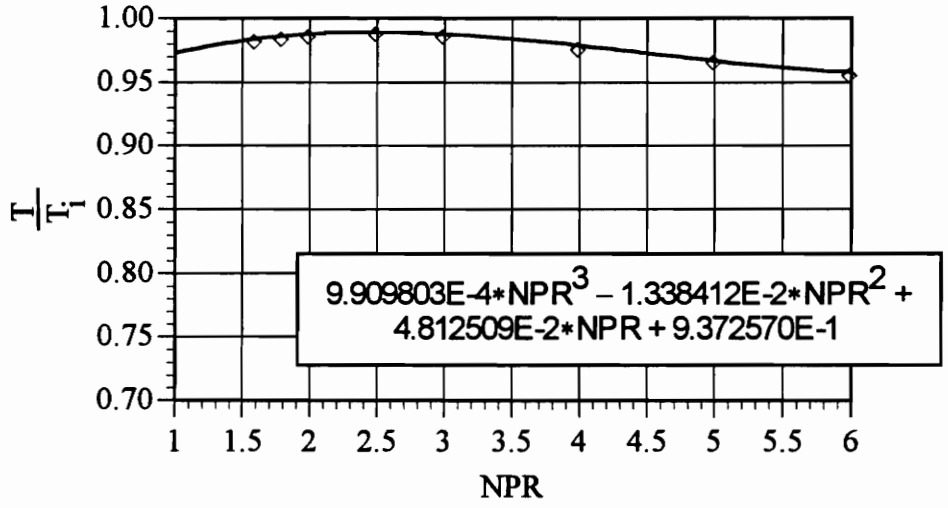

a) $\delta_{v,y}=0°$

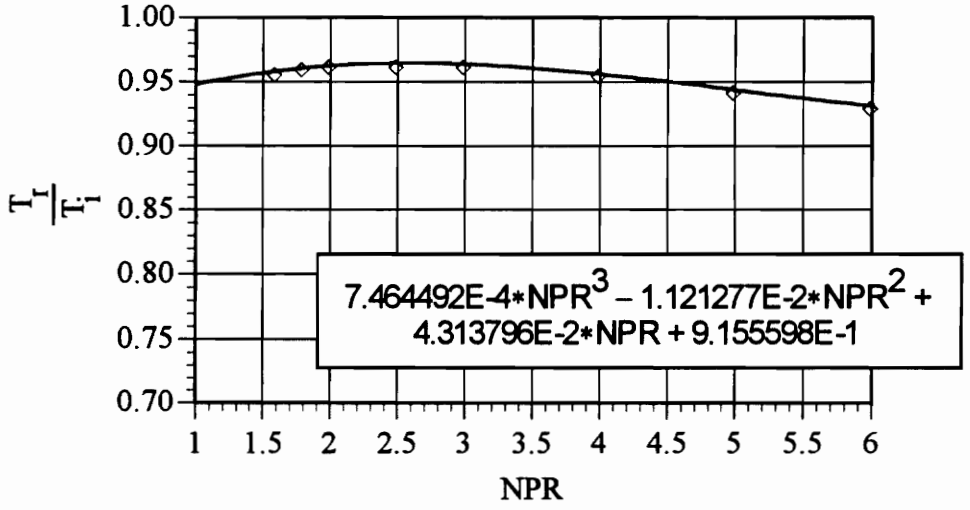

b) $\delta_{v,y}=20°$

Figure 26. Thrust coefficient for 2D, convergent thrust vectoring nozzles, AR=4.0.

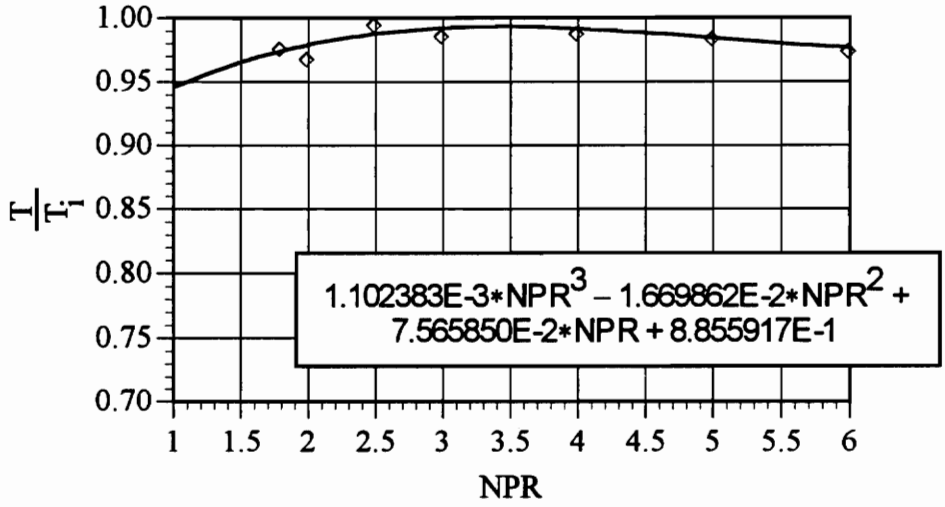

a) $\delta_{v,y}=0°$

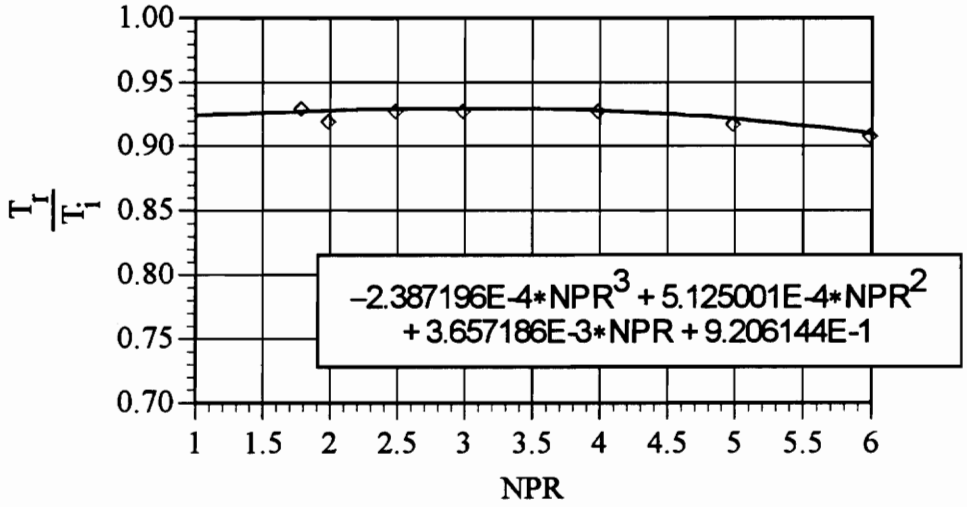

b) $\delta_{v,y}=20°$

Figure 27. Thrust coefficient for 2D, C-D thrust vectoring nozzles, AR=1.5.

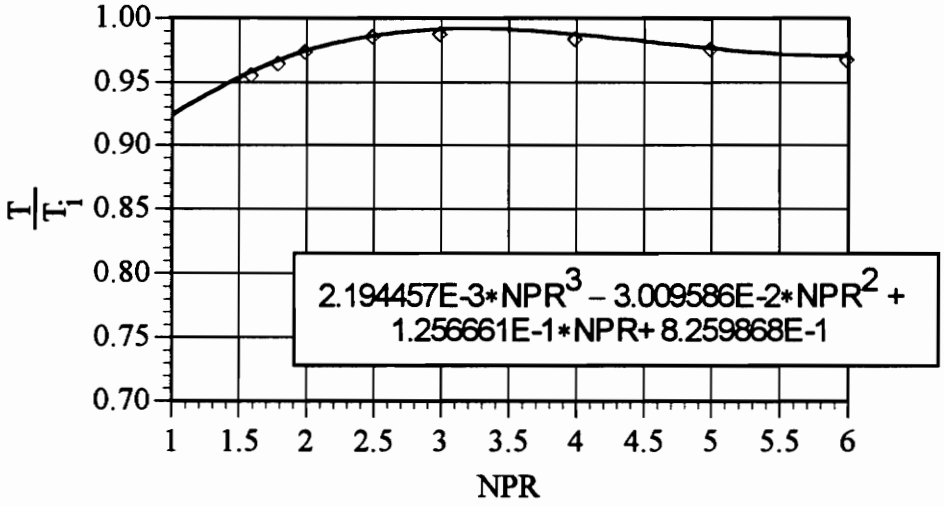

a) $\delta_{v,y}=0°$

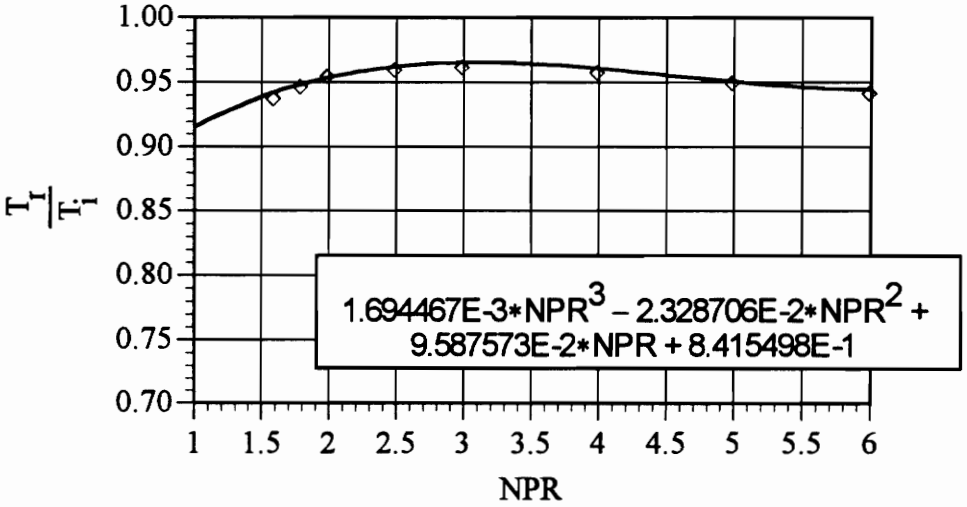

b) $\delta_{v,y}=20°$

Figure 28. Thrust coefficient for 2D, C-D thrust vectoring nozzles, AR=4.0.

nozzles with area ratios of 1.5 and 4.0, and yaw angles of 0° and 20°, in figures 25 through 28. The convergent-divergent nozzle appears to have no significant advantage (in terms of thrust coefficient) over the convergent nozzle. In all cases, turning the flow caused significant reductions in the thrust coefficient. The high aspect ratio nozzles were less effective in turning the flow through the same angle as the geometric pitch vector. Conceptually, this makes sense, as the center of the flow is less strongly influenced by the side flaps for high aspect ratios.

4.4 Summary

Thus, it can be demonstrated that thrust vectoring can be achieved with axisymmetric nozzles with only slight reductions in resultant thrust. This is not the case with nonaxi-symmetric nozzles, which suffer comparatively large losses, even though the flow was turned subsonically in both nozzle types. Axisymmetric nozzles also produce flow pitch angles roughly equivalent to the geometric pitch vector, while 2D nozzles turned the flow through a greater angle than the geometric pitch vector. Nonaxisymmetric nozzles can also be easily used for yaw vectoring, but have been shown here to suffer significant losses.

The nozzles presented in the previous sections have been added to ACSYNT to expand the library of nozzles available to the user. As ACSYNT is not yet capable of utilizing a non-axial thrust component, the data for the thrust vectoring nozzles at non-zero pitch or yaw angles has not been used, and is presented here for completeness and future reference. In addition, the thrust calculation routine has been modified to easily accept additional nozzle types.

5.0 Conclusions

Nearly twenty new routines have been developed to predict the drag and internal performance for the mixed compression inlets. Both planar and axisymmetric inlet types have been successfully modelled. The results of the newly developed routines are typically within ten to fifteen percent of the predicted results, as given by experiments. More importantly, the proper trends are displayed, and it is felt that nearly any geometry may be successfully represented. A detailed accounting of the methods used to predict drag and internal losses is presented, along with the results of these routines.

The nozzle performance calculations were also significantly enhanced. The modifications made addressed the following concerns:

- Prior to this work, only two nozzle types were supported, convergent and convergent-divergent axisymmetric.
- Program logic made addition of new nozzle types cumbersome.
- Nozzle exit conditions were being calculated in a manner inconsistent with the assumptions made for nozzle flow.

These problems were readily solved. The nozzle library has been expanded to include convergent and convergent-divergent nonaxisymmetric nozzles, and several thrust vectoring configurations. Currently, there are more than twenty different nozzle geometries supported, and additional nozzle types may readily be added. Further, the calculations solving for nozzle exit conditions have been modified to be consistent with the nozzle geometry.

6.0 Recommendations for Future Work

There are several propulsion related areas in which work might be done to further enhance the capabilities of ACSYNT. They are listed here in order of increasing complexity.

- The first of these is the ducting of air from the inlet to the engine, and from the engine to the exhaust nozzle. Currently, there are no provisions for ducting losses for aircraft designs where the engine is buried in the fuselage, as when minimization of radar cross section or IR visibility is desired. One potentially important diffuser duct type would be a transition duct, that connects a 2D inlet to an (axisymmetric) compressor.
- Also desirable is some method of calculating thrust using an arbitrary nozzle geometry, using a modular technique similar to that used for inlet design. The user should be able to pick a base nozzle type and then specify the necessary geometric parameters to describe that nozzle. While the work done here has done much to expand the selections of nozzles available, this would allow a continuous spectrum of nozzles available to the user.
- Some provisions for non-zero angle of attack conditions should be made in the inlet calculation. At the least, calculation of pressure recovery should account for this phenomena, although inlet drag will also be strongly affected.
- Lastly, the incorporation of non-axial thrust components, for use in designing STOL or highly maneuverable aircraft is seen as desirable. The addition of this type of technology would affect a large number of calculations within ACSYNT, and may not be feasible in the near future.

References

Andrews, E. H., McClinton, C. R., and Pinckney, S. Z.
"Flow Field and Starting Characteristics of an Axisymmetric Mixed Compression Inlet"
NASA TM X-2072, Jan. 1971

Ball, W. H.
"Propulsion System Installation Corrections", vols. 1 - 4
Boeing Company, Seattle Washington, Research and Engineering Division
AFFL-TR-72-147, December 1972

Brook, J. W.
"An Approximate Method for Determining the Wave Drag of Axisymmetric Conical Cowls"
J. Aero. Sci., No. 5, Vol. 25, May 1958

Capone, F. J., Mason, M. L., and Leavitt, L. D.
"An Experimental Investigation of Thrust Vectoring Two-Dimensional Convergent-Divergent Nozzles Installed in a Twin-Engine Fighter Model at High Angles of Attack"
NASA TM-4155, Feb 1990

Chyu, W. J., Howe, G. W. and Shih, T. I-P.
"Bleed Boundary Conditions for Numerically Simulated Mixed-Compression Supersonic Flow"
Journal of Propulsion and Power, No. 4, Vol. 8, July—Aug 1992

Curry, Lt. S. G., Barnes, G. R., Jones, T. J. and Hartill, W. R.
"Exhaust Nozzle Concepts of STOL Tactical Aircraft"
AIAA 83-1226, 1983

Fujimoto, A., Niwa, N., and Sawada, K.
"Numerical Investigation of Supersonic Inlet with Realistic Bleed and Bypass Systems"
Journal of Propulsion and Power, No. 4, Vol. 8, July—Aug 1992

Kapoor, K., Pai, T. G., and Pamadi, B. N.
"Subcritical Flow Studies on Two-Dimensional External Compression Supersonic Inlets"
Journal of Propulsion and Power, No. 4, Vol. 8, July—Aug 1992

Mason, M. L. and Berrier, B. L.
"Static Performance of Nonaxisymmetric Nozzles with Yaw Thrust-Vectoring Vanes"
NASA TP-2813, May 1988

Mason, M. L. and Burley, J. R. II
"Static Investigation of Two STOL Nozzle Concepts with Pitch Thrust-Vectoring Capability"
NASA TP-2559, April 1986

Moeckel, W. E.
"Approximate Method for Predicting Form and Location of Detached Shock Waves Ahead of Plane or Axially Symmetric Bodies"
NACA Technical Note 1921, 1949

Osmon, R. V.
"Improved Methods of Spillage Drag Prediction for Two-Dimensional Supersonic Inlets"
AIAA Paper 67-449, 1967

Petersen, M. W. and Tamplin, G. C.
"Experimental Review of Transonic Spillage Drag of Rectangular Inlets"
North American Aviation Inc., Los Angeles, CA AFAPL-TR-66-30, May 1966

Raymer, D. P.
Aircraft Design: A Conceptual Approach
AIAA, 1989

Seddon, J. and Goldsmith, E. L.
Intake Aerodynamics
AIAA and Collins, 1985

Sibulkin, M.
"Theoretical and Experimental Investigation of Additive Drag"
NACA Report 1187, 1954

Smeltzer, D. B. and Sorensen, N. E.
"Analytic and Experimental Performance of Two Isentropic Mixed Compression Axisymmetric Inlets at Mach Numbers 0.8 to 2.65"
NASA TN D-7320, June 1973

Taylor, J. G.
"Internal Performance of a Hybrid Axisymmetric/Nonaxisymmetric Convergent-Divergent Nozzle"
NASA TM-4230, Jan. 1991

Willis, J. H. and Randall, D. G.
"The Theoretical Wave Drag of Open Nose Axisymmetric Forebodies with Varying Fineness Ratio, Area Ratio, and Nose Angle"
RAE TN Aero 2360, 1955

Wolfe, Capt. L. D. and Fanning, Capt. A. E.
"Advanced Nozzle Technology"
AGARD Cp 241, 1977

Wong, N. D., and Anderson, W. E.
"Experimental Investigation of a Large-Scale, Two-Dimensional, Mixed-Compression Inlet System"
NASA TN D-7445, 1973

Appendix A

Derivation of the ideal thrust ratio

Begin with standard expression for thrust:

$$T = \dot{m}V_e - A_e\left(P_e - P_\infty\right)$$

Nondimensionalize thrust by $P_o A_t$ to get

$$\frac{T}{P_o A_t} = \frac{\dot{m}}{P_o A_t}V_e - \frac{A_e}{A_t}\left(\frac{P_e}{P_o} - \frac{P_\infty}{P_o}\right) \text{ where:}$$

$$V_e = \sqrt{2C_p\left(T_o - T_e\right)} \text{ and, assuming choked flow at nozzle throat}$$

$$\frac{\dot{m}}{P_o A_t} = \frac{\rho^* A^* V^*}{P_o A_t} = \frac{P^*}{P_o}\frac{A^*}{A_t}\frac{V^*}{RT^*} = \left(\frac{2}{\gamma+1}\right)^{\frac{\gamma}{\gamma-1}}\sqrt{\frac{\gamma}{RT^*}} = \sqrt{\frac{\gamma}{R}\left(\frac{2}{\gamma+1}\right)^{\frac{\gamma+1}{\gamma-1}}}\left[\frac{1}{\sqrt{T_o}}\right]$$

$$\frac{T}{P_o A_t} = \gamma\sqrt{\frac{2}{\gamma-1}\left(\frac{2}{\gamma+1}\right)^{\frac{\gamma+1}{\gamma-1}}}\sqrt{1-\left(\frac{P_e}{P_o}\right)^{\frac{\gamma-1}{\gamma}}} + \frac{A_e}{A_t}\left(\frac{P_e}{P_o} - \frac{P_\infty}{P_o}\right)$$

But, for a perfectly expanded Con-Di nozzle, ideal thrust is given by:

$$\frac{T_i}{P_o A_t} = \gamma\sqrt{\frac{2}{\gamma-1}\left(\frac{2}{\gamma+1}\right)^{\frac{\gamma+1}{\gamma-1}}}\sqrt{1-\left(\frac{P_e}{P_o}\right)^{\frac{\gamma-1}{\gamma}}} \quad \text{since } P_e = P_\infty.$$

For a convergent nozzle $\frac{P_e}{P_o} = \frac{P^*}{P_o}$ and $A_e = A_t$, so thrust is given by:

$$\frac{T}{P_o A_t} = \gamma \sqrt{\frac{2}{\gamma - 1}\left(\frac{2}{\gamma + 1}\right)^{\frac{\gamma+1}{\gamma-1}}} \sqrt{1 - \left(\frac{2}{\gamma+1}\right)} + \left(\frac{2}{\gamma+1}\right)^{\frac{\gamma}{\gamma-1}} - \frac{P_\infty}{P_o}$$

$$\frac{T}{P_o A_t} = \gamma \sqrt{\frac{2}{\gamma - 1}\left(\frac{2}{\gamma + 1}\right)^{\frac{\gamma+1}{\gamma-1}} - \frac{2}{\gamma - 1}\left(\frac{2}{\gamma+1}\right)^{\frac{2\gamma}{\gamma-1}}} + \left(\frac{2}{\gamma+1}\right)^{\frac{\gamma}{\gamma-1}} - \frac{P_\infty}{P_o}$$

$$\frac{T}{P_o A_t} = (\gamma + 1)\left(\frac{2}{\gamma+1}\right)^{\frac{\gamma}{\gamma-1}} - \frac{P_\infty}{P_o}$$

Thus, the ideal thrust ratio is:

$$\frac{T}{T_i} = \frac{(\gamma + 1)\left(\frac{2}{\gamma+1}\right)^{\frac{\gamma}{\gamma-1}} - \frac{P_\infty}{P_o}}{\gamma \sqrt{\frac{2}{\gamma-1}\left(\frac{2}{\gamma+1}\right)^{\frac{\gamma+1}{\gamma-1}}} \sqrt{1 - \left(\frac{P_\infty}{P_o}\right)^{\frac{\gamma-1}{\gamma}}}}$$

Appendix B — Implementation

This appendix describes the implementation of the previously described inlet drag and total pressure recovery prediction methods. First, a brief description, the required input, and the output is given for each subroutine, along with the section of the thesis where the methods used are discussed. This listing is followed by structure charts for the newly developed routines. Finally, sample ACSYNT input and output comparing an axisymmetric external compression inlet to a 2D mixed compression inlet is provided. The only difference in input is the section that is highlighted with bold letters.

Planar mixed compression inlet subroutines

Freestream conditions include Mach number, static pressure, and static temperature for all routines listed here.

SUBROUTINE ADDMC

Purpose:

Calculates the additive drag of the 2D mixed compression inlet.

Methods refer to:

Sections 2.2, 3.3.4, Figures 4, 5, 7

Input:

Mass flow rate, freestream conditions, capture height, inlet height, ramp angles, width, reference mass flow ratio, mass flow ratio, sideplates toggle, ramp lengths, start/unstart toggle

Output:

Additive drag coefficient

SUBROUTINE DIMMC

Purpose:

Dimensions the 2D mixed compression inlet — after inlet sizing is performed, this determines critical dimensions of the inlet

Methods refer to:

N/A. This routine uses simple geometry and isentropic flow relationships

Input:

Capture area, design Mach number, ramp angles, area ratio, cowl angle, ratio of cowl height to maximum height

Output:

Width, capture height, inlet height, maximum height, ramp lengths

SUBROUTINE DRAGMC

Purpose:

Calls other drag prediction routines, sums results

Methods refer to:

N/A. Utility routine for convenience only

Input:

Mass flow, freestream conditions, ramp angles, capture height, inlet height, maximum height, width, sideplates toggle, diverter angle, cowl angle, ramp lengths, capture area, started toggle, mass flow ratio

Output:

Spillage, wave, profile, and total inlet drag coefficients

SUBROUTINE MAXMMC

Purpose:

Determines the maximum mass flow the inlet can process for the given freestream conditions

Methods refer to:

N/A. Uses isentropic flow relationships

Input:

Freestream conditions, capture height, inlet height, ramp angles, width, ramp lengths, started toggle

Output:

Reference mass flow ratio, maximum mass flow rate

SUBROUTINE MC2D

Purpose:

This is the routine called by INLDRG for inlet types 7 and 8. It calls the supporting routines that do the actual calculation of inlet drag and total pressure recovery

Methods refer to:

N/A

Input:

Ramp angles, freestream conditions, freestream total pressure and temperature, design Mach number, design total temperature and pressure, total pressure

recovery table, incremental total pressure recovery, auxiliary mass flow ratio, ratio of diverter wedge area to inlet capture face area, area at the engine face, Mach number at the engine face, corrected engine mass flow, capture area scale factor, bleed and bypass drag scale factors, cowl angle, aspect ratio, diverter wedge angle, maximum cowl height, inlet type, pressure recovery method

Output:

Supersonic, subsonic, and combined total pressure recovery, capture area, bypass area ratio, bleed area ratio, forebody length, mass flow ratio, width, spillage drag coefficient, wave drag coefficient, and profile drag coefficient

SUBROUTINE MCMT2D

Purpose:

Determine the throat Mach number

Methods refer to:

Section 3.3.3

Input:

Design Mach number, ramp angles, supersonic total pressure recovery, freestream conditions, started toggle, iteration count, mass flow rate, throat area

Output:

Throat Mach number

SUBROUTINE PRRC2D

Purpose:

Determines the supersonic total pressure recovery

Methods refer to:

Section 2.3, 3.2.3, 3.3.2

Input:

Pressure recovery method, ramp angles, specific heats ratio, freestream Mach number, total pressure recovery table, incremental total pressure recovery, start/unstart toggle

Output:

Supersonic total pressure recovery

SUBROUTINE NSPOSN

Purpose:

Determine the maximum number of oblique shocks ahead of the normal shock — this routine ignores mass flow conditions, and thus can be used to determine if started conditions are **possible**.

Methods refer to:

N/A. Uses compressible flow relationships and correlations to find the minimum Mach number for an oblique shock to attach to a wedge.

Input:

Ramp angles, freestream Mach number, specific heat ratio

Output:

Number of oblique shocks upstream of the normal shock (0, 1, 2 or 3)

Axisymmetric mixed compression inlet subroutines

Freestream conditions include Mach number, static pressure, and static temperature for all routines listed here.

SUBROUTINE ADDMCX

Purpose:

Calculates the additive drag for the axisymmetric mixed compression inlet

Methods refer to:

Sections 2.2, 3.4.3, Figures 10, 11, 13

Input:

Mass flow rate, freestream conditions, cowl radius, cone radius at the cowl face, cone half angle, factor representing flow angle cosine at capture face

Output:

Additive drag coefficient

SUBROUTINE AXINS

Purpose:

Determines the maximum number of shocks upstream of the normal shock

Methods refer to:

N/A. Uses conical shock methods and correlations to determine minimum Mach number for attached shocks

Input:

Cone half angle, cowl internal angle, specific heat ratio, freestream Mach number

Output:

Number of shocks upstream of the normal shock

SUBROUTINE AXMCMX

Purpose:

Determine the maximum mass flow the inlet can process for the given freestream conditions

Methods refer to:

N/A. Uses isentropic flow relationships, shock relationships

Input:

Freestream conditions, cowl radius, cone radius at the cowl face, cone half angle, cone length, started toggle

Output:

Reference mass flow ratio, maximum mass flow rate, factor which makes the additive drag zero at full flow.

SUBROUTINE DIMMCX

Purpose:

Dimensions the axisymmetric mixed compression inlet -- after inlet sizing is performed, this determines critical dimensions of the inlet

Methods refer to:

N/A. Uses isentropic flow and conical shock relationships

Input:

Capture area, design Mach number, cone half angle, cowl angle, maximum cowl length, ratio of cowl radius to maximum inlet radius

Output:

Cowl radius, cone radius at the cowl face, maximum radius, cone length

SUBROUTINE DRAGMX

Purpose:

Calls the other drag prediction routines, sums results

Methods refer to:

N/A. Utility routine for convenience only

Input:

Mass flow, freestream conditions, design Mach number, cone half angle, cowl radius, cone radius at the cowl face, maximum radius, cowl external and internal angles, capture area, mass flow ratio

Output:

Spillage, wave, profile, and total inlet drag coefficients

SUBROUTINE MCAXI

Purpose:

This is the routine called by INLDRG for inlet type 9. It calls the supporting routines that do the actual calculation of inlet drag and total pressure recovery

Methods refer to:

N/A

Input:

Cone half angle, freestream conditions, freestream total pressure and temperature, design Mach number, design total pressure and temperature, total pressure recovery table, incremental total pressure recovery, auxiliary mass flow ratio,

Mach number at the engine face, area at the engine face, corrected engine mass flow, capture area scale factor, bleed and bypass drag scale factors, cowl external angle, maximum cowl radius, pressure recovery method

Output:

Supersonic, subsonic, and combined total pressure recovery, capture area, bypass area ratio, bleed area ratio, cone length, mass flow ratio, spillage drag coefficient, wave drag coefficient, profile drag coefficient

SUBROUTINE MCMTAX

Purpose:

Determines the throat Mach number for subsonic pressure recovery correlation

Methods refer to:

N/A. Uses isentropic flow and shock relationships similar to that described in section 3.3.3

Input:

Design Mach number, cone half angle, cone internal angle, supersonic pressure recovery, freestream conditions, started toggle, iteration count, mass flow rate, throat area

Output:

Throat Mach number

SUBROUTINE PRRCAX

Purpose:

Determines the supersonic total pressure recovery

Methods refer to:

Section 2.3, 3.2.3, 3.4.2

Input:

Pressure recovery method, freestream Mach number, cone half angle, internal cowl angle, specific heats ratio, total pressure recovery table, start/unstart toggle

Ouput:

Supersonic total pressure recovery

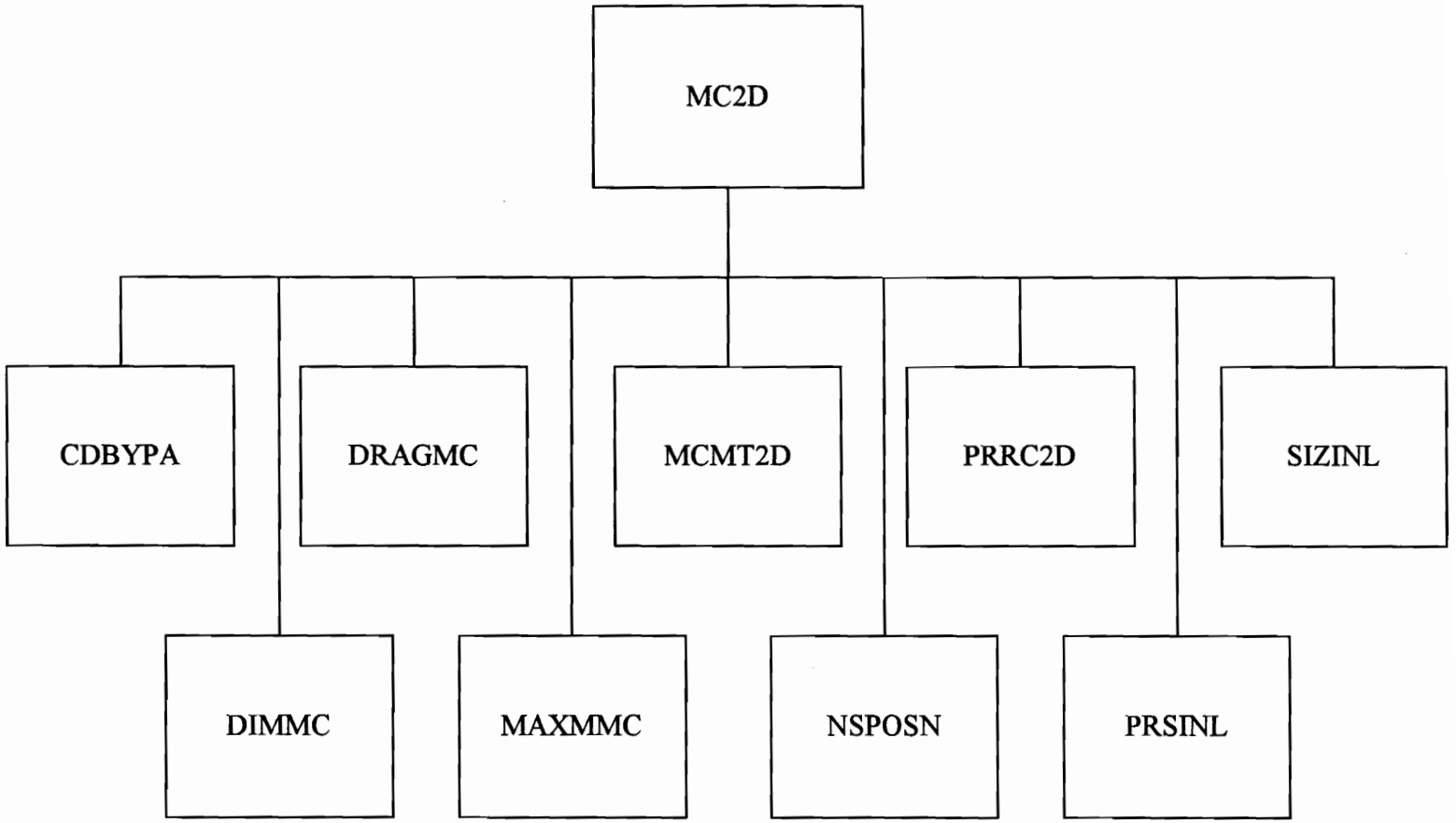

Figure 29. 2D Mixed Compression Inlet Structure Chart

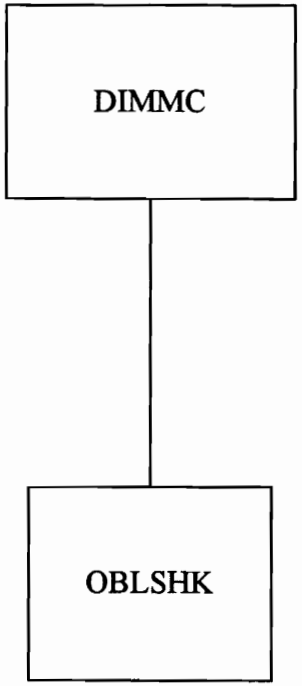

Figure 29a. 2D Mixed Compression Inlet Structure Chart, cont.

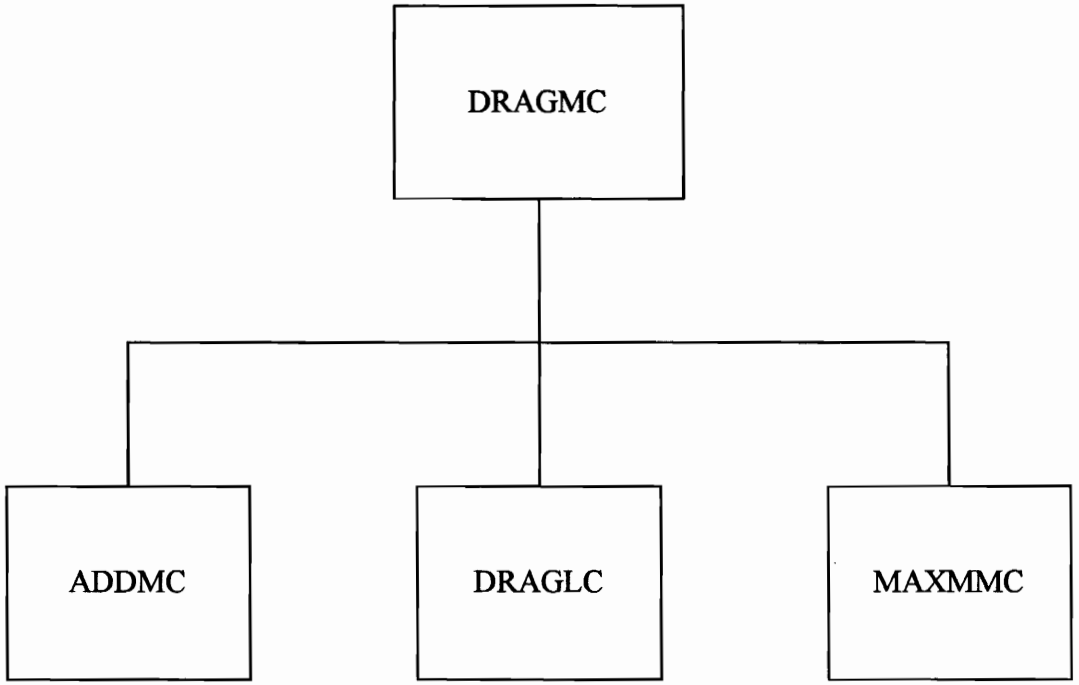

Figure 29b. 2D Mixed Compression Inlet Structure Chart, cont.

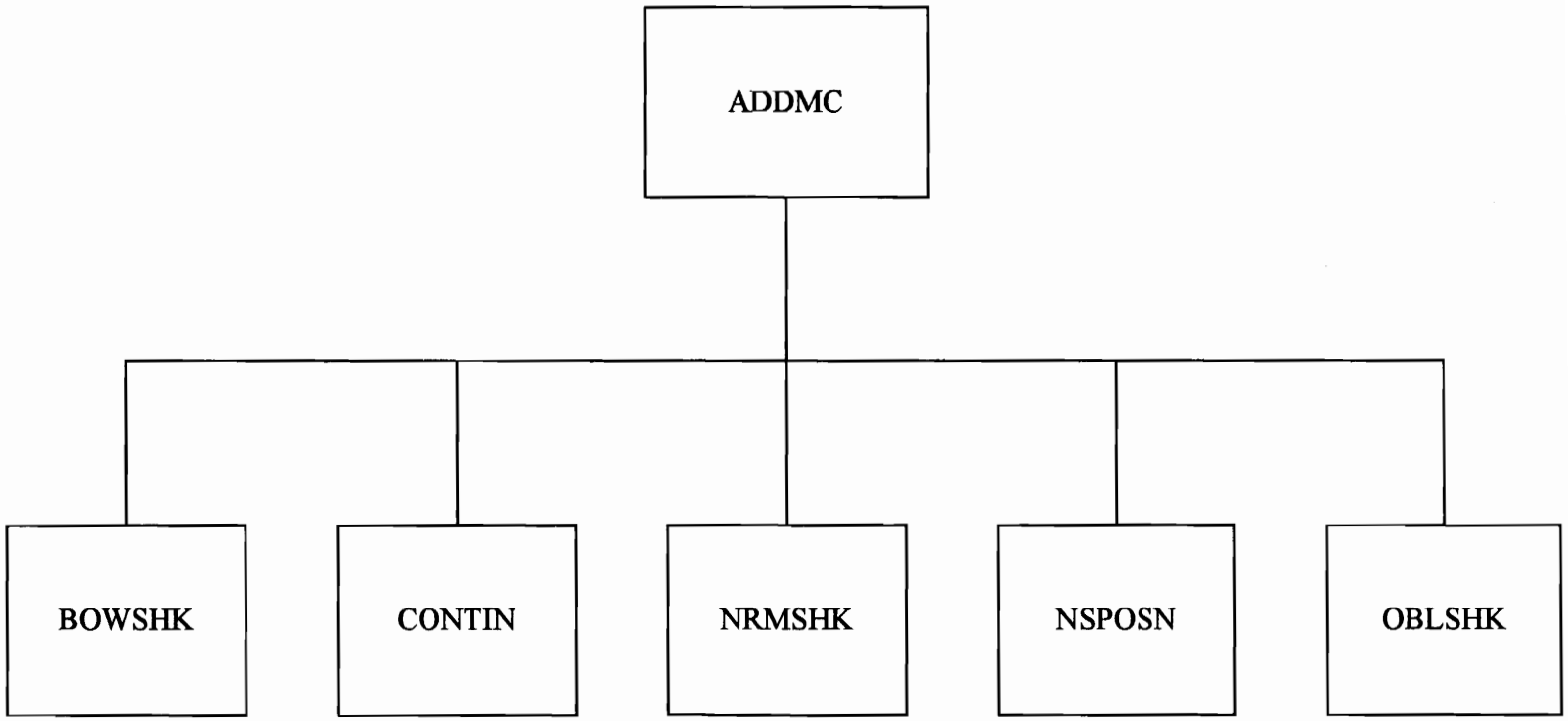

Figure 29c. 2D Mixed Compression Inlet Structure Chart, cont.

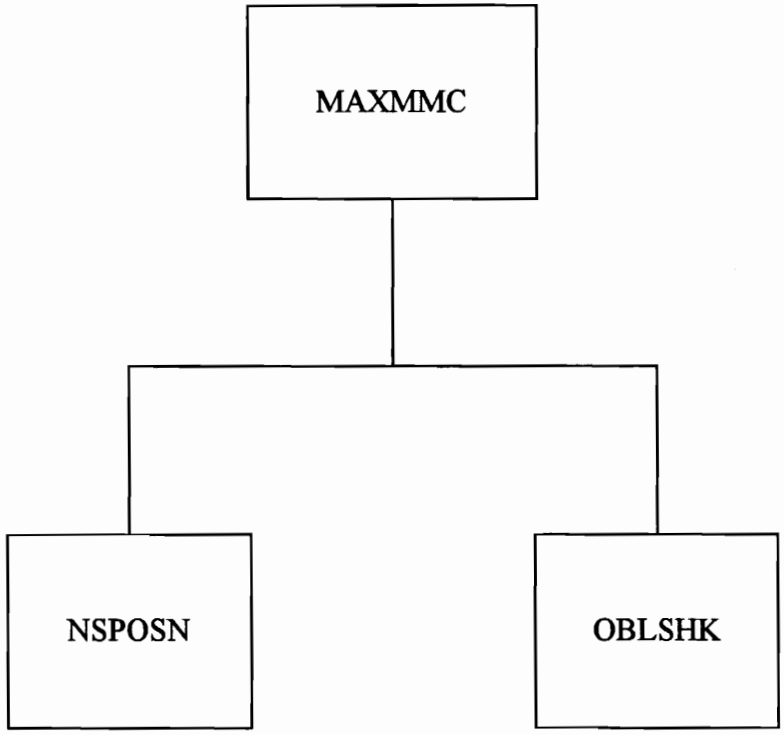

Figure 29d. 2D Mixed Compression Inlet Structure Chart, cont.

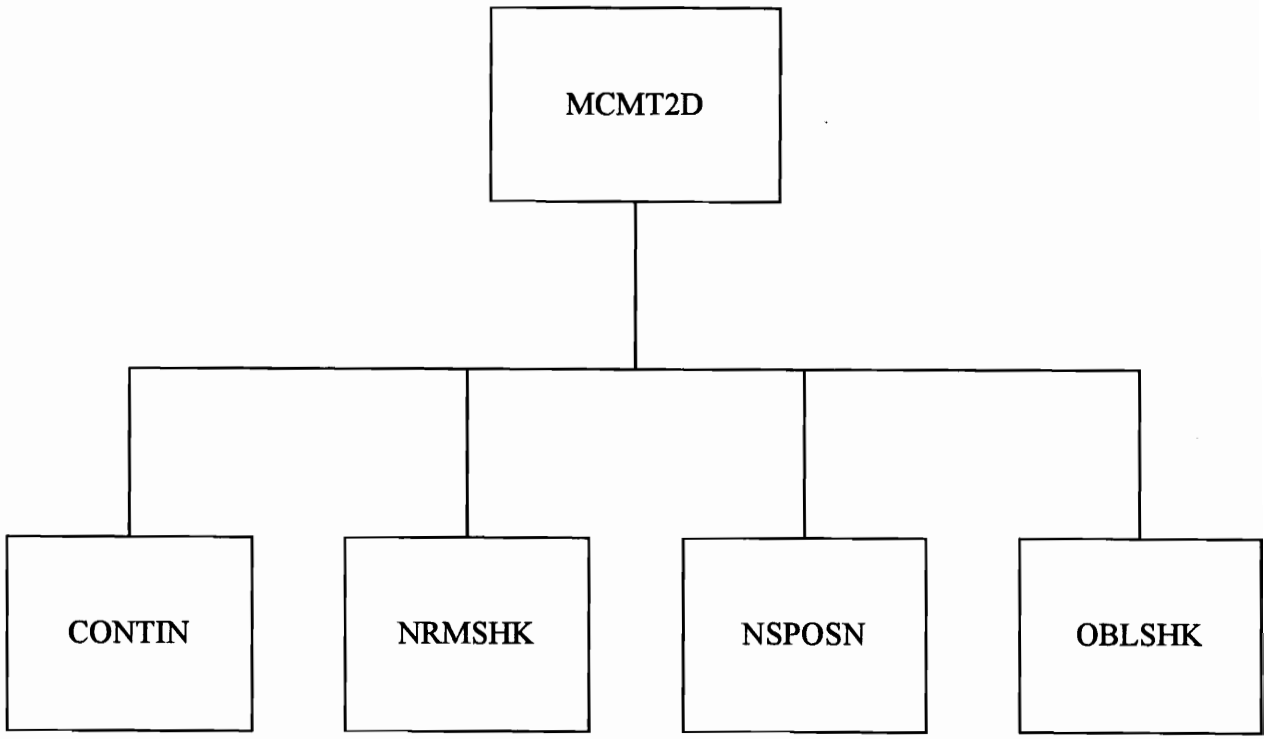

Figure 29e. 2D Mixed Compression Inlet Structure Chart, cont.

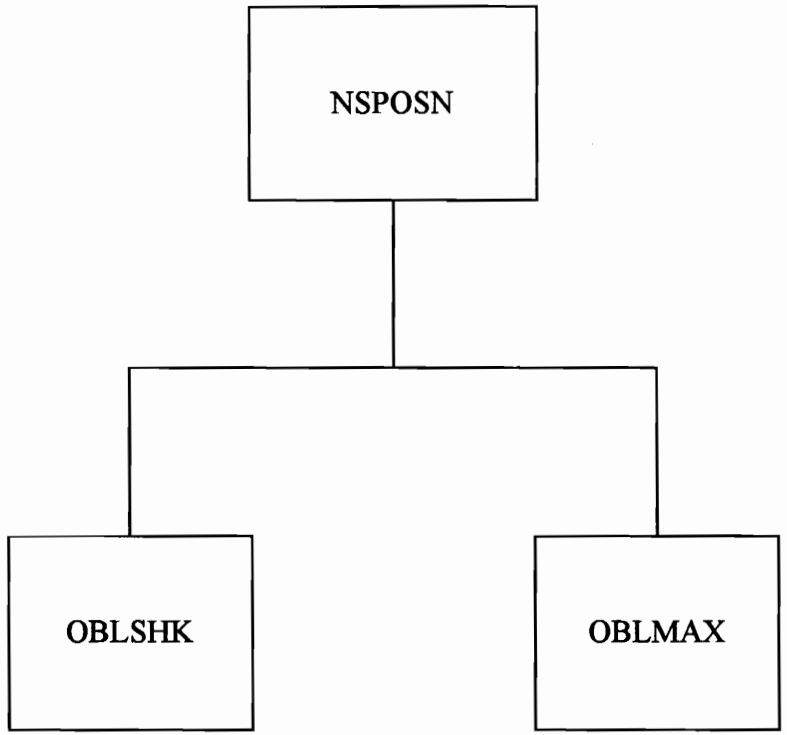

Figure 29f. 2D Mixed Compression Inlet Structure Chart, cont.

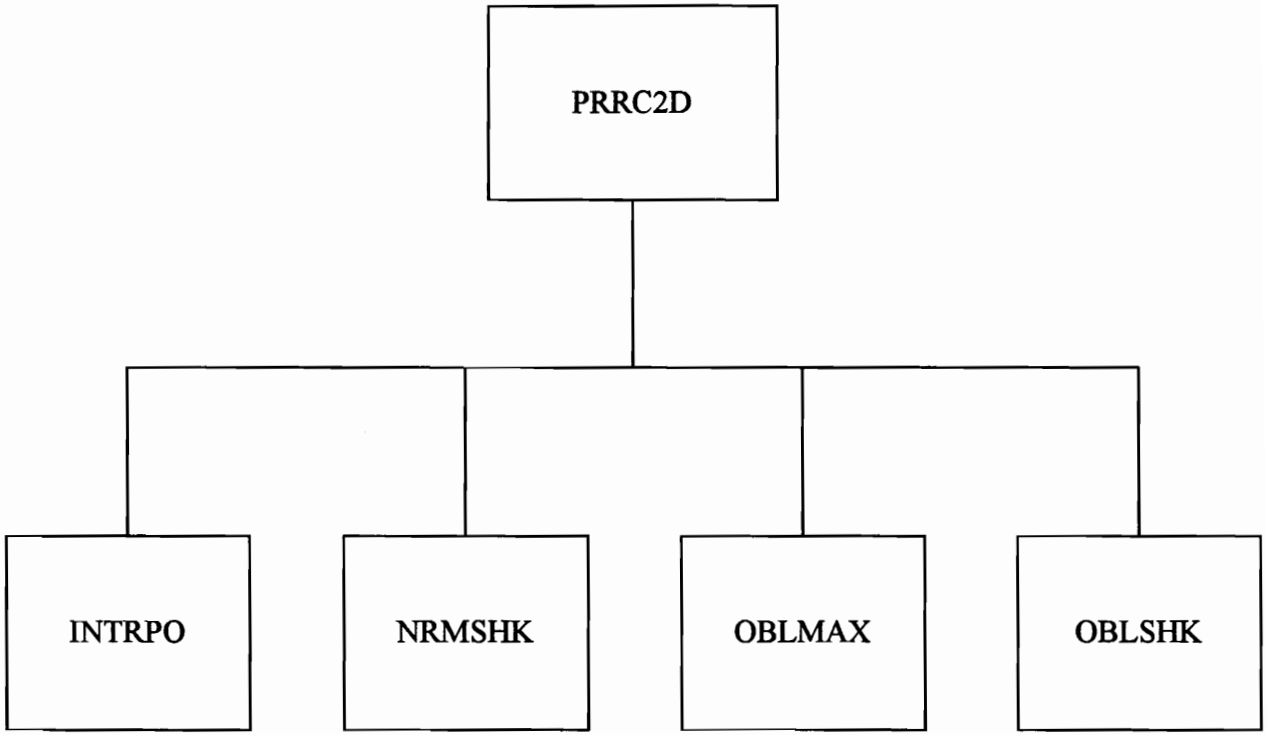

Figure 29g. 2D Mixed Compression Inlet Structure Chart, cont.

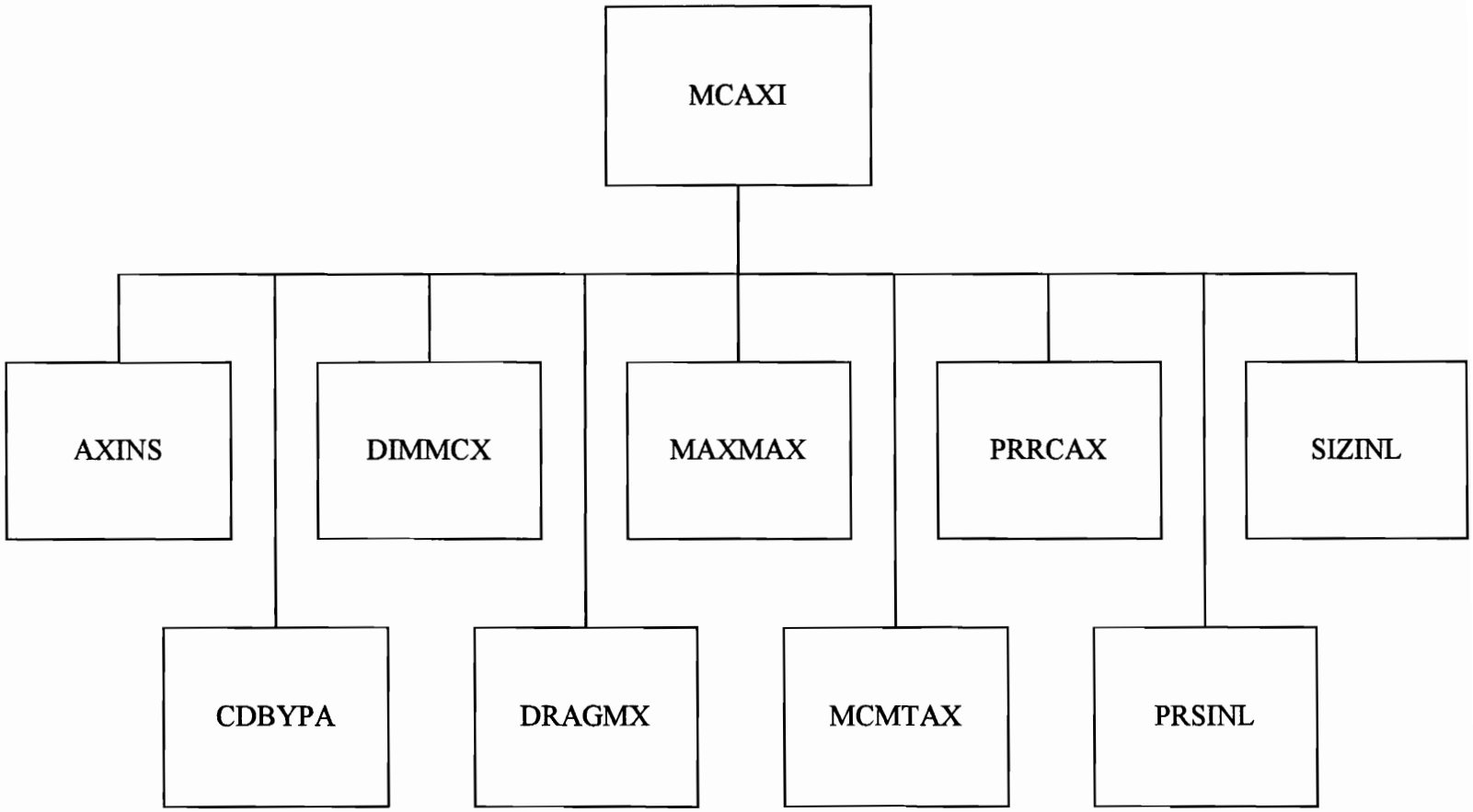

Figure 30. Axisymmetric Mixed Compression Inlet Structure Chart

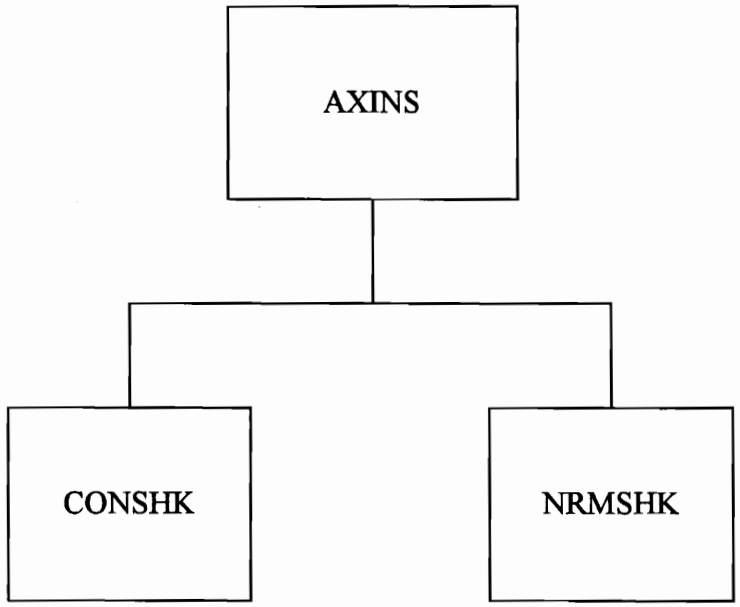

Figure 30a. Axisymmetric Mixed Compression Inlet Structure Chart, cont.

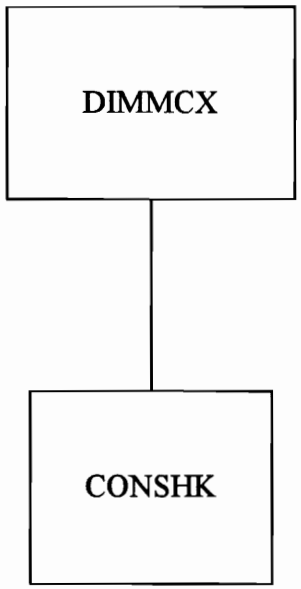

Figure 30b. Axisymmetric Mixed Compression Inlet Structure Chart, cont.

Figure 30c. Axisymmetric Mixed Compression Inlet Structure Chart

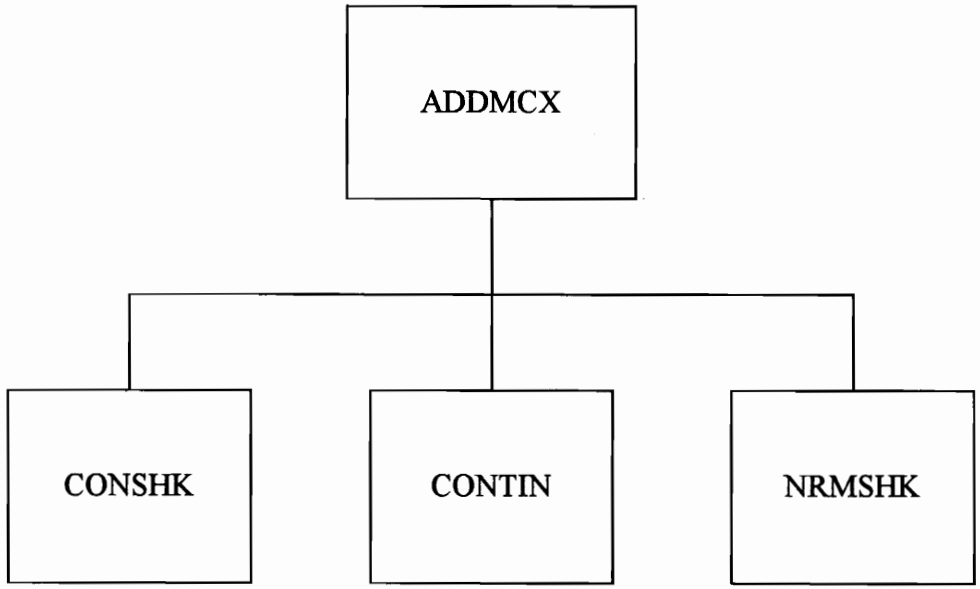

Figure 30d. Axisymmetric Mixed Compression Inlet Structure Chart, cont.

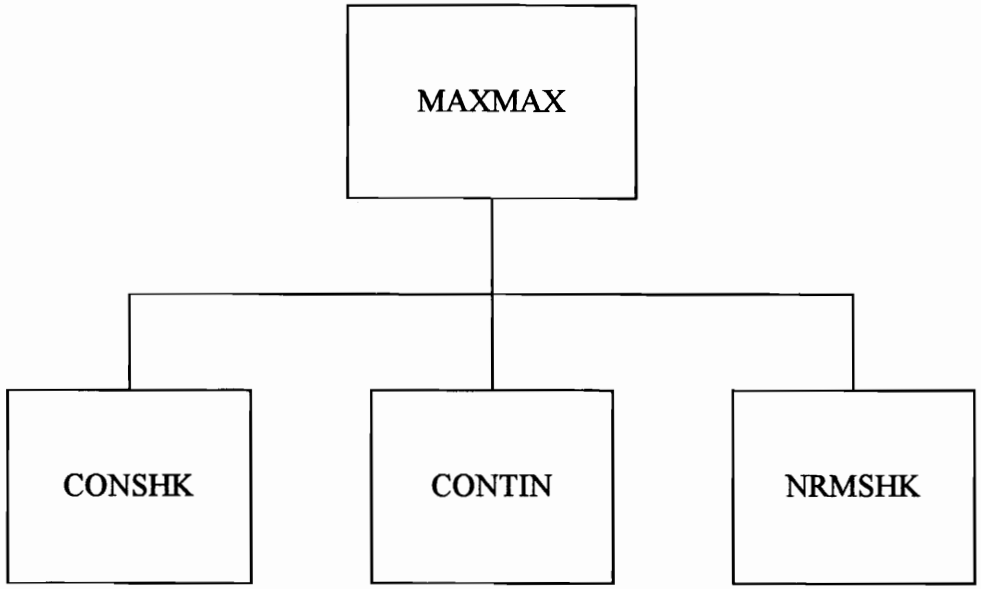

Figure 30e. Axisymmetric Mixed Compression Inlet Structure Chart, cont.

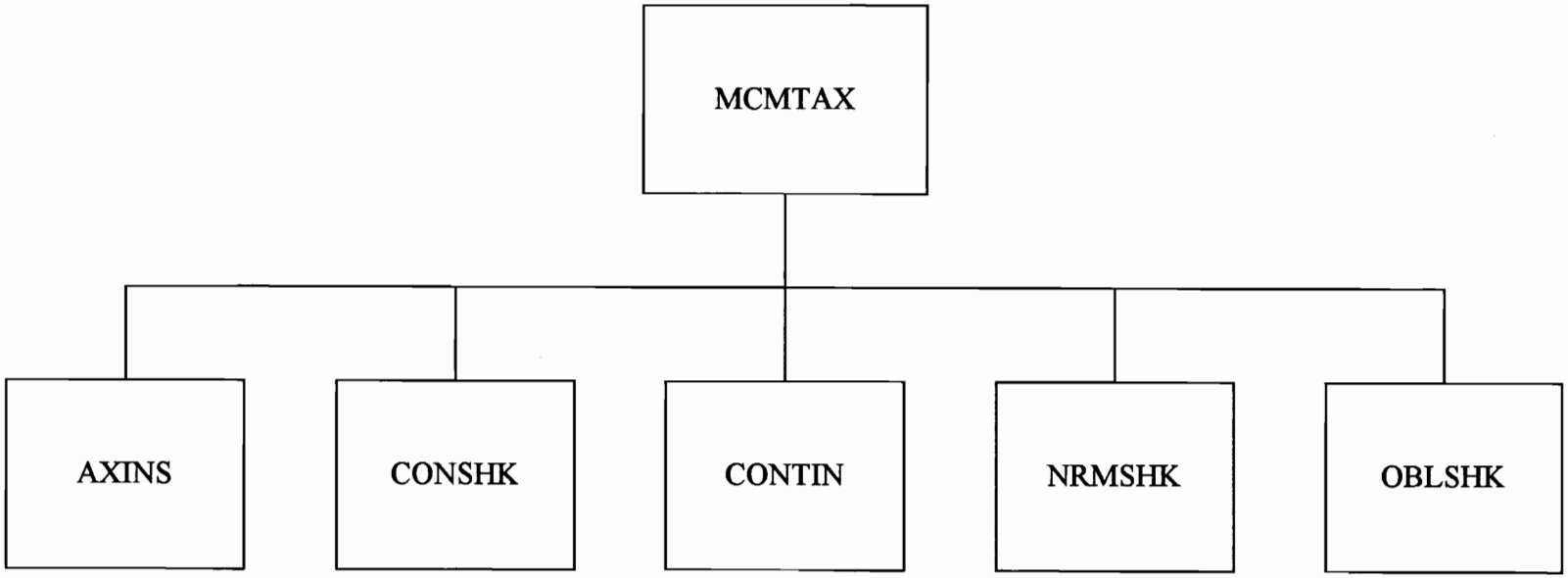

Figure 30f. Axisymmetric Mixed Compression Inlet Structure Chart, cont.

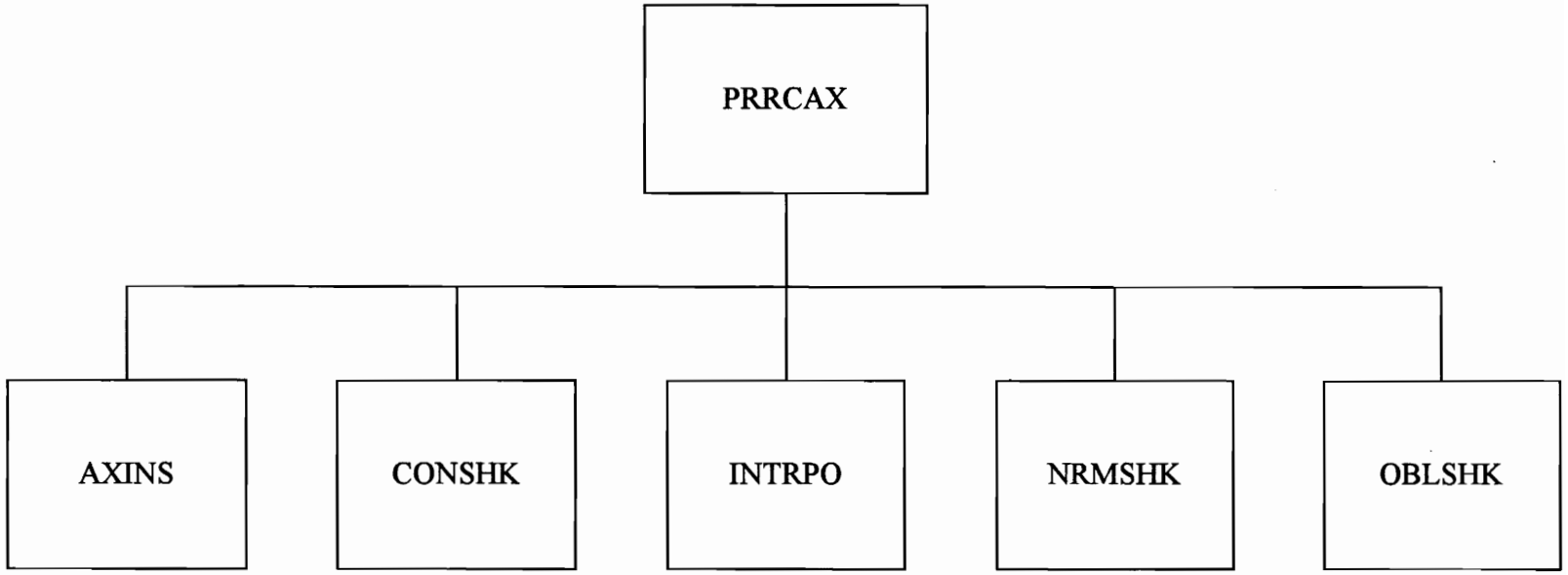

Figure 30g. Axisymmetric Mixed Compression Inlet Structure Chart, cont.

Axisymmetric External Compression inlet — sample input and results

```
  Input for Module #  2
  ********************************************************************************
                            TRAJECTORY INPUT


 TIMTO1 = 5.0        MENDUR =     0.     NCRUSE = 2     IPLOT = 4
 TIMTO2 =  .5          QMAX =  1700.     IPSIZE =-2     HMINP =     0.
 FRFURE =  .22        XDESC = 100.0      IPSTO1 = 5     HMAXP = 40000.
  DESLF = 2.50       WKFUEL = 1.000      IPSTO2 = 1     DELHP =  4000.
  ULTLF = 3.75       CRMACH = 2.400       IBREG = 0    SMMINP =  .300
  RANGE =  4000.     WKLAND =  .570      IENDUR = 0    SMMAXP =  .900
  WFUEL = 324293.     FLFAC =  .600      IPRINT = 0     DELMP =  .100
  WFEXT =      0.     DECEL =  .250      KERROR = 2    WCOMBP =      .70
 WFTRAP =    100.    NLEGCL = 0          NLEGCR = 0    NLEGLO = 0
 FWGMAX = 1.200         TOL =  .001      MILCOM = 0     NMISS = 1
  NCODE = 0          MMPROP = 1


 MISSION  1

          MACH NO.   ALTITUDE      HORIZONTAL     NO.  VIND
 PHASE    START END  START  END     DIST  TIME     TURN  "G"S  WKFUEL M IP IX W B A P
 -------  ---- ----  -----  -----   ------ -----   ---- -----  ------ - -- -- - - - -
 COMBAT   1.30  .00  50000      0      5.0    .0    .0    .0   .0001 1  1  0 0 0 0 0
 COMBAT   1.40  .00  50000      0      5.0    .0    .0    .0   .0001 1  1  0 0 0 0 0
 COMBAT   1.50  .00  50000      0      5.0    .0    .0    .0   .0001 1  1  0 0 0 0 0
 COMBAT   1.60  .00  50000      0      5.0    .0    .0    .0   .0001 1  1  0 0 0 0 0
 COMBAT   1.70  .00  50000      0      5.0    .0    .0    .0   .0001 1  1  0 0 0 0 0
 COMBAT   1.80  .00  50000      0      5.0    .0    .0    .0   .0001 1  1  0 0 0 0 0
 COMBAT   1.90  .00  50000      0      5.0    .0    .0    .0   .0001 1  1  0 0 0 0 0
 COMBAT   2.00  .00  50000      0      5.0    .0    .0    .0   .0001 1  1  0 0 0 0 0
 COMBAT   2.10  .00  50000      0      5.0    .0    .0    .0   .0001 1  1  0 0 0 0 0
 COMBAT   2.20  .00  50000      0      5.0    .0    .0    .0   .0001 1  1  0 0 0 0 0
 COMBAT   2.30  .00  50000      0      5.0    .0    .0    .0   .0001 1  1  0 0 0 0 0
 COMBAT   2.40  .00  50000      0      5.0    .0    .0    .0   .0001 1  1  0 0 0 0 0


  Input for Module #  4
  ********************************************************************************
1                       PROPULSION INPUT
                         VERSION 04-76

 *****  Proposed LARC HSCT24E Propulsion System *****


  AENDIA =     4.000  AENLE  =    22.000  AENWT  =  7000.000
  ALTI   =      .000  AM     =      .000  ATURB  =      .242
  AENTW  =      .000
  AUAENG =      .000  AWAENG =      .000  BA     =      .000
  DELPR  =      .000  DELT57 =   370.000  DEPWCC =     5.000
  DIA1   =     3.960  EAB1   =      .750  EB1    =      .910
  ED1    =      .750  ETAC1  =      .900  ETAF1  =      .900
  ETAT1  =      .885  HTR    =      .400  HVF    = 18600.000
  MACH1  =      .930  MACH2  =     2.020  PCDFAC =     1.000
  POSA   =    29.920  PRFD   =     1.000  PWCC   =   100.000
  P11P1  =     1.000  P2P1   =    12.070  R10A   =    -2.000
  R32    =      .950  R54    =      .940  R54N   =      .940
  R711   =      .980  R711N  =      .980  SCPR   =     1.480
  SFADP  =     1.000  SFADSP =     1.000  SFAUXP =     1.000
  SFBEP  =     1.000  SFBPP  =     1.000  SFBTP  =     1.000
  SFDIVP =     1.000  SFINSP =     1.000  SFIP   =     1.000

  nInl   =         4  InType =         5  sfInlP =     1.000
```

```
sfSplP =     1.000  spPrfP =     1.000  sfWavP =     1.000
Lm =        12.000  YcOYm  =      .850  AR     =     1.000
theta  =    10.000  psi    =      .000  eta    =    10.000
lipRat =      .010

SFSFC1 =      .800  SFSFC2 =      .700  SFSFC3 =      .700
SM1    =      .600  SODG   =     1.000  TOSA   =   518.000
TR     =   520.000  TWAB   =    49000.  TWOAB  =    35000.
TWTO   =      .500  T3     =     2430.  T5M    =     3400.
T51    =     2800.  T7M    =     3400.  T71    =       0.
VC1    =      .980  WCWA1  =      .000  XMDES  =     2.400
XMT    =      .990  YREN   =       95.  FRBT   =     2.730
FRPN   =     4.220  RDIAM  =     1.980  RLENG  =     1.710


IPR    =         3  IPRINT =         1  IPLOT  =         1
KERROR =         0  KODE   =         0  KT5    =         2
KT7    =         0  MINPR  =         0  NAB    =         6
NOZZ   =         1  NPROP  =         6  NSUMM  =         8
                                         IENG   =         1 (J85 )


THESE VARIABLES ARE USED BY TABLE LOOK UP
ESF    =      .550  NDTAIL   = 0  IPDBUG  = 0  IIPRINT = 0


ALTD  =    50000.    50000.    50000.    50000.    50000.    50000.
XMACH =     1.400     1.600     1.800     2.000     2.200     2.400
XMPRI =      .302      .930     1.200     2.000     2.100     3.000
XPRI  =      .986      .990      .986      .937      .600      .400
XMPRI1 =     .000      .000      .000      .000      .000      .000      .000      .000
   .000      .000
XPRI1 =      .000      .000      .000      .000      .000      .000      .000      .000
   .000      .000
XMPRI2 =     .000      .000      .000      .000      .000      .000      .000      .000
   .000      .000
XPRI2 =      .000      .000      .000      .000      .000      .000      .000      .000
   .000      .000



 Output for Module #  2
 ********************************************************************************
                        TRAJECTORY OUTPUT


Block Time                          =     .092 hrs
Block Range                         =       .0 n.m.
Block Fuel                          =  2860.2 lb.

Takeoff Field Length (total run)    =  785850. ft
Landing Field Length (total run)    =   96616. ft   Decel @ .250 Gs
Landing Field Length (ground run)   =   38767. ft
Weight for Landing calculation      =  644067. lbs
Landing Thrust to Weight ratio      =     .390
Takeoff Weight                      =  646064. lbs
Landing Weight                      =  643204. lbs


 Output for Module #  4
 ********************************************************************************
1                     ENGINE SUMMARY


               ENGINE DIAMETER =     4.00 FEET
               ENGINE LENGTH   =    22.00 FEET
               ENGINE WEIGHT   =  7000.00 POUNDS
```

```
                BYPASS RATIO    =       .00
                NO OF ENGINES   =        4.
                DRAG REF AREA   =  7500.00 SQ FEET
                PWCC   = PERCENT OF ENGINE CORRECTED AIRFLOW
                THRUST = ENGINE THRUST (POUNDS PER ENGINE)
                SFC    = ENGINE SPECIFIC FUEL CONSUMPTION
                THRUSTU= THRUST PER ENGINE IN LBS, W/O INSTAL DRAG CORR
                SFCU   = SFC,1/HR, W/O INSTALLATION DRAG CORR
                CDINS  = TOT INSTALLATION DRAG COEF PER A/C (SWING REF)
1


    MACH      ALT      PWCC   THRUST THRUSTU      SFC     SFCU    CDINS
   1.400   50000.     100.    8449.   9349.     .965     .872    .0014
                        95.    7713.   8708.     .989     .876    .0016
                        90.    6342.   7439.    1.012     .863    .0018
                        85.    5019.   6248.    1.062     .853    .0020
                        80.    3741.   5146.    1.167     .848    .0022
                        75.    2547.   4137.    1.382     .851    .0025
                        70.    1455.   3228.    1.921     .866    .0028
                        65.     474.   2427.    4.618     .902    .0031
   1.600   50000.     100.    9323.  10366.     .967     .869    .0013
                        95.    8793.   9975.     .998     .879    .0014
                        90.    8168.   9503.    1.036     .890    .0016
                        85.    6489.   7982.    1.083     .880    .0018
                        80.    4917.   6573.    1.170     .875    .0020
                        75.    3468.   5289.    1.337     .877    .0022
                        70.    2094.   4136.    1.758     .890    .0025
                        65.     817.   3123.    3.528     .923    .0028
   1.800   50000.     100.    9903.  11041.     .974     .874    .0011
                        95.    9443.  10690.     .999     .883    .0012
                        90.    8816.  10284.    1.042     .893    .0014
                        85.    8137.   9832.    1.095     .906    .0016
                        80.    6368.   8295.    1.178     .904    .0019
                        75.    4511.   6674.    1.341     .906    .0021
                        70.    2821.   5225.    1.703     .919    .0023
                        65.    1309.   3955.    2.874     .951    .0026
   2.000   50000.     100.   10001.  11225.     .997     .889    .0010
                        95.    9673.  10961.    1.014     .895    .0010
                        90.    9041.  10626.    1.063     .904    .0012
                        85.    8330.  10228.    1.124     .916    .0015
                        80.    7558.   9775.    1.202     .929    .0017
                        75.    5790.   8330.    1.348     .937    .0020
                        70.    3653.   6523.    1.697     .951    .0022
                        65.    1744.   4946.    2.784     .981    .0025
   2.200   50000.     100.    9416.  10798.    1.080     .941    .0009
                        95.    9215.  10681.    1.095     .944    .0009
                        90.    8770.  10471.    1.135     .950    .0011
                        85.    8057.  10178.    1.213     .960    .0014
                        80.    7266.   9813.    1.313     .972    .0016
                        75.    6405.   9383.    1.446     .987    .0019
                        70.    4674.   8090.    1.738    1.004    .0022
                        65.    2287.   6145.    2.783    1.036    .0025
   2.400   50000.     100.    8118.   9572.    1.219    1.034    .0008
                        95.    8113.   9680.    1.225    1.027    .0009
                        90.    7852.   9665.    1.264    1.027    .0010
                        85.    7182.   9541.    1.370    1.031    .0013
                        80.    6410.   9321.    1.512    1.040    .0016
                        75.    5547.   9018.    1.711    1.053    .0019
                        70.    4604.   8640.    2.006    1.069    .0022
                        65.    2956.   7564.    2.802    1.095    .0025


    SEA-LEVEL STATIC THRUST =    49000.  (MAX)
    SEA-LEVEL SFC           =     1.021
```

```
  Output for Module # 11
  ********************************************************************************
1         SUMMARY --- ACSYNT OUTPUT --- NASA, AMES RESEARCH CENTER

ENGLISH UNITS -
 Langley Research Center HSCT24E
   DISTANCES IN FEET

   WEIGHTS IN LBS.
    GENERAL            FUSELAGE                          WING   CANARD  VTAIL
   FORCES IN LBS.

   PRESSURES IN LBS/FT**2
 WG     320734.   LENGTH          284.0   AREA          7500.0      .0  450.0
 W/S        42.8  DIAMETER         12.0   WETTED AREA 15003.0      .0  466.8
 T/W         .30  VOLUME        26893.0   SPAN           150.0      .0   17.0
 N(Z) ULT   3.8   WETTED AREA    7644.9   L.E. SWEEP      45.1    89.4   52.9
 CREW         0.  FINENESS RATIO  23.7   C/4 SWEEP       38.0      .0   38.8
 PASENGERS250.                           ASPECT RATIO    3.00     .01    .64
                                         TAPER RATIO      .20     .00    .20
    ENGINE              WEIGHTS          T/C ROOT         .02     .00    .10
                                         T/C TIP          .02     .00    .06
 NUMBER       4.                 W     WG  ROOT CHORD     83.3      .0   44.1
 LENGTH    22.0    STRUCT. 160962. 50.2   TIP CHORD       16.7      .0    8.8
 DIAM.      3.9    PROPUL.  36120. 11.3   M.A. CHORD      57.4      .0   30.4
 WEIGHT 7000.0     FIX. EQ. 63285. 19.7   LOC. OF L.E.   139.1      .0  239.1
 TSLS   49000.     FUEL      3604.  1.1
 SFCSLS   1.02     PAYLOAD  50000. 15.6


                              MISSION SUMMARY

 PHASE     MACH      ALT     FUEL    TIME     DIST    L/D     THRUST    SFC       Q
 =======   ====   ======   ======   =====   ======   =====   =======   =====   ======
 TAKEOFF    .00       0.    2860.     5.5    785    850.4
 COMBAT    1.30   50000.       0.      .0       .0   11.47    53860.8   1.120    288.2
 COMBAT    1.40   50000.       0.      .0       .0   11.39    59415.3   1.108    334.2
 COMBAT    1.50   50000.       0.      .0       .0   11.65    64577.5   1.108    383.7
 COMBAT    1.60   50000.       0.      .0       .0   11.65    70161.1   1.104    436.5
 COMBAT    1.70   50000.       0.      .0       .0   11.67    75599.8   1.105    492.8
 COMBAT    1.80   50000.       0.      .0       .0   11.67    80940.0   1.107    552.5
 COMBAT    1.90   50000.       0.      .0       .0   11.56    86071.6   1.112    615.6
 COMBAT    2.00   50000.       0.      .0       .0   11.48    91022.7   1.119    682.1
 COMBAT    2.10   50000.       0.      .0       .0   11.00    95605.0   1.142    752.0
 COMBAT    2.20   50000.       0.      .0       .0   11.03    99767.8   1.172    825.4
 COMBAT    2.30   50000.       0.      .0       .0   10.94   103542.5   1.205    902.1
 COMBAT    2.40   50000.       0.      .0       .0   10.86   106905.0   1.241    982.2
 LANDING                                  96615.9

 Block Time  =    .092 hr  (without air and ground manuever allowances)
 Block Range =     .0 nm

                              COMBAT PHASES

 MACH    ALT   PS1G  NZS  CLS    CDS    ALS  NZI   PSI    CLI   CDI    ALI   CBE
 1.30 50000.    -5. 1.0  .298   .0260  3.3  2.5  -391.  .734  .1173  8.6     0.
 1.40 50000.     7. 1.1  .270   .0237  3.2  2.5  -375.  .631  .0947  8.0     0.
 1.50 50000.    24. 1.2  .261   .0224  3.1  2.5  -320.  .549  .0717  6.8     0.
 1.60 50000.    38. 1.3  .249   .0214  3.0  2.5  -292.  .482  .0585  6.1     0.
 1.70 50000.    53. 1.4  .238   .0204  3.0  2.5  -264.  .426  .0483  5.6     0.
 1.80 50000.    68. 1.5  .228   .0195  3.0  2.5  -239.  .379  .0408  5.1     0.
 1.90 50000.    82. 1.5  .215   .0186  3.0  2.5  -224.  .340  .0356  4.9     0.
 2.00 50000.    97. 1.6  .204   .0178  3.0  2.5  -208.  .306  .0313  4.6     0.
 2.10 50000.   107. 1.6  .186   .0169  3.1  2.5  -222.  .277  .0294  4.8     0.
 2.20 50000.   122. 1.7  .178   .0161  3.1  2.5  -202.  .252  .0259  4.5     0.
 2.30 50000.   134. 1.8  .167   .0153  3.1  2.5  -192.  .231  .0235  4.4     0.
 2.40 50000.   146. 1.8  .157   .0145  3.1  2.5  -184.  .212  .0214  4.3     0.
```

2D Mixed Compression inlet — sample input and results

```
  Input for Module #  2
  ********************************************************************************
                            TRAJECTORY INPUT


 TIMTO1 = 5.0        MENDUR =    0.     NCRUSE = 2     IPLOT = 4
 TIMTO2 =  .5          QMAX =  1700.    IPSIZE =-2     HMINP =     0.
 FRFURE =  .22        XDESC = 100.0     IPSTO1 = 5     HMAXP = 40000.
  DESLF = 2.50       WKFUEL = 1.000     IPSTO2 = 1     DELHP =  4000.
  ULTLF = 3.75       CRMACH = 2.400      IBREG = 0   SMMINP =  .300
  RANGE =  4000.     WKLAND =  .570     IENDUR = 0   SMMAXP =  .900
  WFUEL = 324293.     FLFAC =  .600     IPRINT = 0    DELMP =  .100
  WFEXT =      0.     DECEL =  .250     KERROR = 2   WCOMBP =      .70
 WFTRAP =    100.    NLEGCL = 0         NLEGCR = 0   NLEGLO = 0
 FWGMAX = 1.200         TOL =  .001     MILCOM = 0    NMISS = 1
  NCODE = 0          MMPROP = 1


 MISSION  1

          MACH NO.   ALTITUDE      HORIZONTAL     NO.  VIND
 PHASE   START END   START  END     DIST  TIME     TURN  "G"S  WKFUEL M IP IX W B A P
 ------- ---- ----  ----- -----    ------ -----    ---- -----  ------ - -- -- - - - -
 COMBAT  1.30  .00  50000     0      5.0     .0     .0    .0   .0001 1  1  0 0 0 0 0
 COMBAT  1.40  .00  50000     0      5.0     .0     .0    .0   .0001 1  1  0 0 0 0 0
 COMBAT  1.50  .00  50000     0      5.0     .0     .0    .0   .0001 1  1  0 0 0 0 0
 COMBAT  1.60  .00  50000     0      5.0     .0     .0    .0   .0001 1  1  0 0 0 0 0
 COMBAT  1.70  .00  50000     0      5.0     .0     .0    .0   .0001 1  1  0 0 0 0 0
 COMBAT  1.80  .00  50000     0      5.0     .0     .0    .0   .0001 1  1  0 0 0 0 0
 COMBAT  1.90  .00  50000     0      5.0     .0     .0    .0   .0001 1  1  0 0 0 0 0
 COMBAT  2.00  .00  50000     0      5.0     .0     .0    .0   .0001 1  1  0 0 0 0 0
 COMBAT  2.10  .00  50000     0      5.0     .0     .0    .0   .0001 1  1  0 0 0 0 0
 COMBAT  2.20  .00  50000     0      5.0     .0     .0    .0   .0001 1  1  0 0 0 0 0
 COMBAT  2.30  .00  50000     0      5.0     .0     .0    .0   .0001 1  1  0 0 0 0 0
 COMBAT  2.40  .00  50000     0      5.0     .0     .0    .0   .0001 1  1  0 0 0 0 0


  Input for Module #  4
  ********************************************************************************
1                       PROPULSION INPUT
                         VERSION 04-76

 *****  Proposed LARC HSCT24E Propulsion System *****


  AENDIA =     4.000  AENLE  =    22.000  AENWT  =  7000.000
  ALTI   =      .000  AM     =     .000  ATURB  =      .242
  AENTW  =      .000
  AUAENG =      .000  AWAENG =     .000  BA     =      .000
  DELPR  =      .000  DELT57 =  370.000  DEPWCC =     5.000
  DIA1   =     3.960  EAB1   =     .750  EB1    =      .910
  ED1    =      .750  ETAC1  =     .900  ETAF1  =      .900
  ETAT1  =      .885  HTR    =     .400  HVF    = 18600.000
  MACH1  =      .930  MACH2  =    2.020  PCDFAC =     1.000
  POSA   =    29.920  PRFD   =    1.000  PWCC   =   100.000
  P11P1  =     1.000  P2P1   =   12.070  R10A   =    -2.000
  R32    =      .950  R54    =     .940  R54N   =      .940
  R711   =      .980  R711N  =     .980  SCPR   =     1.480
  SFADP  =     1.000  SFADSP =    1.000  SFAUXP =     1.000
  SFBEP  =     1.000  SFBPP  =    1.000  SFBTP  =     1.000
  SFDIVP =     1.000  SFINSP =    1.000  SFIP   =     1.000

  nInl   =         4  InType =        7  sfInlP =     1.000
```

```
 sfSplP =     1.000  spPrfP =     1.000  sfWavP =     1.000
 Lm =        12.000  YcOYm  =      .850  AR     =     2.200
 theta  =     6.250  psi    =      .000  eta    =     4.500
 lipRat =      .010

 SFSFC1 =      .800  SFSFC2 =      .700  SFSFC3 =      .700
 SM1    =      .600  SODG   =     1.000  TOSA   =   518.000
 TR     =   520.000  TWAB   =    49000.  TWOAB  =    35000.
 TWTO   =      .500  T3     =     2430.  T5M    =     3400.
 T51    =     2800.  T7M    =     3400.  T71    =       0.
 VC1    =      .980  WCWA1  =      .000  XMDES  =     2.400
 XMT    =      .990  YREN   =       95.  FRBT   =     2.730
 FRPN   =     4.220  RDIAM  =     1.980  RLENG  =     1.710


 IPR    =         3  IPRINT =         1  IPLOT  =         1
 KERROR =         0  KODE   =         0  KT5    =         2
 KT7    =         0  MINPR  =         0  NAB    =         6
 NOZZ   =         1  NPROP  =         6  NSUMM  =         8
                                         IENG   =         1 (J85 )


 THESE VARIABLES ARE USED BY TABLE LOOK UP
 ESF    =      .550  NDTAIL   = 0  IPDBUG  = 0  IIPRINT = 0


 ALTD  =    50000.    50000.    50000.    50000.    50000.    50000.
 XMACH =     1.400     1.600     1.800     2.000     2.200     2.400
 XMPRI =      .302      .930     1.200     2.000     2.100     3.000
 XPRI  =      .986      .990      .986      .937      .600      .400
 XMPRI1 =     .000      .000      .000      .000      .000      .000      .000      .000
    .000      .000
 XPRI1 =      .000      .000      .000      .000      .000      .000      .000      .000
    .000      .000
 XMPRI2 =     .000      .000      .000      .000      .000      .000      .000      .000
    .000      .000
 XPRI2 =      .000      .000      .000      .000      .000      .000      .000      .000
    .000      .000



 Output for Module #  2
 ********************************************************************************
                        TRAJECTORY OUTPUT


Block Time                          =     .092 hrs
Block Range                         =       .0 n.m.
Block Fuel                          =   2860.2 lb.

Takeoff Field Length (total run)    =  748223. ft
Landing Field Length (total run)    =   96616. ft   Decel @ .250 Gs
Landing Field Length (ground run)   =   38767. ft
Weight for Landing calculation      =  644067. lbs
Landing Thrust to Weight ratio      =     .400
Takeoff Weight                      =  646064. lbs
Landing Weight                      =  643204. lbs


 Output for Module #  4
 ********************************************************************************
1                     ENGINE SUMMARY


               ENGINE DIAMETER =     4.00 FEET
               ENGINE LENGTH   =    22.00 FEET
               ENGINE WEIGHT   =  7000.00 POUNDS
```

```
                BYPASS RATIO    =       .00
                NO OF ENGINES   =        4.
                DRAG REF AREA   =  7500.00 SQ FEET
                PWCC   = PERCENT OF ENGINE CORRECTED AIRFLOW
                THRUST = ENGINE THRUST (POUNDS PER ENGINE)
                SFC    = ENGINE SPECIFIC FUEL CONSUMPTION
                THRUSTU= THRUST PER ENGINE IN LBS, W/O INSTAL DRAG CORR
                SFCU   = SFC,1/HR, W/O INSTALLATION DRAG CORR
                CDINS  = TOT INSTALLATION DRAG COEF PER A/C (SWING REF)
1
```

MACH	ALT	PWCC	THRUST	THRUSTU	SFC	SFCU	CDINS
1.400	50000.	100.	8640.	9566.	.961	.868	.0015
		95.	7930.	8911.	.980	.872	.0016
		90.	6580.	7617.	.994	.858	.0017
		85.	5286.	6402.	1.027	.848	.0018
		80.	4045.	5277.	1.099	.842	.0020
		75.	2885.	4248.	1.243	.844	.0022
		70.	1832.	3321.	1.554	.858	.0024
		65.	895.	2503.	2.493	.891	.0026
1.600	50000.	100.	10526.	11315.	.918	.854	.0010
		95.	10034.	10888.	.938	.864	.0010
		90.	9454.	10375.	.960	.875	.0011
		85.	7745.	8734.	.973	.863	.0012
		80.	6157.	7213.	1.002	.855	.0013
		75.	4703.	5827.	1.057	.853	.0014
		70.	3391.	4583.	1.165	.862	.0015
		65.	2139.	3490.	1.445	.886	.0017
1.800	50000.	100.	12314.	12805.	.881	.847	.0005
		95.	11814.	12395.	.898	.856	.0006
		90.	11254.	11925.	.918	.866	.0006
		85.	10642.	11402.	.941	.879	.0007
		80.	8804.	9655.	.958	.874	.0008
		75.	6871.	7813.	.990	.871	.0009
		70.	5133.	6166.	1.052	.876	.0010
		65.	3599.	4723.	1.175	.895	.0011
2.000	50000.	100.	14074.	14953.	.887	.834	.0007
		95.	13580.	14584.	.904	.842	.0008
		90.	12999.	14129.	.925	.851	.0009
		85.	12341.	13598.	.949	.862	.0010
		80.	11615.	12999.	.978	.874	.0011
		75.	9639.	11150.	1.013	.876	.0012
		70.	7206.	8845.	1.076	.877	.0013
		65.	5066.	6832.	1.199	.889	.0014
2.200	50000.	100.	15749.	16480.	.890	.850	.0005
		95.	15332.	16248.	.907	.856	.0006
		90.	14790.	15892.	.928	.863	.0007
		85.	14138.	15426.	.953	.873	.0008
		80.	13388.	14863.	.982	.885	.0010
		75.	12552.	14213.	1.017	.899	.0011
		70.	10512.	12360.	1.066	.906	.0012
		65.	7565.	9602.	1.160	.914	.0013
2.400	50000.	100.	16154.	16718.	.916	.885	.0003
		95.	16034.	16761.	.927	.887	.0004
		90.	15630.	16631.	.949	.892	.0005
		85.	15072.	16346.	.976	.900	.0007
		80.	14376.	15924.	1.008	.910	.0008
		75.	13558.	15380.	1.047	.923	.0010
		70.	12631.	14728.	1.093	.938	.0011
		65.	10647.	13019.	1.163	.951	.0013

```
 SEA-LEVEL STATIC THRUST =    49000.  (MAX)
 SEA-LEVEL SFC           =     1.021
```

Output for Module # 11

1 SUMMARY --- ACSYNT OUTPUT --- NASA, AMES RESEARCH CENTER

Langley Research Center HSCT24E

GENERAL		FUSELAGE			WING	CANARD	VTAIL
WG	320773.	LENGTH	284.0	AREA	7500.0	.0	450.0
W/S	42.8	DIAMETER	12.0	WETTED AREA	15003.0	.0	466.8
T/W	.30	VOLUME	26893.0	SPAN	150.0	.0	17.0
N(Z) ULT	3.8	WETTED AREA	7644.9	L.E. SWEEP	45.1	89.4	52.9
CREW	0.	FINENESS RATIO	23.7	C/4 SWEEP	38.0	.0	38.8
PASENGERS	250.			ASPECT RATIO	3.00	.01	.64
				TAPER RATIO	.20	.00	.20
ENGINE		WEIGHTS		T/C ROOT	.02	.00	.10
				T/C TIP	.02	.00	.06
NUMBER	4.		W WG	ROOT CHORD	83.3	.0	44.1
LENGTH	22.0	STRUCT.	161001. 50.2	TIP CHORD	16.7	.0	8.8
DIAM.	3.9	PROPUL.	36120. 11.3	M.A. CHORD	57.4	.0	30.4
WEIGHT	7000.0	FIX. EQ.	63285. 19.7	LOC. OF L.E.	139.1	.0	239.1
TSLS	49000.	FUEL	3604. 1.1				
SFCSLS	1.02	PAYLOAD	50000. 15.6				

MISSION SUMMARY

PHASE	MACH	ALT	FUEL	TIME	DIST	L/D	THRUST	SFC	Q
TAKEOFF	.00	0.	2860.	5.5	748223.4				
COMBAT	1.30	50000.	0.	.0	.0	11.47	54131.6	1.120	288.2
COMBAT	1.40	50000.	0.	.0	.0	11.34	60740.2	1.104	334.2
COMBAT	1.50	50000.	0.	.0	.0	11.58	66603.1	1.106	383.7
COMBAT	1.60	50000.	0.	.0	.0	11.40	77775.0	1.069	436.5
COMBAT	1.70	50000.	0.	.0	.0	11.33	87158.2	1.054	492.8
COMBAT	1.80	50000.	0.	.0	.0	11.23	96610.1	1.043	552.5
COMBAT	1.90	50000.	0.	.0	.0	11.04	105966.4	1.037	615.6
COMBAT	2.00	50000.	0.	.0	.0	10.71	122319.1	1.041	682.1
COMBAT	2.10	50000.	0.	.0	.0	10.07	137616.6	1.045	752.0
COMBAT	2.20	50000.	0.	.0	.0	9.91	152732.7	1.055	825.4
COMBAT	2.30	50000.	0.	.0	.0	9.73	167872.8	1.068	902.1
COMBAT	2.40	50000.	0.	.0	.0	9.78	182566.3	1.086	982.2
LANDING					96615.9				

Block Time = .092 hr (without air and ground manuever allowances)
Block Range = .0 nm

COMBAT PHASES

MACH	ALT	PS1G	NZS	CLS	CDS	ALS	NZI	PSI	CLI	CDI	ALI	CBE
1.30	50000.	-4.	1.0	.298	.0260	3.3	2.5	-390.	.734	.1173	8.6	0.
1.40	50000.	10.	1.1	.274	.0242	3.3	2.5	-372.	.631	.0946	8.0	0.
1.50	50000.	28.	1.2	.268	.0231	3.2	2.5	-315.	.549	.0716	6.8	0.
1.60	50000.	57.	1.4	.270	.0237	3.3	2.5	-272.	.481	.0582	6.1	0.
1.70	50000.	83.	1.5	.267	.0235	3.4	2.5	-231.	.424	.0480	5.5	0.
1.80	50000.	111.	1.7	.261	.0233	3.5	2.5	-193.	.377	.0405	5.1	0.
1.90	50000.	139.	1.8	.253	.0229	3.6	2.5	-163.	.338	.0352	4.8	0.
2.00	50000.	191.	2.0	.256	.0239	3.8	2.5	-107.	.303	.0308	4.6	0.
2.10	50000.	240.	2.2	.245	.0243	4.2	2.5	-79.	.274	.0288	4.7	0.
2.20	50000.	296.	2.4	.244	.0246	4.4	2.5	-14.	.248	.0253	4.5	0.
2.30	50000.	356.	2.5	.236	.0243	4.5	2.5	46.	.226	.0228	4.3	0.
2.40	50000.	419.	2.5	.217	.0222	4.4	2.5	108.	.207	.0207	4.2	0.

Vita

The author was raised in a small (pop. ~800) town in coastal Maine. He was raised on a farm with pigs, goats, sheep, and other typical farm animals. While this was a good character building way to grow up, it undoubtedly influenced his educational goals and his desire to never clean animal stalls again. He studied Mechanical Engineering at the University of Maine at Orono from 1987 to 1991. Upon graduating, he (virtually) immediately left for the warmer climate of Virginia to attend the Virginia Polytechnic Institute and State University, and continue his engineering studies, well out of reach of the nearest pitchfork.